Universidade de Aveiro
2014

Secção Autónoma de Ciências da Saúde

Sílvia Isabel Ferreira da Silva

A PPA é uma proteína fundamental na espermatogénese

APP is a critical protein in spermatogenesis

Universidade de Aveiro
2014

Secção Autónoma de Ciências da Saúde

Sílvia Isabel Ferreira da Silva

A PPA é uma proteína fundamental na espermatogénese

APP is a critical protein in spermatogenesis

Dissertação apresentada à Universidade de Aveiro para cumprimento dos requisitos necessários à obtenção do grau de Mestre em Biomedicina Molecular, realizada sob a orientação científica da Professora Doutora Odete Abreu Beirão da Cruz e Silva, Professora Auxiliar com Agregação da Secção Autónoma de Ciências da Saúde da Universidade de Aveiro, e co-orientação da Doutora Dânia Sofia da Silva Teixeira, Investigadora do Centro de Biologia Celular (Secção Autónoma de Ciências da Saúde) da Universidade de Aveiro.

Este trabalho contou com o apoio do Centro de Biologia Celular (CBC) da Universidade de Aveiro, e é financiado por fundos FEDER através do Programa Operacional Factores de Competitividade – COMPETE e por Fundos nacionais da FCT – Fundação para a Ciência e a Tecnologia no âmbito do projeto PTDC/BEX-BCM/0493/2012.

o júri

presidente

Professora Doutora Ana Gabriela da Silva Cavaleiro Henriques
Professora Auxiliar Convidada da Secção Autónoma de Ciências da Saúde da Universidade de Aveiro

Professora Doutora Odete Abreu Beirão da Cruz e Silva
Professora Auxiliar com Agregação da Secção Autónoma de Ciências da Saúde da Universidade de Aveiro

Professora Doutora Maria de Lourdes Gomes Pereira
Professora Associada com Agregação do Departamento de Biologia da Universidade de Aveiro

agradecimentos

Um agradecimento muito especial à Professora Doutora Odete Abreu Beirão da Cruz e Silva pela oportunidade de realização deste trabalho e pela orientação dada, que permitiu o meu enriquecimento pessoal, científico e profissional.

À Doutora Dânia Sofia da Silva Teixeira pela ajuda e apoio dado ao longo de todo o percurso deste trabalho.

Ao Professor João Carlos Sousa, do ICVS da Universidade do Minho, por ter fornecido os tecidos sem os quais este trabalho não seria possível. Muito obrigado pela disponibilidade e por toda a ajuda dada.

Ao Centro de Biologia Celular da Universidade de Aveiro e à FCT pelo financiamento deste estudo.

Muito obrigado aos colegas de laboratório de Neurociências, em especial à Filipa Martins, Joana Oliveira, Joana Rocha, Regina Cerqueira e Ana Marote, pelo suporte, amizade e companhia.

Aos colegas do Mestrado de Biomedicina Molecular, em especial à Rita Cardoso, Margarida Oliveira e Cláudia Nunes. Obrigado por todos os momentos partilhados.

Obrigada às minhas companheiras de casa, Inês Santana e Liliana Carvalho, pela amizade.

Por último, muito obrigada à minha família, em especial à minha mãe, que me apoia incondicionalmente.

palavras-chave

proteína precursora de amilóide, proteína tau, fosforilação, proteína serina/treonina fosfatase, espermatogénese.

resumo

A proteína precursora de amilóide (PPA) e a proteína Tau estão relacionadas com os marcos histológicos da doença de Alzheimer, uma doença neurodegenerativa progressiva e complexa. A PPA é uma glicoproteína integral transmembranar que tem duas predominantes vias de processamento proteolítico, a via não-amiloidogénica e a via amiloidogénica. A proteína Tau encontra-se associada aos microtúbulos, sendo a afinidade dessa ligação regulada pela fosforilação de resíduos de serina e treonina. A expressão da PPA e da proteína Tau também já foi reportada no testículo. No entanto, ainda não foram estabelecidas as suas funções e modificações pós-traducionais neste tecido. Assim, analisamos a expressão destas duas proteínas e o seu padrão de fosforilação durante a espermatogénese usando como modelos murganhos e ratos *wild-type*. Através de imuno-histoquímica revelamos que a PPA, a proteína Tau, a proteína serina/treonina fosfatase (PP) 1α e a PP1γ são expressas em toda a espermatogénese. Fosforilação da PPA e da proteína Tau foi detetada durante a meiose. Em contraste com a localização da PPA-total, a PPA fosforilada na treonina 668 está especialmente localizada no núcleo dos espermatócitos. Estes resultados sugerem que a fosforilação da PPA e da proteína Tau contribui para a espermatogénese, especialmente na meiose. No entanto, são necessários estudos futuros para validar os nossos resultados e desvendar a função específica da PPA e da proteína Tau durante a espermatogénese e na meiose.

keywords amyloid precursor protein, tau protein, phosphorylation, serine/threonine protein phosphatase, spermatogenesis.

abstract The Amyloid precursor protein (APP) and Tau protein are related to histopathological hallmarks of Alzheimer's disease, a progressive and complex neurodegenerative disease. APP is a type 1 integral transmembrane glycoprotein. There are two predominant proteolytic processing pathways of APP, the nonamyloidogenic pathway, and the amyloidogenic pathway. Tau is one of the microtubule-associated proteins, and its binding affinity for microtubules is regulated by phosphorylation of serine and threonine residues. APP and Tau protein expression has also been reported in the testis. However, their function and posttranslational modifications in the testis have not been established. Thus, we analyzed the expression of these two proteins and their phosphorylation patterns during spermatogenesis using wild-type mice and rats as models. Through immunohistochemistry we revealed that APP, Tau protein, Serine/Threonine Protein Phosphatase (PP) 1α and PP1γ are expressed throughout spermatogenesis. APP and Tau are phosphorylated during meiosis. In contrast to total-APP localization, phosphorylated APP at Thr668 was specially localized in spermatocyte nuclei. These results suggest that phosphorylation of APP and Tau protein contribute to spermatogenesis, especially in meiosis. However, further research is required to validate our results and unravel the specific function of APP and Tau protein during spermatogenesis and meiosis.

Index

List of Figures

List of Tables

Acronyms, Abbreviations, and Initials

a.a.	amino acids
AD	Alzheimer's Disease
ADAM	A Disintegrin And Metalloprotease
AICD	Amyloid Precursor Protein Intracellular Domain
Ala	Alanine
Aph	Anterior Pharynx Defective
APL	β-Amyloid-Like Protein (*Caenorhabditis elegans*)
APLP	Amyloid Precursor-Like Protein
APOE	Apolipoprotein E gene
APP	Amyloid Precursor Protein
APPL	β-Amyloid-Like Protein (*Drosophila melanogaster*)
APS	Ammonium Persulphate
Asp	Aspartic acid
Aβ	β-Amyloid Peptide
BACE	β-Site Amyloid Precursor Protein-Cleaving Enzyme
BCA	Bicinchoninic Acid
BSA	Bovine Serum Albumin
CDK	Cyclin-Dependent Kinase
CHAPS	3[(3-Cholamidopropyl)dimethylammonio]-propanesulfonic acid
CNS	Central Nervous System
CS GAG	Chondroitin Sulphate Glycosaminoglycan
C-terminal	Carboxy-terminal
CTF	Carboxy-Terminal Fragment
CuBD	Copper-Binding Domain
DE	Acidic Region
DNA	Deoxyribonucleic acid
ECL	Enhanced Chemiluminescence
FBS	Foetal Bovine Serum

FPKM	Fragments Per Kilobase of transcript per Million fragments mapped
FSH	Follicle Stimulating Hormone
GSK	Glycogen Synthase Kinase
HFBD/GFLD	Heparin-Binding/Growth-Factor-Like Domain
HRP	Horseradish Peroxidase
Ig	Immunoglobulin
IHC	Immunohistochemistry
Ile	Isoleucine
JNK	c-Jun N-terminal Kinase
KPI	Kunitz Protease Inhibitor Domain
Leu	Leucine
LH	Luteinizing Hormone
MAP	Microtubule-Associated Protein
MAPT	Microtubule-Associated Protein Tau
MCI	Mild Cognitive Impairment
Met	Methionine
MPM	Metaphase Protein Marker
mRNA	messenger Ribonucleic Acid
MT	Microtubule
NFTs	Neurofibrillary Tangles
N-terminal	Amino-Terminal
PBS	Phosphate Buffered Saline
PDPK	Proline-Directed Protein Kinases
Pen	Presenilin Enhancer
PGCs	Primordial Germ Cells
PHF	Paired Helical Filament
PMSF	Phenylmethylsulfonyl Fluoride
PP	Serine/Threonine Protein Phosphatase
Pro	Proline

PS	Presenilin
PSEN	Presenilin gene
RC	Random Coil
sAPP	soluble Amyloid Precursor Protein
SDS	Sodium Dodecyl Sulphate
Ser	Serine
TACE	Tumour Necrosis Factor-α Converting Enzyme
TBS	Tris Buffered Saline
TBS-T	Tris Buffered Saline-Tween
TEMED	N,N,N',N'-Tetramethylethylenediamine
Thr	Threonine
TM	Transmembrane
Tyr	Tyrosine
Val	Valine
ZnBD	Zinc-Binding Domain

1. Introduction

1.1. Alzheimer's Disease

Over the last decades societies have been growing older, with the most intensive growth in the number of individuals above 85 years old. This scenario represents one of the biggest challenges for health care and social systems. Gradual improvement of health care, arising from advances in science research, and the social support given to senior citizens has significantly contributed to this beneficial tendency. Still, ageing populations contribute to an increase in the ratio of age-related diseases, and consequently, an increase in the burden for the health care system, thus changing the main concerns of science research [1].

Alzheimer's disease (AD) was first described in 1907 by Dr. Alois Alzheimer, a German psychiatrist and neuropathologist, as "an unusual illness of the cerebral cortex" [2]. It's a progressive and complex neurodegenerative disease, and is characterized by an irreversible memory loss and intellectual function decline, severe enough to interfere with daily functions (reviewed in Thies and Bleiler, 2013 [3]).

AD is the most common type of dementia, accounted for an estimated 60% to 80% of cases. According to Alzheimer's Association (http://www.alz.org/) the term dementia describes "a variety of diseases and conditions that develop when neurons die or no longer function normally", consequently causing "changes in one's memory, behaviour, and ability to think clearly". Besides AD, other types of dementia include vascular dementia, dementia with Lewy bodies, frontotemporal lobar degeneration, mixed dementia, Parkinson's disease, Creutzfeldt-Jakob disease, and normal pressure hydrocephalus. Each type of dementia is associated with distinct symptom patterns and brain abnormalities. AD affects people in different ways, but the common symptoms are: memory loss that disrupts daily life; challenges in planning or solving problems; difficulty completing familiar tasks; confusion with time or place; trouble understanding visual images and spatial relationships; new problems with words in speaking or writing; misplacing things and losing the ability to retrace steps; decreased or poor judgment; withdrawal from work or social activities; changes in mood and personality. Later symptoms include impaired judgment, disorientation, confusion, behaviour changes, and difficulty speaking, swallowing, and walking (reviewed in Thies and Bleiler, 2013 [3]).

World Health Organization estimated that 44.4 million people worldwide were living with dementia in 2013, and there are 7.7 million new cases of dementia each year [4]. In 2010, Western Europe was the global burden of disease region with the highest number of people with dementia (7.0 million), followed by East Asia with 5.5 million, South Asia with 4.5 million and North America with 4.4 million [5]. According to the Alzheimer Association, in the United States of America an estimated 5.2 million of people of all ages have AD in 2013 (reviewed in Thies and Bleiler, 2013 [3]). Of those with AD, about 4% are less than 65 years old, 13% are 65 to 74 years old, 44% are 75 to 84 years old, and 38% are 85 years or older

[6] (reviewed in Thies and Bleiler, 2013 [3]). By 2050, the total estimated prevalence expected is 13.8 million of people in United States of America [6] (reviewed in Thies and Bleiler, 2013 [3]) and 115.4 million of people worldwide [7].

1.1.1. AD Hallmarks

AD has as microscopic hallmarks brain abnormalities the extracellular senile plaques (also known as neuritic plaques) and intracellular neurofibrillary tangles (NFTs), as represented in Figure 1 [8]. These histological features go along with decreases in synaptic density, increases in neuronal loss, neuroinflammatory glial activity and neurodegeneration [1]. For a neuropathological diagnosis of AD, both senile plaques and NFTs are mandatory [9], and can only be confirmed post-mortem at the autopsy [10].

Senile plaques are neurotoxic and consist of a dense amyloid core of β-amyloid peptide (Aβ) of 40 and 42 amino acids (a.a.) in length [11]. These plaques are surrounded by dystrophic neurites and, precipitate and deposit outside and around neurons, predominantly those in the limbic system and cortex. This mechanism will finally lead to neuronal death, which is proposed to be responsible for phenotypical dementia in affected patients [9].

Tau is a microtubule-associated protein (MAP), and the major constituent of NFTs. Tau's function is regulated by phosphorylation. In AD, Tau protein is abnormally hyperphosphorylated, which leads to Tau polymerization, disruption of microtubule (MT) dynamics, and impaired axonal transport. That consequently results in the formation of intraneuronal NFTs and finally neuronal death [9].

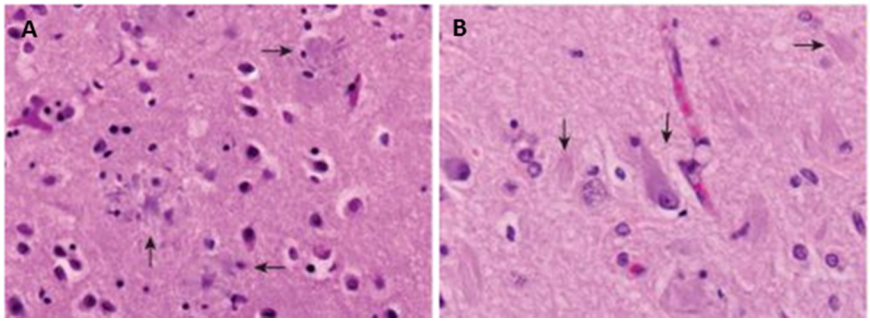

Figure 1: Alzheimer disease histopathological features in the brain.
A) Plaques with dystrophic neurites surrounding amyloid cores (arrows). **B)** Neurofibrillary tangle is present within one neuron, and several extracellular tangles are also present (arrows) (taken from [12]).

Nowadays, the "amyloid hypothesis" is generally supported. According to this hypothesis the abnormal production and aggregation of Aβ, principally the more fibrillogenic $A\beta_{42}$ isoform, are the primary pathogenic events in AD, and NFTs are further downstream in the neuropathogenesis. This hypothesis is controversial, because senile

plaques and NFTs have been found in the brain of non-demented persons as well, although in lower abundance. Additionally, the precise sequence and repercussion of the different biological processes involved in AD are not yet entirely clear. Though neurodegeneration, senile plaques, and NFTs are broadly accepted as part of the AD, it remains difficult to determine to what magnitude these factors contribute to dementia and to what magnitude they are interconnected with each other. However, some studies have shown that soluble oligomers of Aβ can disrupt synaptic function, facilitate neuronal dysfunction in AD, and are both essential and sufficient to disrupt learning behaviour in a way that is both potent, rapid, and transient [9].

1.1.2. AD Forms

There are two forms of AD: the familial form, which has an earlier onset (symptoms tend to develop before age 65), faster progression, and affects around 1% of the patients; and the sporadic form, which has a later onset (symptoms develop at age 65 or older), and is the most common condition. Nonetheless, the clinical and histopathological features of both forms are undistinguishable [1,3].

The familial AD is caused by mutations in three genes: the amyloid precursor protein (APP) gene, and the presenilin genes, PSEN1 and PSEN2, which are involved in the cleavage of APP and production of Aβ [1,3]. Mutations in the substrate and in the proteases can contribute to amyloid deposition, which forms one of the corner stones of the "amyloid hypothesis" [13]. Mutations in the APP gene, on chromosome 21q21.3, are estimated to represent about 5% of familial AD. To date, a total of 51 mutations have been identified in the APP gene, but not all are pathogenic. Two well-studied mutations found in familial AD families have been expressed in transgenic mice. In the first case, the "London mutation", a missense mutation, a valine is replaced by an isoleucine at codon 717 (V717I). In the second case, the "Swedish mutation", where, immediately upstream of the Aβ domain, mutations at codons 670 and 671 resulted in a double base pair substitution, whereby a lysine and a methionine are replaced by aspartic acid and leucine (K670D/M671L, APPsw) [14].

Mutations in the PSEN1 gene, on chromosome 14q24.3, are the most common cause of autosomal dominant early-onset AD, accounting for up to 70% of cases [15], with about 207 mutations identified in this gene. While in the PSEN2 gene, on chromosome 1q31-q42, only 25 mutations have been described so far, and not all have been confirmed to be pathogenic, accounting for less than 5% of early-onset AD cases [16,17]. Mutations in PSEN1 and PSEN2 genes result in the production of abnormal presenilin (PS) proteins, which interfere with the γ-secretase complex function, mainly due to a defective PS1. Consequently this alters APP processing, because PS/γ-secretase can cleave APP at different positions. That leads to variable effects on the spectrum of Aβ peptides released,

which are the overproduction of the longer and toxic version of Aβ peptides (≥$A\beta_{42}$) and the underproduction of the shorter version of Aβ peptides (≤$A\beta_{40}$). Copies of the toxic peptide fragment stick together and build up in the brain, forming the senile plaques [13].

The MAPT gene is located on chromosome 17q21.1, and codes for human microtubule-associated protein Tau [18]. No mutations have been identified in familial AD. However, exonic and intronic mutations were identified in the Tau gene that were associated to frontotemporal dementia with parkinsonism-17, a familial dementia related to AD. These findings prove that dysfunction of Tau in itself can cause neurodegeneration and consequently contribute to dementia. Besides frontotemporal dementia, Tau mutations can cause diseases as varied as subcortical gliosis, cortico-basal degeneration and pallido-ponto-nigral degeneration [14].

1.1.3. AD Risk Factors

AD is a complex multifactorial disease attributable to various interrelated and interacting environmental and genetic factors. Many factors contribute to the development of AD. Advanced age is the greatest risk factor for AD, but this disease is not a typical part of ageing. Another risk factor is the family history, because individuals who have a first-degree relative with AD are more likely to develop the disease than those who do not. People with mild cognitive impairment (MCI), especially MCI involving memory problems, are more likely to develop dementia than people without it. Cardiovascular diseases and factors that increase the risk of cardiovascular diseases, like smoking, alcohol intake, high body mass index, diabetes mellitus, high cholesterol, and hypertension, are also associated with a higher risk of developing AD and other dementias. A healthy heart and healthy blood vessels help ensure that the brain is supplied with the oxygen- and nutrient-rich blood, required for normal brain function. Apolipoprotein E gene (APOE) is one of the genetic risk factors for AD, and is associated with sporadic AD. The APOE gene, on chromosome 19q13.2, has three allelic variants, ε2, ε3 and ε4, and studies suggest that the ε3 allele neither increases nor decreases one's risk of AD, but having the ε2 allele may decrease one's risk. However, having the ε4 allele increases the risk of developing AD and of developing it at a younger age. People who inherit two copies of the ε4 allele have an even higher risk of developing AD, although inheriting the ε4 allele does not guarantee that a person will develop this illness [3,19].

On the preventive side, physical activity and consumption of a diet low in saturated fats and rich in fruits, vegetables and vegetable-based oils are two factors that protect the heart as well the brain and reduce the risk of developing dementia. Other protective factors are education, and social and cognitive engagement. This can be explained by the fact that having more years of education, and remaining socially and cognitively active builds a "cognitive reserve". According to this hypothesis, having more years of education, and

remaining socially and cognitively active increases the connections between neurons in the brain and empowers the brain to compensate more fully for the early brain changes of AD or other dementias by using alternative routes of neuron-to-neuron communication to complete a cognitive task [3,19].

1.2. APP

APP is evolutionary highly conserved and it´s family includes the mammalian amyloid precursor-like protein (APLP) 1 and 2, the *Drosophila melanogaster* β-amyloid-like protein APPL, and the *Caenorhabditis elegans* β-amyloid-like protein APL-1 (reviewed in Jacobsen and Iverfeldt, 2009 [20]).

All APP family members are type 1 integral transmembrane (TM) glycoproteins, and are composed by a large ectoplasmic amino-terminal (N-terminal) region, a single membrane-spanning domain, and a shorter cytoplasmic carboxy-terminal (C-terminal) region [21,22] (reviewed in Jacobsen and Iverfeldt, 2009 [20]). The APP sequence can be divided into several distinct domains, as demonstrated in Figure 2. The ectoplasmic region of APP, which represents the larger part of the protein, can be divided into the E1 and E2 domains. The E1 domain can be further divided into a number of subdomains, including a heparin-binding/growth-factor-like domain (HFBD/GFLD), a copper-binding domain (CuBD) and a zinc-binding domain (ZnBD). The E1 domain is followed by an acidic region rich in aspartic acid and glutamic acid (DE) and a Kunitz protease inhibitor domain (KPI), which is not present in APP695 (an APP alternatively spliced isoform). The E2 region consists of another HFBD/GFLD and a random coil (RC) region. The cytoplasmic region of APP contains a protein interaction motif, namely the YENPTY sequence (including the NPXY internalization signal), which is conserved in all APP homologues. The sequences of all APP homologues can be divided into similar domain structures as APP (Figure 2) (reviewed in Jacobsen and Iverfeldt, 2009 [20]).

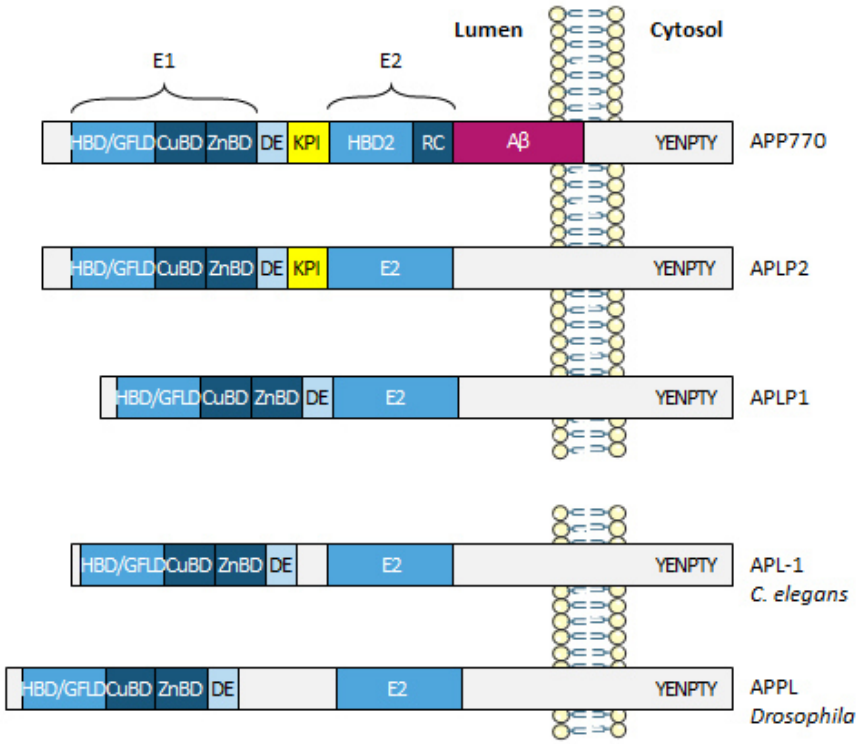

Figure 2: Schematic diagram of APP and its homologues domain organization.
All APP family members are type I integral membrane proteins that have relatively large extracellular domains and short intracellular domains. They contain heparin-binding/growth-factor-like domains (HBD/GFLD), copper- and zinc-binding domains (CuBD and ZnBD), an acidic domain (DE), and a protein interaction motif (YENPTY) in the carboxy-terminal. Other abbreviations: APL-1, *Caenorhabditis elegans* β-Amyloid-Like Protein; APLP, Amyloid Precursor-Like Protein; APP770, an Amyloid Precursor Protein alternatively spliced isoform; APPL, *Drosophila melanogaster* β-Amyloid-Like Protein; Aβ, β-Amyloid Peptide; KPI, Kunitz Protease Inhibitor Domain; RC, Random Coil (adapted from [20]).

APP is ubiquitously expressed and is encoded by a single gene on chromosome 21q21.3. However, APP exists in 11 isoforms produced by alternative splicing of three exons in a 19-exon gene, of which exons 7, 8 and 15 can be alternatively spliced [23], and the different isoforms can be preferentially expressed in different cell types [20]. There are three major isoforms of APP in mammals: APP695 (exons 1–6, 9–18), APP751 (exons 1–7, 9–18), and APP770 [20,23]. The main difference between APP isoforms is the presence or absence of the KPI domain and a chondroitin sulphate glycosaminoglycan (CS GAG) attachment site. The APP695 isoform is mainly found in cells of neuronal origin [20], while APP751 and APP770 are the predominant isoforms expressed in non-neuronal cells [24]. In mouse the presence of three APP splicing forms (APP695, APP751, and APP770) was described, the tissue distributions of these three forms are similar to that seen in humans [25,26].

1.2.1. APP Proteolytic Processing

There are two proteolytic processing pathways of APP, the nonamyloidogenic pathway, and the amyloidogenic pathway, represented in Figure 3. Both pathways are mediated by at least three cleavage events. The nonamyloidogenic processing of APP is initiated through cleavage by α-secretase, which leads to the release and secretion of the soluble N-terminal ectodomain sAPPα from the cell surface leaving an 83 a.a. long C-terminal membrane-bound fragment (C83). This fragment can be further processed by γ-secretase, leading to the release and secretion of a small non-pathogenic peptide p3 and a free APP intracellular domain (AICD). In the amyloidogenic pathway, APP is initially cleaved by β-secretase and releases the large soluble N-terminal ectodomain sAPPβ. The remaining C-terminal stub of 99 a.a. (C99) can then be further processed by γ-secretase, in a similar way to the nonamyloidogenic pathway, generating Aβ and AICD. The AICD can be translocated into the nucleus, where it may function as a transcription factor. Aβ is a normal soluble cellular metabolite encompassing two main forms with different C-terminal regions, $A\beta_{40}$ and $A\beta_{42}$ [20,23].

γ-Secretase cleavage between Val711 and Ile712 (in the APP770 isoform) generates $A\beta_{40}$, and cleavage between Ala713 and Thr714 results in production of $A\beta_{42}$. After γ-secretase cleavage, the remaining C-terminal fragments are 57 or 59 a.a. long (C57 and C59), and have been identified as AICD. Consequently, the final processing step has been suggested to be a result of three cleavage events. The C99 fragment is first cleaved at the ε-site between Leu720 and Val721, followed by cleavage at the ζ-site at the Val717-Ile718 bond, and finally the peptide is cut at the γ-site [8,20].

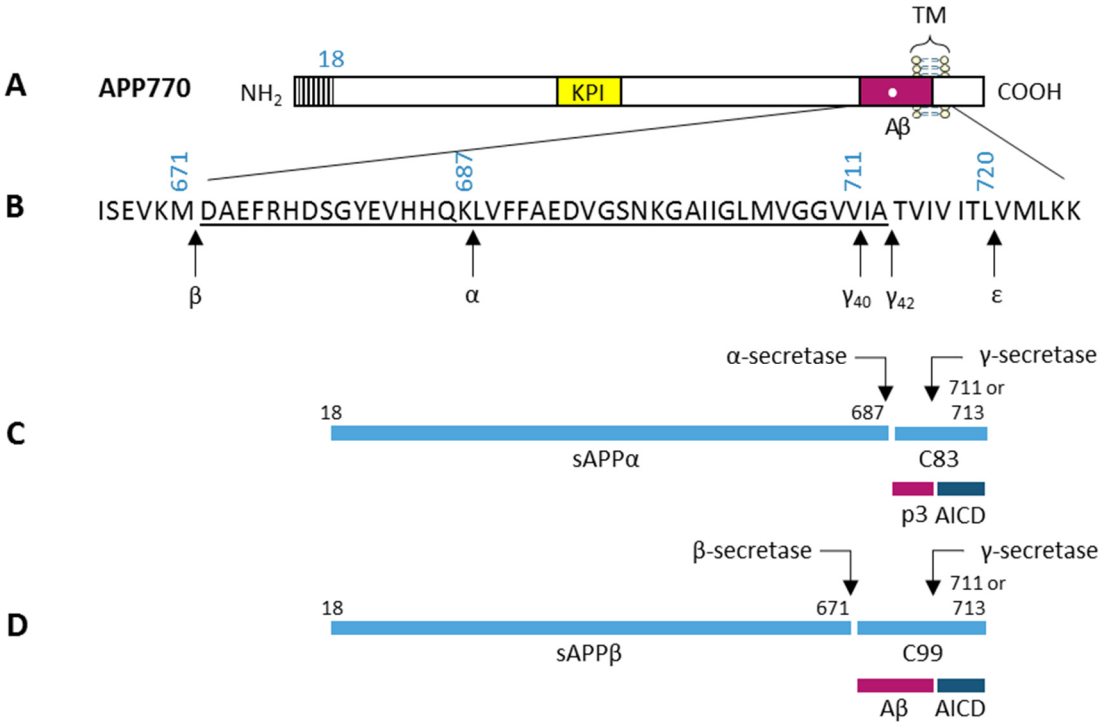

Figure 3: Schemes of the amyloid precursor protein (APP) and its two proteolytic processing pathways and principal proteolytic derivatives.
A) The largest of the known APP alternative splice forms, APP770, comprising 770 amino acids (a.a.). Regions of interest: a) a 17-residue signal peptide occurs at the N-terminal; b) two alternatively spliced exons of 56 and 19 a.a. are inserted at residue 289; the first contains a serine protease inhibitor domain of the Kunitz type (KPI); c) a single transmembrane domain (TM) at a.a. 700–723. The β-amyloid peptide (Aβ) includes 28 residues just outside the membrane plus the first 12–14 residues of the TM. **B)** The a.a. sequence within APP that contains the Aβ and TM regions. The underlined residues represent the $A\beta_{42}$ peptide. Three-digit numbers represent codon numbers (APP770 isoform). **C)** The nonamyloidogenic pathway. The first arrow indicates a site (after residue 687; same as white dot in Aβ box in A) of cleavage by α-secretase that enables secretion of the large, soluble ectodomain sAPPα into the medium and retention of the 83-residue C-terminal fragment (C83) in the membrane. C83 can undergo cleavage by γ-secretase principally at residue 711 or residue 713 to release the p3 peptides. **D)** The amyloidogenic pathway. The alternative proteolytic cleavage after residue 671 by β-secretase that results in the secretion of the slightly truncated sAPPβ molecule and the retention of a 99-residue C-terminal fragment in the membrane. C99 can also undergo cleavage by γ-secretase to release the Aβ peptides. Cleavage of both C83 and C99 by γ-secretase at the ε-site (in B) releases the APP intracellular domain (AICD) into the cytoplasm. The order and interdependency of the γ- and ε-cleavages have not been established (adapted from [8]).

Although APP processing has been widely studied, all the processing events and the enzymes involved have not yet been fully elucidated.

a) α-Secretase

α-Secretase is a zinc metalloproteinase that cleaves APP at the Lys687-Leu688 bond (in the APP770 isoform) [8,20], and metabolizes about 90% of APP [9]. Several enzymes can act as α-secretase, and they are all members of the ADAM (A Disintegrin And Metalloprotease)

family. The enzymes are ADAM9, ADAM10 and ADAM17, also known as tumour necrosis factor-α converting enzyme (TACE) [9,20]. ADAMs are type 1 integral membrane proteins, ~750 a.a. long, with a multidomain structure, including signal peptide, pro-domain, catalytic metalloprotease domain, disintegrin/cystein-rich domain, TM domain, and a short cytoplasmic domain [20], represented in Figure 4. All members of this family have four potential functions: cell fusion, cell adhesion, intracellular signalling and proteolysis [23]. Apparently, they have redundant α-secretase cleavage activities but differential expression patterns [9].

Figure 4: Structure of α-secretase.
Processing of APP by α-secretase is mediated by a series of proteases, mostly members of the ADAM (A Disintegrin And Metalloprotease) family, which are all membrane bound and consist of several extracellular domains, including a signal peptide (SP), a pro-domain (Pro), a catalytic metalloprotease domain, a disintegrin domain (which in some instances provides interaction with integrin receptors), and a cysteine-rich domain. Other abbreviations: TM, Transmembrane (adapted from [27]).

b) β-Secretase

The APP cleavage at the Met671-Asp672 bond (in the APP770 isoform) is carried out by β-secretase (Figure 5), an aspartyl protease, which constitutes the first step towards Aβ generation. BACE (β-Site Amyloid Precursor Protein-Cleaving Enzyme) 1 and BACE2 are the two β-secretases that have been identified. BACE is a single domain integral protein with the active site located on the ectoplasmic side of the membrane. The optimal pH of BACE activity is approximately 4.5, indicative that the β-site cleavage of APP takes place in the more acidic cellular compartments, like the endosomes. BACE cleavage has also been proposed to occur in lipid rafts (reviewed in Jacobsen and Iverfeldt, 2009 [20]). BACE1 is widely expressed in the brain [20], particularly in the neurons [9].

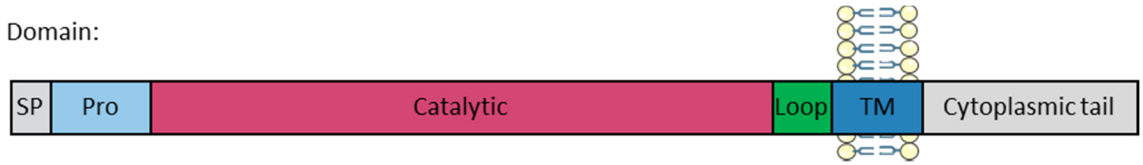

Figure 5: Structure of β-secretase.
β-Secretase activity is specifically mediated by the β-Site Amyloid Precursor Protein-Cleaving Enzyme 1 (BACE1). BACE1 is a membrane-bound enzyme that is synthesized with a signal peptide (SP), a pro-domain (Pro), and a catalytic domain. Other abbreviations: TM, Transmembrane (adapted from [27]).

c) γ-Secretase

γ-Secretase is an aspartyl protease, with a low sequence specificity that cleaves the substrate within its TM domain. The protein is a complex holoenzyme that consists of

several individual enzymes, including PS1 or PS2, anterior pharynx defective 1 (Aph-1), nicastrin, and presenilin enhancer 2 (Pen-2), as demonstrated in Figure 6. The stoichiometry (proportions in which elements are combined) of the γ-secretase components is likely 1:1:1:1, but was also suggested the possibility that also larger multimers are formed or that additional proteins are incorporated into the complex. PS is a polytopic protein with nine TM domains, and is considered to possess the active site of the enzyme. The core of the catalytic site of PS consists of two highly conserved aspartate residues (Asp257 and Asp385 in human PS1) within TM6 and TM7. Nicastrin is an evolutionarily conserved type I integral membrane protein that is highly glycosylated. This protein has one TM and a large ectodomain, proposed to function as a gate keeper to the PS1 active site, restricting access of substrates to the complex. Nicastrin also functions as a substrate receptor and is important for the assembly process of the γ-secretase complex. Aph-1 has a seven TM structure with the C-terminal located in the cytoplasm. Pen-2 displays a hairpin-like structure with two TM domains and both termini located at the luminal side. The functions of Aph-1 and Pen-2 are not yet completely understood. Still, Aph-1 has been implicated in stabilization of PS1 and plays a significant role during assembly of the complex. Additionally, Pen-2 stabilizes the final complex and is involved in endoproteolysis of PS1 [13,20].

PS/γ-secretase cleaves with remarkable relaxed sequence specificity TM domains of several proteins, like APP, APLP-1, APLP-2, Notch 1, 2, 3 and 4, among others (reviewed in Wakabayashi and De Strooper, 2008 [13]). It is essential that the substrates have a type I conformation of the TM domain and a very short (<50 a.a.) extracellular ectodomain [28,29]. Bulky extracellular ectodomains greater than 200-300 a.a. residues prevent γ-secretase cleavage and are usually removed by membrane bound (metallo)-proteases or “sheddases” at the cell surface. This first cleavage can be triggered by ligand binding, as is the case for Notch, whereas for other substrates, e.g., APP, shedding is largely constitutive. γ-Secretase cleavage occurs at different positions in the membrane domain of its substrates, generating a series of small peptides, like Aβ or p3, and AICD (APP), Nβ and NICD (Notch), etc., which are secreted at the extracellular side of the membrane (reviewed in Wakabayashi and De Strooper, 2008 [13]).

Both PS proteins (PS1 and PS2) share approximately 63% homology with the highest similarity in the TM domains, where most of the familial AD-linked mutations are found (reviewed in Parent and Thinakaran, 2010 [30]). Both PS have been targets of intense study. Knockouts, knockins, and transgenic models have been used to study these proteins [9].

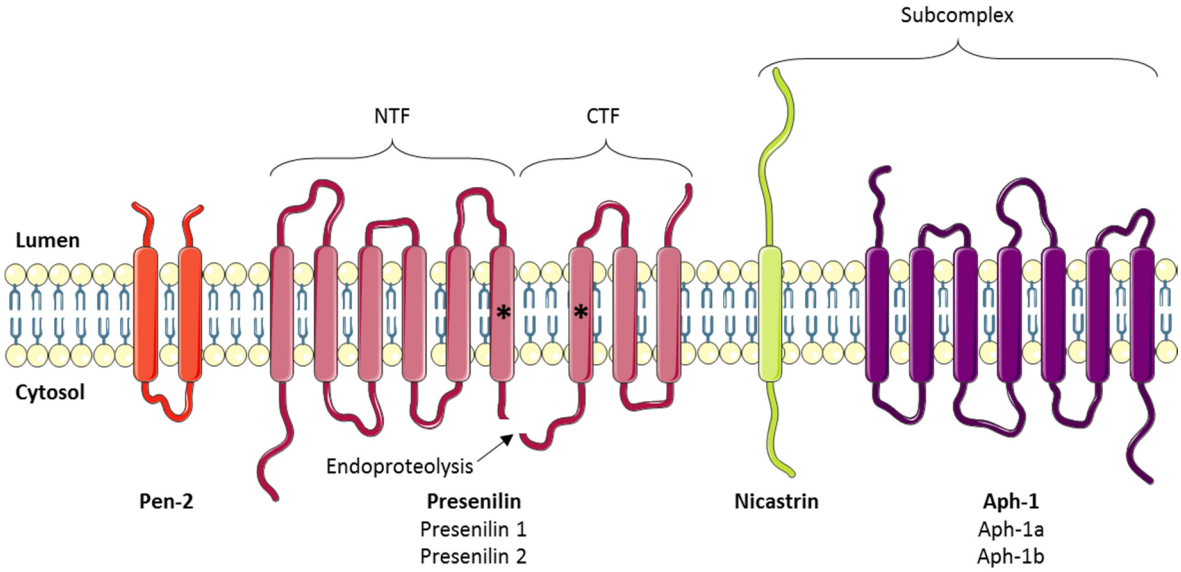

Figure 6: Scheme of the γ-secretase complex.
γ-Secretase is a highly hydrophobic complex composed of four integral membrane proteins: presenilin enhancer 2 (Pen-2), presenilin (presenilin 1 or presenilin 2), nicastrin, and anterior pharynx defective 1 (Aph-1). Presenilin 1 and presenilin 2, and Aph-1a and Aph-1b are encoded by different genes, and all subunits can combine to generate at least four different complexes. Alternative splicing of these genes adds further complexity. Presenilin provides the active site with two catalytic aspartates located in transmembrane (TM) domains 6 and 7 (indicated as stars). Nicastrin and Aph-1 first form a stable subcomplex, followed by incorporation of presenilin and Pen-2 in the early secretory compartment. Once all four components assemble, presenilin undergoes endoproteolysis by unknown "presenilinase" activity within the large intracellular loop between TM6 and TM7 (indicated by an arrow), and the amino-terminal fragment (NTF) and the carboxy-terminal fragment (CTF) remain noncovalently bound. Only fully assembled complexes reach the cell surface and endocytic compartments (adapted from [13]).

1.2.2. APP Functions

Despite all the findings with respect to APP and its homologues, its biological functions are still not fully understood, and will require further research in the future. It is clear that proteins from the APP family have redundant and partially overlapping functions, and their biological functions are not restricted to the nervous system. Several *in vitro* and *in vivo* studies suggest that APP, APLP1, and APLP2 are involved in the developing and adult nervous system, cell adhesion and migration, neurite outgrowth, neuronal survival and apoptosis, synaptogenesis, vesicular transport, neuronal migration, modulation of synaptic plasticity, axonal transport, and can act as modulators of insulin and glucose homeostasis. In particular, APP functions as a cell surface receptor and is involved in transcription regulation through protein-protein interactions (reviewed in Jacobsen and Iverfeldt, 2009 [20]).

1.2.3. APP Post-translational Modifications

The APP family proteins are post-translationally modified in several different ways. All family members undergo *N*-glycosylation within its extracellular domain. Both APP and APLP2 have been shown to be subject to *O*-glycosylation within its extracellular domain, sialylation, and CS GAG modification [20,24]. Some post-translational modification sites are conserved in all homologues, like the APP N^{467} *N*-glycosylation site. Whereas others sites are only conserved within the mammalian homologues, like the APP K^{695} sumoylation site [20]. *N*-glycosylation affects the processing of APLP1, once when it's blocked with tunicamycin additional APLP1 fragments are generated. However, the processing of APP and APLP2 was unaffected by the blocking of *N*-glycosylation [31]. In contrast, sialylation affects APP processing, since overexpression of sialyltransferase enhanced secretion of Aβ [32].

All APP family members have been shown to be phosphorylated, and some of the most studied phosphorylation sites are shown in Table 1. APP is a phosphoprotein that has several phosphorylatable a.a. residues in its intracellular and extracellular domains [20,24]. Among the intracellular domain sites that can be phosphorylated, Thr654, Ser655, and Thr668 (numbering for the APP695 isoform) have been shown to be phosphorylated in adult rat brain [33,34]. The Tyr653, Ser655, Thr668, Ser675, Tyr682, Thr686 and Tyr687 were found to be phosphorylated in post-mortem brain tissue of AD patients [35]. Phosphorylation at these sites has been described to impact APP cellular localization. In addition, Thr668 phosphorylated APP has been found to be enriched in endocytic compartments and to co-localize with BACE in AD brains [35].

Since these residues are located in specific protein interacting sites its phosphorylation may interfere with protein binding and thus interfere with APP and AICD functions. Additionally, some phosphorylation sites may affect the processing of APP [20]. Lee *et al.* (2003) reported that Aβ production was reduced in rat embryonic cortical neurons when treated with a cyclin-dependent kinase (CDK) 5 inhibitor, which reduced Thr668 phosphorylation, or when transfected with Thr668Ala mutant APP [35]. In another study, Thr668 phosphorylation of APP was reported to induce increased β-cleavage, but decreased γ-cleavage, resulting in decreased Aβ production [36]. Phosphorylation of APP at Tyr687 was suggested to regulate α-cleavage of APP since overexpression of the mutant Tyr687Ala decreased the level of the C83 fragment [37].

Alignment of the APP family members shows that the APP Thr668 phosphorylation site is conserved in all APP homologues: APLP1 (Thr624), APLP2 (Thr736), APPL (Thr855), and APL-1 (Thr660). Three other *in vivo* phosphorylated sites in APP, Tyr682, Thr686, and Tyr687 (which are part of the YENPTY motif), are also conserved in all APP homologues. Tyr653, another *in vivo* phosphorylated site in APP, is conserved in both mammalian homologues, but not in APPL or APL-1 (reviewed in Jacobsen and Iverfeldt, 2009 [20]).

Table 1: Some of phosphorylation sites of APP and its homologues, and the different enzymes that mediate the phosphorylation.

Phosphorylatable Amino Acid Residues	Protein Kinase	
Thr654 and Ser655 (APP)	CaMPK II [38]	*in vitro*
Ser655 (APP)	PKC [38]	*in vitro*
Thr668 (APP)	CDK1/CDC2 kinase [33]	in dividing cells, at the G2/M phase of the cell cycle
	JNK3 [39]	during neuronal differentiation
	CDK5 [40] and GSK-3β [41]	in post-mitotic neurons
	JNK1 and JNK2 [42]	in response to cellular stress
Thr736 (APLP2 763 isoform)	CDC2 kinase [43]	*in vitro*

Abbreviations: APLP, Amyloid Precursor-Like Protein; APP, Amyloid Precursor Protein; CaMPK, Calcium/Calmodulin-dependent Protein Kinase; CDC, Cell Division Cycle; CDK, Cyclin-Dependent Kinase; GSK, Glycogen Synthase Kinase; JNK, c-Jun N-terminal Kinase; PKC, Protein Kinase C; Ser, Serine; Thr, Threonine. Residue in bold type was the one addressed in this study.

APP phosphorylation has been shown to regulate intracellular signaling via adaptor proteins. Thr668 phosphorylation was shown to induce large conformational changes of the intracellular domain [44]. It was later shown that the peptidyl-, prolyl cis/trans isomerase Pin1 binds to Thr668-phosphorylated APP both *in vitro* and *in vivo* and thereby accelerates the production of the trans conformation of Pro669 [45]. This proline residue is conserved in APLP2 (Pro737) and APL-1 (Pro662), but not in APLP1 or APPL. It was further demonstrated that the Pin1-catalysed isomerization of APP regulated its processing, since overexpression or knockout of Pin1 reduced or increased the secretion of Aβ, respectively. It has further been shown that Pin1 knockout in mice resulted in age-dependent neuropathy [46].

1.3. Tau

Tau protein regulates MT assembly, dynamic behaviour, and spatial organization under physiological conditions [47,48]. Tau protein has been shown to regulate axonal transport of organelles, including mitochondria [49]. Proteins from the MAP family are present in several species, such as *C. elegans* [50,51], *Drosophila* [52,53], goldfish [54], bullfrog [55],

rodents [56,57], bovines [58,59], goat [60], monkeys [60], and human [61,62]. In human, MAPs are mainly present in neurons [63], although non-neuronal cells usually present trace amounts. For example, glial cells express Tau protein mainly in pathological conditions [64], and it is possible to detect Tau mRNA and proteins in several peripheral tissues like heart, lung, kidney, pancreas, testis, muscle, and fibroblasts [65–67].

The gene encoding human Tau protein MAPT is unique and located on chromosome 17q21.1 [68], spans approximately 150 kb, and contains 16 exons [69] (Figure 7). The exons 4A, 6 and 8 are specific to peripheral Tau protein, therefore are never present in any mRNA of human brain [58,60]. Tau is encoded by a single gene from which nine isoforms are produced through alternative splicing [70], six of which (range from 352 to 441 a.a. and an apparent molecular weight of 48–67 kDa) are the isoforms expressed in human central nervous system (CNS) [61,62,71].

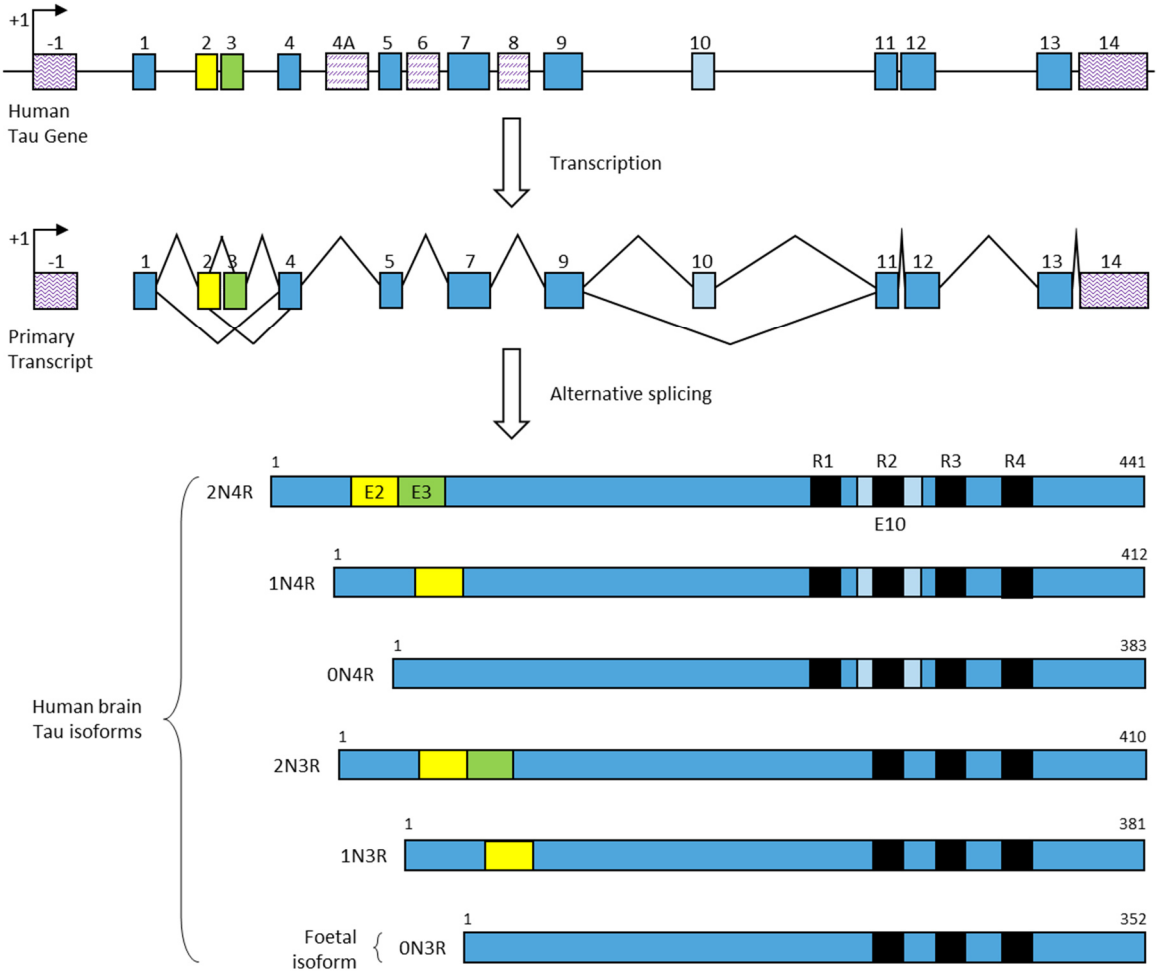

Figure 7: Schematic representation of the human Tau gene, the human Tau primary transcript and the six human central nervous system (CNS) Tau isoforms.
The human Tau gene is located over 100kb on chromosome 17q21.1. It contains 16 exons, with exon -1 being part of the promoter (upper panel). Tau primary transcript contains 13 exons, since exons 4A, 6 and 8 are not transcribed in human brain (middle panel). Exons -1 and 14 are transcribed but not translated. Exons 1, 4, 5, 7, 9, 11, 12, 13 are constitutive, and exons 2, 3, and 10 are alternatively spliced, giving rise to six different mRNAs, translated in six different CNS Tau isoforms (lower panel). These isoforms differ by the absence or presence of one or two 29 amino acids (a.a.) inserts encoded by exon 2 (yellow box) and 3 (green box) in the amino-terminal part, in combination with either three (R1, R3 and R4) or four (R1–R4) repeat-regions (black boxes) in the carboxy-terminal part. The fourth microtubule-binding domain is encoded by exon 10 (light blue box) (lower panel). The adult Tau isoforms include the longest 441-a.a. component (2+3+10+), the 410-a.a. component (2+3+10-), the 412-a.a. component (2+3-10+), the 381-a.a. component (2+3-10-) and the 383-a.a. component (2-3-10+). The shortest 352-a.a. isoform (2-3-10-) is found only in the foetal brain, and thus is referred as foetal Tau isoform (adapted from [72]).

Tau can be subdivided into four regions (Figure 8): i) an acidic region in the N-terminal part; ii) a proline-rich region; iii) a region responsible for binding with MTs (MT-binding domains); and iv) a C-terminal region [73]. There are two aspects that separate Tau isoforms, these are: the absence or presence of one or two inserts (29 or 58 a.a.) in the N-terminal part of the molecule; and the presence of either three or four repeat-regions in the C-terminal part (3R and 4R Tau), an outcome of alternative splicing of exon 10 [58,61,62,74]. There

is evidence that each of these isoforms may have particular biological roles, once they are differentially expressed during development. For example, the only Tau isoform present during foetal stages is the one characterized by the absence of N-terminal inserts and the presence of three C-terminal repeats, 3R Tau (exons 2, 3 and 10 are spliced out). Adult human CNS expresses equal amounts of 3R and 4R isoforms (with one or two N-terminal inserts and three or four C-terminal repeats). These findings demonstrate developmental regulation of exon 10 splicing [75,76]. Therefore, it is highly probable that Tau isoforms have specific functions related to the absence or presence of regions encoded by the cassette exons 2, 3 and 10. Moreover, the relative levels of six Tau isoforms expressed in adult human CNS (3R and 4R isoforms) differ between neurons in different brain regions. Granular cells of the dentate gyrus (hippocampal formation) don't express Tau mRNAs containing exon 10 (4R Tau), only 3R Tau [61,62]. Tau isoforms may be differentially distributed in neuronal subpopulations [72].

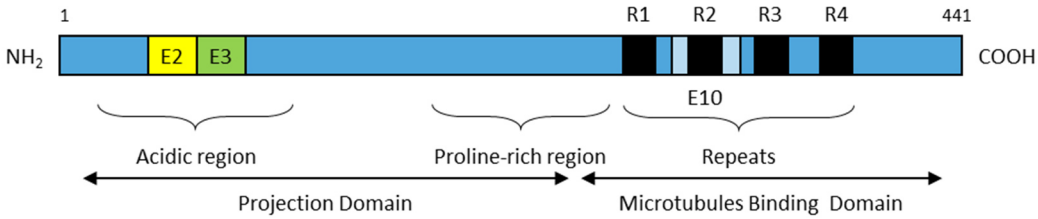

Figure 8: Schematic representation of the functional domains of the longest Tau isoform (2+3+10+). The projection domain, including an acidic and a proline-rich region, interacts with neural plasma membrane and cytoskeletal elements to determine spacings between microtubules in axons. The amino-terminal part is also involved in signal transduction pathways by interacting with proteins as phospholipase C-γ (PLC-γ) and Src-kinases. The carboxy-terminal part, referred to as microtubules binding domain, regulates the rate of microtubules polymerization and stabilization. It is also involved in the binding with functional proteins as protein phosphatase 2A (PP2A) or presenilin 1 (PS1) (adapted from [72]).

1.3.1. Tau Phosphorylation

The exons 9-12 of Tau gene encode four imperfect repeat domains (encompassing 31–32 residues) that mediate the interaction between Tau and tubulin [77]. Within neurons, Tau is predominantly found in axons [78] as a highly soluble phosphoprotein [79]. Tau contains 85 putative phosphorylation sites: 45 are serines, 35 are threonines and only 5 are tyrosines [72,80,81]. Most of these phosphorylation sites are on Ser-Pro and Thr-Pro motives [82]. Table 2 summarizes the four groups of protein kinases that can phosphorylate Tau: i) the Proline-Directed Protein Kinases (PDPKs) which phosphorylate Tau on serine or threonine residues that are followed by a proline residue; ii) the non-PDPK group; iii) protein kinases that phosphorylate Tau on serine or threonine residues followed or not by a proline; iv) and the tyrosine protein kinases (reviewed in Buée *et al.*, 2010 [83]).

Table 2: Most studied protein kinases involved in Tau phosphorylation (reviewed in [72,80]).

PDPK
• Cyclin-Dependent Kinases including CDC2, CDK1 and CDK5;
• MAPK;
• SAP Kinases.
Non-PDPK
• CaMPK II;
• CK1, CK2 and CK1δ;
• DYRK1A;
• MARK;
• Phosphorylase Kinase;
• PKA, PKB, PKC and PKN;
• Rho kinase;
• TTBK1 and TTBK2.
Kinases that phosphorylate on Serine or Threonine residues followed or not by a Proline
• AGC kinases, such as MSK1 (recognition motifs RXRXXS/T);
• GSK-3α and GSK-3β (recognition motifs SXXXS or SXXXD/E).
Tyrosine Protein Kinases
• Src kinases;
• c-Abl;
• c-Met.

Abbreviations: CaMPK, Calcium/Calmodulin-Dependent Protein Kinase; CDC, Cell Division Cycle; CDK, Cyclin-Dependent Kinase; CK, Casein Kinase; DYRK, Dual-Specificity Tyrosine Phosphorylation-Regulated Kinase; GSK, Glycogen Synthase Kinase; MAPK, Mitogen Activated Protein Kinase; MARK, Microtubule-Affinity Regulating Kinase; MSK, Mitogen- and Stress-Activated Protein Kinase; PDPK, Proline-Directed Protein Kinases; PK, Protein Kinase; SAP, Stress-Activated Protein; TTBK, Tau-Tubulin Kinase.

Tau binding affinity for MTs is regulated by the phosphorylation of serine and threonine residues [84,85]. It is believed that through this binding, Tau plays a major role in stabilizing MTs. When phosphorylated, Tau protein is not able to polymerize tubulin into MTs and do not stabilize the latter [86].

Tau's phosphorylation process is also developmentally regulated. During embryogenesis and early development, when only the shortest of the isoforms is expressed, Tau phosphorylation reaches high levels. By contrast, adult brain expresses six isoforms with relatively reduced phosphorylation levels compared with the foetal situation [87].

The different levels of Tau phosphorylation are a dynamic process that results from the activity of several specific kinases (Table 3) and phosphatases (Table 4) towards specific sites.

Table 3: Protein kinases involved in Tau phosphorylation and the respective phosphorylation sites (reviewed in [88]).

Protein Kinase	Phosphorylation Sites
PKA	Ser195, Ser198, Ser199, **Ser202**, **Thr205**, Thr212, Ser214, Thr217, Thr231, Ser324, Ser235, Ser258, Ser262, Ser356, Ser409, Ser412, Ser413, Ser416, Ser422, Ser435
PKB	Thr212, Ser214
PKC	Ser258, Ser293, Ser324, Ser352
PKN	Ser214, Ser258, Ser320, Ser352
RSK	Thr212, Ser214
MSK1	Ser214, Ser262, Ser305
SGK1	Ser214
p70S6K	Thr212, Ser214, Ser262
ROCK	Thr245, Ser262, Thr377, Ser409
p110 kinase	Ser262
CaMPK II	Ser214, Thr217, Thr231, Ser235, Ser262, Ser396, Ser404
AMPK	Thr231, Ser262, Ser396, Ser404
BRSK	Ser262
MARK	Thr17, Thr95, Ser113, Ser131, Thr149, Thr169, Ser184, Ser198, Ser208, Ser214, Ser237, Ser238, Ser262, Ser320, Ser324, Ser356
CK1	Ser241, Ser258, Ser262, Thr263, Ser285, Ser289, Ser305, Ser341, Ser352, Ser356, Thr361, Thr373, Thr386, Ser412, Ser416, Ser433, Ser435
TTBK1/2	Ser198, Ser199, **Ser202**, Ser208, Ser210, Ser422
CDK5	Thr181, Ser199, **Ser202**, **Thr205**, Thr212, Ser214, Thr217, Thr231, Ser235, Ser396, Ser404
MAPK	Ser46, Thr50, Thr153, Thr181, Ser199, **Ser202**, **Thr205**, Thr212, Thr217, Ser235, Ser396, Ser404, Ser422
JNK	Thr181, Ser199, **Ser202**, **Thr205**, Thr212, Thr217, Ser396, Ser404, Ser422
CDC2	Thr153, **Ser202**, **Thr205**, Thr212, Thr231, Ser235, Ser404
GSK-3β	Ser46, Thr50, Thr181, Ser184, Ser199, **Ser202**, **Thr205**, Thr212, Ser214, Thr217, Thr231
DYRK1A	Thr181, Ser199, **Ser202**, **Thr205**, Thr212, Thr217, Thr231, Ser396, Ser400, Ser404, Ser422

SAPK	Thr50, Thr69, Thr153, Thr181, Ser199, **Ser202**, **Thr205**, Thr212, Thr217, Ser235, Ser396, Ser404, Ser422
CK2	Thr39, Ser199, Ser396, Ser400

Abbreviations: AMPK, Adenosine Monophosphate-Activated Protein Kinase; BRSK, Brain-Selective Kinase; CaMPK, Calcium/Calmodulin-Dependent Protein Kinase; CDC, Cell Division Cycle; CDK, Cyclin-Dependent Kinase; CK, Casein Kinase; DYRK, Dual-Specificity Tyrosine Phosphorylation-Regulated Kinase; GSK, Glycogen Synthase Kinase; JNK, c-Jun N-terminal Kinase; MAPK, Mitogen Activated Protein Kinase; MARK, Microtubule-Affinity Regulating Kinase; MSK, Mitogen- and Stress-Activated Protein Kinase; p110 kinase, A 110 kDa Microtubule Affinity-Regulating Kinase; p70S6K, S6 Ribosomal Protein Kinase; PK, Protein Kinase; ROCK, Rho-Associated, Coiled-Coil-Containing Kinase; RSK, Ribosomal Protein S6 Kinase; SAPK, Stress-Activated Protein Kinase; Ser, Serine; SGK, Serum- and Glucocorticoid-Regulated Kinase; Thr, Threonine; TTBK, Tau-Tubulin Kinase. Residues in bold type were the ones addressed in this study.

Table 4: Protein phosphatases involved in Tau dephosphorylation and the respective dephosphorylation sites (reviewed in [88]).

Protein Phosphatase	Dephosphorylation Sites
PP1	Ser198, Ser199, **Ser202**, Thr212, Thr217, Ser262, Ser396, Ser404, Ser422
PP2A	Ser46, Ser198, Ser199, **Ser202**, Ser205, Thr217, Thr231, Ser262, Ser396, Ser404, Ser422
PP2B (calcineurin)	Ser46, Thr181, Ser199, **Ser202**, Thr217, Ser235, Ser262, Ser356, Ser396, Ser404, Ser422
PP5	Ser198, Ser199, **Ser202**, Thr231, Ser235, Ser262, Ser356, Ser396, Ser404, Ser422

Abbreviations: PP, Serine/Threonine Protein Phosphatase; Ser, Serine; Thr, Threonine. Residues in bold type were the ones addressed in this study.

In addition to being phosphorylated, Tau can be *O*-GlcNAcylated, nitrated, and ubiquitinated [89].

1.3.2. Tauopathies

Tauopathies are a class of neurodegenerative disorders, that include AD, and are characterized by the presence of aggregates of abnormally phosphorylated Tau in the CNS [89–93]. In tauopathies, the natively unfolded Tau protein forms intracellular fibrillar structures of aggregated, hyperphosphorylated, and ubiquitinated Tau, which are associated with synaptic and neuronal loss. Upon abnormal phosphorylation, Tau reduces its affinity for and dissociates from MTs [94–96]. In AD brains Tau accumulates as paired helical filaments (PHF) in the neuronal perikarya and processes [97,98]. It has been proposed that at

the single-cell level the defects start with a modification of Tau by phosphorylation, causing destabilization of MTs and consequently resulting in a "pre-tangle" stage [99]. After this stage, the destabilization of MTs leads to loss of dendritic MTs and synapses, plasma membrane degeneration, and finally cell death [100].

Occurrence of fibrillar Tau inclusions in tauopathies strongly supports a key role in the observed clinical symptoms and pathology. Interestingly, Tau is required for Aβ's toxicity both *in vitro* and *in vivo*. This was suggested by the resistance shown by primary cultured neurons from Tau knockout mice when exposed to Aβ [101] as well as by the rescuing premature mortality and preventing memory deficits observed in APP transgenic mice when crossed with Tau knockout mice [102]. This supports a central role of Tau in mediating Aβ toxicity in the early pathogenesis of AD [103].

1.4. Spermatogenesis

Spermatogenesis is a dynamic and multistep process of male germ cell proliferation and differentiation by which spermatozoa are produced from primordial germ cells (PGCs) [104]. This process in mammals is controlled by a complex system of paracrine and endocrine activity within a structurally well-organized tissue [105].

The formation of sperm begins with the embryonic PGCs migrating into the undifferentiated gonad as a response to soluble stem-cell factor. PGCs then differentiate into prospermatogonia and stay in a quiescent state within the testicular seminiferous tubules. At the onset of puberty, gonadotropic stimulation induces spermatogenesis (the meiotic divisions by which spermatogonia develop into sperm; Figure 9) followed by spermiogenesis (the differentiation of haploid round spermatids into flagellated sperm cells; Figure 10) [106]. The mammalian process of spermatogenesis comprises three phases of cellular events, which are: i) the proliferative phase (spermatogonia), in which diploid spermatogonial germ cells divide by mitosis producing new germ cells, to maintain the germ cell pool, and committed cells (primary spermatocytes); ii) the meiotic phase (spermatocyte), in which primary spermatocytes undergo meiosis, reducing both the chromosome number and amount of deoxyribonucleic acid (DNA), and producing haploid daughter spermatids; iii) spermatid phase (spermiogenesis), in which spermatids undergo huge morphological and biochemical changes differentiating into mature sperm cells (spermatozoa) [105,107,108]. Methylation of imprinted genes occurs between the spermatogonial and the spermatocyte phases. During the last stage of spermiogenesis, the nucleus flattens and condenses, as nonhistone basic proteins such as protamines displace the typical histones that associate with nuclear DNA, transcriptional activity in the spermatid is silenced, and nucleosomal structure is lost. At the same time, the remaining

cytoplasm is jettisoned as a "cytoplasmic droplet" [106]. The resulting sperm cells ultimately separate from the adherent Sertoli cells and, once released into the lumen of the seminiferous tubule, passively migrate to the epididymis for further maturation [105]. These maturation processes are required for fully functional spermatozoa (capable of motility and fertilization). Sperm cells are stored until they are ejaculated from the male reproductive tract. By the last stages of spermiogenesis, when sperm are released into the lumen of the seminiferous tubule, their ribosomes are nearly absent, and their endoplasmic reticulum has been lost from the cytoplasm. Given that they have no machinery to produce proteins, all of the factors that sperm will require for ascending the female reproductive tract must either be synthesized in advance and stored or must be provided from the outside – for example, by the cells of the cauda epididymis [106].

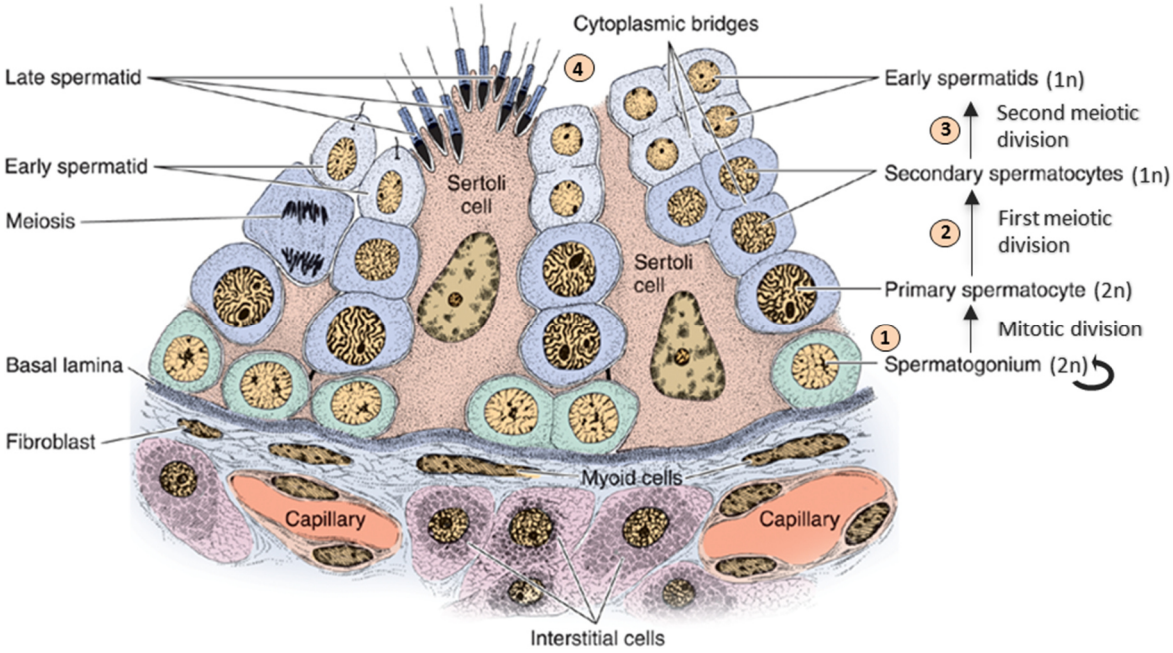

Figure 9: Schematic representation of part of a seminiferous tubule with its surrounding cells.
The seminiferous epithelium is formed by two cell populations: the cells of the spermatogenic lineage and the Sertoli cells (supporting cells). Surrounding the seminiferous tubule there is a layer of myoid cells, as well as connective tissue, blood vessels and interstitial cells. **1)** Nearest the basement membrane are spermatogonia (diploid cells, 2n), which divide by mitosis to produce more germ cells and cells committed to meiosis (primary spermatocyte). **2)** Primary spermatocytes replicate their deoxyribonucleic acid (DNA) shortly after they form and before meiosis begins, resulting in 2n 4d primary spermatocytes. Haploid secondary spermatocytes (1n 2d) are the result of the first meiotic division. **3)** The secondary spermatocytes divide quickly again in the second meiotic division (no DNA replication precedes meiosis II) to become haploid spermatids (1n 1d). **4)** These latter cells differentiate as sperm cells (spermiogenesis) that will be motile. These last events take place near the apical ends of the Sertoli cells at the lumen of the seminiferous tubules. Usually all stages of this process (spermatogenesis) do not take place within one small area of tubule as shown schematically here (adapted from [109,110]).

Central to this system are the Sertoli cells (also called supporting or sustentacular cells), which in response to endocrine and paracrine stimulation by factors such as follicle stimulating hormone (FSH) and luteinizing hormone (LH)-stimulated testosterone provide

both paracrine regulation and structural support to the differentiating germ cells. Sertoli cells adhere to germ cells to form a highly complex epithelium, in which various tight and adherent junctions form the blood-testis-barrier and regulate germ cell location and movement toward the lumen during differentiation. As secretory cells, Sertoli cells produce growth and anti-apoptotic factors such as Steel (kit-ligand), as well as seminiferous tubule fluid with its proteins and other constituents. Sertoli cells also have the function of phagocytosis of the degenerating germ cells and the residual body (excess cytoplasm) that remains from the released sperm. These supporting cells are essential to control the diverse environmental niches in which male germ cells develop [105,111]. Leydig cells (interstitial cells), other specialized cell type that also support spermatogenesis, are in the interstitial tissue of the testis, and are uniquely positioned to provide testosterone to the seminiferous tubules to drive spermatogenesis [108].

Sperm morphogenesis is accomplished inside the testis, but testicular sperm remain physiologically “immature”. During transit, mammalian sperm undergo epididymal maturation, but they remain unable to fertilize oocytes. Capacitation, the final preparatory step, occurs only when sperm have resided in the female genital tract for some time. This ill-defined process appears to be necessary for sperm to undergo a further morphological and physiological transition, the acrosome reaction, once they encounter the zona pellucida of the egg. The acrosome, a caplike structure covering the anterior portion of the sperm nucleus, contains multiple hydrolytic enzymes that are released by exocytosis prior to fertilization. Simultaneously, extensive changes occur in all sperm compartments (head and flagellum, membrane, cytosol, and cytoskeleton). Factors originating from epididymal fluid and seminal plasma are lost or redistributed, membrane lipids and proteins are reorganized, and complex signal-transduction mechanisms are initiated [106].

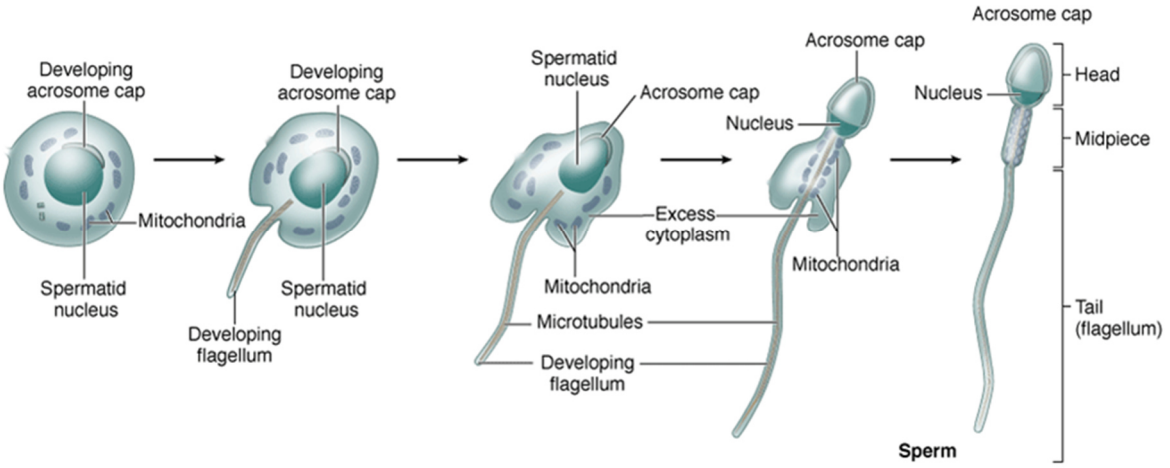

Figure 10: Spermiogenesis diagram.
Major morphological changes occur within spermatids as they undergo the differentiation process and become highly specialized sperm cells. These changes involve flattening of the nucleus, formation of an acrosome which resembles a large lysosome, growth of a flagellum (tail) from the basal body, reorganization of the mitochondria in the midpiece region, and shedding of unneeded cytoplasm as a residual body (taken from [110]).

Humans vs. Rodents

Like in AD research, rodent (rat, mouse and hamster) models are also used in studies of gametogenesis. Despite both being mammals, there are several differences between humans and rodents spermatogenesis and testes. In Table 5 some characteristics that differentiate between human and the species addressed in this study (rat and mouse) are indicated. Spermatogonia, which constitute the first phase, are the most immature spermatogenic cells and reside on the basement membrane of the seminiferous epithelium. These cells are classified into three types in humans and four types in rodent, based on the appearance of the nuclei (presence and distribution of heterochromatin) [107,111]. The human types are: type A dark spermatogonia; type A pale spermatogonia; and type B spermatogonia [107]. The rodent types are: undifferentiated type A spermatogonia (A single, A paired, A aligned); differentiated type A spermatogonia (A_1, A_2, A_3, A_4); intermediate spermatogonia (In); and type B spermatogonia (B) (Table 5). However, presently, it is not possible to identify spermatogonial germ cells by routine microscopy, only by electron microscopy [111].

Table 5: Characteristics that differentiate spermatogenesis and testes of humans and rodents, which are constant and specific in each species.

	Humans	Rodents	
		Rat	Mouse
Number of cycles of the seminiferous epithelium	4.6 [107]	4.5 [111]	
Cycle lengths	16 days [107]	12.9 days [112]	8.6-8.9 days [111]
Duration to complete the spermatogenesis	74 days [107]	58 days	39-40 days [111]
Spermatogonial generations [111]	2 (A_{pale}, B) [c]	6 (A_{1-4}, In, B) [c]	6 (A_{1-4}, In, B) [c]
Meiotic index [a] [111]	1.3 (68%) [d]	3.4 (15%) [d]	2.3-3.1 (23-43%) [d]
Overall rate of spermatogenesis [b] [111]	3.2 (80%) [d]	97 (62%) [d]	44-84 (67-83%) [d]
Sperm cell head (the black areas represent portions of the nucleus covered by the acrosome)			
Layers of peritubular myoid cells [113]	multiple (five till seven)	one	
Other features [113]	higher proportions of testis occupied by nongerminal components such as tunic, interstitium, tubule boundary tissue and Sertoli cells	higher proportions of parenchyma, seminiferous tubules, seminiferous epithelium and germinal cells in the rat testis	

[a] Meiotic Index: Number of spermatids formed per each primary spermatocyte.
[b] Overall Rate of Spermatogenesis: Number of spermatids formed per each differentiated type A_1 spermatogonia.
[c] Type A spermatogonia (A); intermediate spermatogonia (In); and type B spermatogonia (B).
[d] Number in parentheses show the percentage of germ cell loss (apoptosis) based on the theoretical yield.

Germ cell loss (apoptosis) occurs normally during spermatogenesis in all mammals, and play a critical role in determining total sperm output. Significant germ cell loss occurs during the spermatogonial phase, called “density-dependent regulation”. One explanation is that the degeneration is a homeostatic mechanism to limit germ cells to the number that

can be supported by available Sertoli cells. Apoptosis is also frequent during meiosis (Table 5), especially in humans, and is probably related to chromosomal damage. In addition to apoptosis, missing generations of spermatocytes and spermatids in the seminiferous epithelium also contribute to the low efficiency of human spermatogenesis. Thus, humans are less efficient at sperm production than rodents. In conclusion, the greatest influences on germ cell production are the capacity for mitosis, and the number of generations of spermatogonial divisions, which will determine, at least in part, the number of cells that enter meiosis [111].

1.5. AD-related Proteins and Fertility

Infertility is described as "the inability of a couple to conceive despite trying for a year" [114]. It affects about 10 to 15% of the reproductive-age population [104,115], with approximately equal contributions from both genders [104]. The causes of male and female infertility are multifactorial [104,114], with several nutritional, behavioural, environmental and genetic factors affecting fertility [104]. Genetic abnormalities contribute to infertility with estimates reaching 50%, and just a small part is described. Infertility diagnoses are very descriptive and reflect the lack of understanding of the many and varied factors that regulate male and female gamete production, maturation, and function [114].

Even with growing knowledge of the physiology of male and female reproduction and the availability of new diagnostic tools, the pathogenesis of testicular [116] and premature ovarian insufficiency [117] remain undefined for the majority of cases and this is denoted as "idiopathic infertility". Idiopathic infertility is likely to have a genetic origin because the number of genes and proteins involved in gametogenesis is around thousands and only a small fraction of them have been identified and screened in infertile men and women [116].

Similar to AD research, knockout models are also used in studies of gametogenesis, especially mouse models. Knowledge obtained from these models has helped elucidate both intrinsic and acquired infertility, and the findings seem to be applicable to humans [106].

1.5.1. APP and Fertility

Supporting the hypothesis that APP is fertility-related are the findings using the double APP and APLP2 knockout mice. Contrary to APP knockout mice and APLP2 knockout mice (that are viable, normal, healthy and fertile [118,119]), the double APP and APLP2 knockout mice show high levels of mortality within the first week after birth (80%), and the surviving animals mate poorly, despite apparent normal ovarian and testicular development [120]. These findings suggest that these two proteins, that can substitute for

each other functionally, are required for early postnatal development and may be involved in gametogenesis [120].

APP's three major isoforms in mammals (APP695, APP751 and APP770) are present in mouse oocytes, pre-implantation embryos, and post-implantation embryonic stages to the late embryonic period [121]. In rat testis, mRNAs encode APP751 and APP770 isoforms (APP isoforms KPI-positive) [122]. Shoji and Kawarabayashi (1990) described the presence of native APP in acrosomes and in growing flagella, and suggested that APP appears in the head and tail formation phase in spermatids [122]. Beer *et al.* (1995) demonstrated that APP is highly expressed in follicle cells (ovary) and in soma and processes of Sertoli cells (testis), and at low levels in germ cells (testis) [123]. Supporting the Shoji and Kawarabayashi (1990) findings is the study from the da Cruz e Silva group, which describes distinct distributions of the APP family members in human sperm. This study was performed using a battery of antibodies that detect APP-specific epitopes, or epitopes common with other APP family members, showing that in rat testis 47% of the mRNA is APP770, 20% is APP751, and 20% is L-APP752. Results also show that in human sperm, the tail main piece mainly expresses full-length APP KPI-positive, the mid-piece mainly expresses APLP2 variants KPI-positive, the equatorial region of the spermhead is likely to contain mainly KPI-containing APLP2 variants, and the surface of the entire spermatozoon, with particular abundance on the head, contain plasma membrane APP and/or APLPs (Figure 11). According to the authors of this study, the presence of APP family members on the surface of the spermatozoa strongly suggest that these proteins may have a very important role in the sperm interactions with the matrix or the oocyte, and in other sperm-specific functions [124].

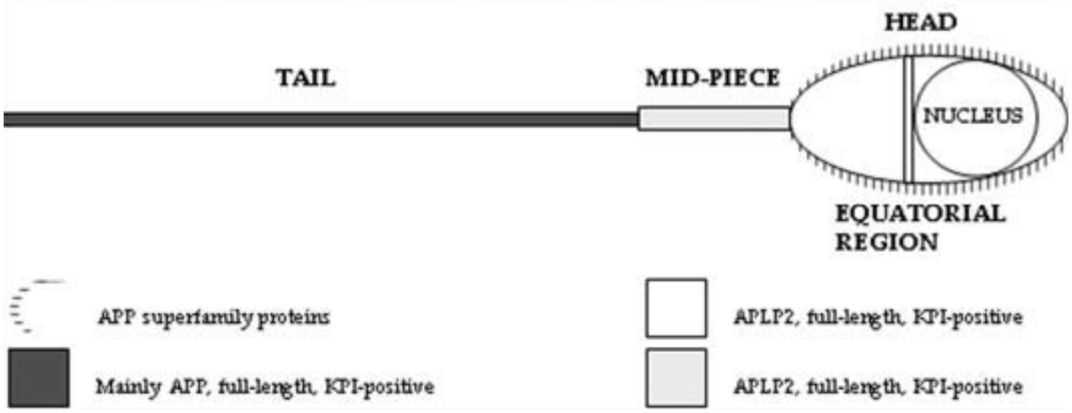

Figure 11: Schematic representation of the amyloid precursor protein (APP) family members expression in the human sperm.
Abbreviations: APLP, Amyloid Precursor-Like Protein; APP, Amyloid Precursor Protein; KPI, Kunitz Protease Inhibitor Domain (taken from [124]).

1.5.2. Tau and Fertility

Despite the fact that Tau knockout mice shown no overt phenotype or malformations [125–127] (reviewed in Ke *et al.*, 2012 [103]) and only when aged, did they develop behavioural impairments and motor deficits [128,129] (reviewed in Ke *et al.*, 2012 [103]), there is evidence that this protein may be involved in spermatogenesis. Contrary to what was thought for a long time, Tau's expression is not limited to the nervous system. Ashman *et al.* (1992) identified this protein in rat and bovine testis [130]. Through immunohistochemistry (IHC), Tau was observed, in bull testis, in the spermatid manchette, a transient, cross-linked MT network of unknown function. As spermatid elongation begins, the manchette forms a sheath around the posterior aspect of the nucleus, but, by the completion of nuclear condensation, the manchette is largely disassembled. Tau immunoreactivity was also observed in late stage I spermatids prior to manchette formation. These findings suggest that Tau not only plays a structural role in the manchette, but may also have a function in manchette assembly [130]. Recently, Inoue and colleagues (2014) showed the expression of Tau and its phosphorylation in testes of mice at 12 weeks of age. This study revealed, through IHC, that Tau phosphorylation was strongly detected in spermatocytes during meiosis, while the expression of acetylated tubulin was inversely weakened during the same stage. According to the authors, these results suggest that Tau phosphorylation contributes to spermatogenesis, particularly in meiosis [73].

1.5.3. Other AD-related proteins and Fertility

As previously described, the three ADAM proteins that can act as α-secretase and participate in the nonamyloidogenic proteolytic processing pathway of APP are ADAM9, ADAM10 and ADAM17 proteins. Results from these three proteins single knockout mice do not show that they are fertility-related. ADAM9 knockout mice are viable and show no apparent abnormalities. This knockout also does not show aberrant APP processing, indicating functional compensation by or redundancy with other proteases. ADAM17 knockout models are lethal embryonically and show little similarity to Notch knockouts. ADAM10 deficient mice are also lethal embryonically and die early in embryogenesis showing major defects in development of the CNS and the vascular system with similar histological abnormalities as observed in Notch deficiency induced in mice. Conditional knockout experiments of ADAM10 in mice have demonstrated a key role in the formation of the brain cortex with aberrant neuronal differentiation in the null mice [131].

BACE1 and BACE2 are two proteins that can act as β-secretase in the amyloidogenic pathway, as mentioned before. Like ADAM proteins, which can act as α-secretase, BACE proteins apparently are not fertility-related. BACE1 [132,133] and BACE2 [133] single knockout mice are viable, healthy and fertile with no changes in morbidity. They are also normal in terms of gross morphology and anatomy, tissue histology, haematology and clinical

chemistry. Double (BACE1 and BACE2) knockout mice despite showing ~60% of neonatal mortality, revealed that surviving animals were fertile, and a detailed pathological examination do not reveal any abnormality [133].

The PS proteins might be also involved in gametogenesis. Supporting this idea are findings that the *C. elegans* TM sperm protein spe-4, homologue of PS, is involved in trafficking of proteins during sperm differentiation, suggesting a role for PS1 in protein trafficking and in sperm morphogenesis [134], but further studies are needed in this regard. Additionally, in neonatal mouse testis, it was reported that PS1 was present in both spermatogonia and Sertoli cells. This suggests a potential role for this protein through Notch signalling in the regulation of the fate of spermatogonial stem cells during the process of spermatogenesis [135]. PS1 knockout mice [136] and double PS1 and PS2 knockout mice [137] die early in embryogenesis, due to disturbances in somitogenesis. This suggests that the PS proteins play an important role in directing the development of the axial skeleton [136]. To overcome this issue, conditional knockouts were developed, in which the loss of the gene was limited to the postnatal stage [9]. However, to date, it was not reported the development of a PS1-null testis mice for the study of this protein in this tissue.

In contrast, PS2 knockout mice are viable and fertile, and develop only mild pulmonary fibrosis and haemorrhage with age [137].

2. Objectives

APP and Tau have been the target of intense study, since they are related to the histopathological hallmarks of AD, a severe neurodegenerative disorder. However, their biological functions are still not fully clear, especially in peripheral tissues.

The general aim of this research was to expand the knowledge of APP and Tau, and more specifically to study the expression of these two proteins in mouse and rat testis, contributing to a better characterization of spermatogenesis. Thus, the specific objectives are to:

- Determine and characterize the expression of APP and phosphorylated APP in testis;
- Determine and characterize the expression of Tau and phosphorylated Tau in testis;
- Determine if APP and Tau could potentially be involved in spermatogenesis;
- Determine the profiles for APP in testis with ageing.

3. Materials and Methods

3.1. Animals

Male C57BL/6 mice with a range of age between 2 and 15 months, and male Wistar Han rats with a range of age between 5 and 29 months were used. All animals were anesthetized with pentobarbital (30 mg/kg) via intramuscular injection in the lower right abdominal quadrant and transcardialy perfused with 0.9% saline solution before being used for tissue collection. After surgical removal of a testicle, the animals were transcardialy perfused with 4% paraformaldehyde fixative and the other testicle was removed surgically. This procedure was carried out at the University of Minho (Braga, Portugal), under the supervising of Professor Doctor João Carlos Sousa.

All experiments were conducted in accordance with the Portuguese national authority for animal experimentation, Direcção Geral de Veterinária (ID: DGV9457). Animals were kept and handled in accordance with the guidelines for the care and handling of laboratory animals in the Directive 2010/63/EU of the European Parliament and of the Council. Efforts were made to minimize the number of animals used and their suffering.

3.2. Antibodies

Antibodies belong to the class of serum proteins known as immunoglobulins (Ig) that are present in the blood of immunized animals. There are five major classes of antibodies found in the blood of higher vertebrates: IgG, IgA, IgM, IgD, and IgE (listed in order of decreasing quantity found in plasma or serum) [138,139]. IgG is the most common and a frequently used antibody for laboratorial techniques. The IgG molecule is composed of two light chains and two heavy chains linked by disulphide bonds and noncovalent interactions to form a Y-shaped structure. The terminal regions of each arm vary in a.a. sequence and are known as variable domains. This variability in a.a. content provides specificity for a particular epitope and enables the antibody to bind specifically to the antigen against which it was raised [138].

Antibodies are the pivotal reagent in many laboratorial techniques. There are two types of antibodies: i) the monoclonal antibodies, that are a homogeneous population of Ig directed against a single epitope; ii) and the polyclonal antibodies, that are a heterogeneous mixture of antibodies directed against various epitopes of the same antigen [140]. Table 6 is a summary of the different antibodies used in this study.

Table 6: Summary of the primary antibodies used for detection of the target proteins in the different assays.

Antibody	Antibody type	Target Epitope	Dilution
Anti-APP, clone 22C11 (Chemicon)	Mouse monoclonal	a.a. 66-81 of APP (N-terminal), recognizing all three isoforms of APP (APP695, 751, 770), sAPP (α and β), and APLP2	IHC 1:20 IB 1:250
Anti-APP, PAD CT695 (Invitrogen)	Rabbit polyclonal	reacts with full-length and N-terminal truncated forms of APP, C-terminal membrane-anchored fragment of APP that remains after α- or β-secretase cleavage (CTF)	IHC 1:100 IB 1:500
Anti-Phospho-APP (Thr668) (Cell Signaling)	Rabbit polyclonal	detects different isoforms of endogenous APP only when phosphorylated at Thr668 (in the APP695 isoform) or the corresponding position on other isoforms	IHC 1:400 IB 1:1000
Anti-Tau, clone Tau-5 (Chemicon)	Mouse monoclonal	a.a. 210-241 of Tau, recognizing phosphorylated and non-phosphorylated isoforms of Tau (total-Tau)	IHC 1:200 IB 1:750
Anti-Phospho-PHF-Tau (pSer202+Thr205), clone AT8 (Thermo Scientific)	Mouse monoclonal	recognizes PHF Tau phosphorylation at Ser202 and Thr205	IHC 1:100 IB 1:500
Anti-PP1α (CBC2C) [141]	Rabbit polyclonal	reacts with PP1α	IHC 1:250
Anti-PP1γ (CBC3C) [141]	Rabbit polyclonal	detects both PP1γ isoforms, PP1γ1 and PP1γ2	IHC 1:500
Anti-γ-Tubulin (GeneTex)	Rabbit polyclonal	a.a. 1-184 of γ-Tubulin, detecting γ-Tubulin	IHC 1:500
Anti-β-Tubulin, clone 2-28-33 (Invitrogen)	Mouse monoclonal	reacts with β-Tubulin	IB 1:1000

Abbreviations: a.a., amino acids; APP, Amyloid Precursor Protein; C-terminal, Carboxy-terminal; CTF, Carboxy-Terminal Fragment; IB, Immunoblotting; IHC, Immunohistochemistry; N-terminal, amino-terminal; PAD, Polyclonal Antibody Designation; PHF, Paired Helical Filament; PP, Serine/Threonine Protein Phosphatase; sAPP, soluble Amyloid Precursor Protein; Ser, Serine; Thr, Threonine.

3.3. Immunohistochemistry

IHC is a technique for identifying antigens (cellular or tissue constituents) through antigen-antibody interactions. The site of antibody binding can be identified either by direct labelling of the antibody (the primary antibody is conjugated directly to the label), or by a secondary labelling method. In the latter a labelled secondary antibody directed against the immunoglobulin of the animal species in which the primary antibody was raised visualizes an unlabelled primary antibody. The secondary labelling method is more sensitive than the direct technique, once multiple secondary antibodies may react with different antigenic sites on the primary antibody, thus increasing the signal amplification. Another advantage is the versatility offered for this technique, once the same labelled secondary antibody can be used with a variety of primary antibodies raised from the same animal species. The conjugate of a labelled antibody, primary or secondary, may be either an enzyme or, more commonly, a fluorochrome [138].

Ensuring preservation of tissue architecture and cell morphology is a very important requirement for all routine histological and cytological research, and is done by adequate and appropriate fixation. There are a great variety of fixatives, and the choice will depend on the individual laboratory. To achieve consistent demonstration of tissue antigens a quick fixation of thin slices of tissue is essential. Delayed or poor fixation may cause loss of antigenicity or diffusion of antigens into the surrounding tissue. Following fixation, most material is routinely processed to paraffin wax to facilitate section cutting. The chemical processes involved in fixation and paraffin processing can mask antigens. Intermolecular and intramolecular cross-linkages are formed with certain structural proteins in these processes, and are responsible for the masking of the tissue antigens. This adverse effect has been thought to be the result of the formation of methylene bridges between reactive sites on tissue proteins. These reactive sites include primary amines, amide groups, thiols, alcoholic hydroxyl groups, and cyclic aromatic rings. The degree of masking of the antigenic sites depends upon the length of time in fixative, fixative concentration, temperature, and availability of other nearby proteins able to undergo cross-linkage. Some of the most common manual methods for antigen unmasking include: microwave oven irradiation, proteolytic enzyme digestion, combined microwave oven irradiation and proteolytic enzyme digestion, pressure cooker heating, autoclave heating, water bath heating, and steamer heating [138]. In the particular case of immunofluorescence, an antigen retrieval technique can be used to enhance intensity and reduce autofluorescence [142].

Another important step is the blocking one. The blocking buffer has as the main function to reduce background and unspecific staining. The ideal blocking buffer will bind to all potential sites of non-specific interaction (reactive sites). This will improve the sensitivity of the assay by improving the signal:noise ratio and eliminating background altogether without altering or obscuring the epitope for antibody binding. There are several

blocking buffers, once no single protein or mixture of proteins works best for all IHC experiments. The blocking buffer choice will depend on the specific antibodies and detection system that will be used. The universal blocking buffer has normal serum, protein solutions, and a buffer, usually Phosphate Buffered Saline (PBS). Foetal Bovine Serum (FBS) is a common blocking reagent, because the serum carries antibodies that bind to reactive sites and therefore prevents non-specific binding of the secondary antibodies used in the assay. Besides serum, concentrated protein buffers made with gelatine, non-fat dry milk or 0.1 to 5% w/v Bovine Serum Albumin (BSA) are often used to coat all proteins in the sample, working as blocking and stabilizer reagent. This approach basically forces primary antibodies to out-compete the blocking protein for binding to cognate ligands while reducing non-specific binding. This is based on the principle that antibodies have no greater binding affinity for non-specific epitopes than do the buffer proteins. To detect intracellular antigens, the blocking buffer is not complete without a penetration enhancer reagent, like Triton X-100. This detergent is one of the most popular reagents for increasing the cell permeability and so improving antibody penetration, given that it partially dissolves the cell membranes. It is recommended, for best results, that the blocking buffer must be made fresh prior to use and stored at 4°C [138,143].

Fluorescent IHC (Paraffin-Embedded Tissue) Protocol

Mouse testes were removed surgically, fixed with 4% paraformaldehyde fixative, embedded in paraffin wax and sectioned using a microtome. Cross-sections (4 μm) were deparaffinised in xylene, hydrated in graduated ethanol (100% for 10 minutes, 90% and 80% for 5 minutes, and 70% for 10 minutes) and in running tap water for 10 minutes. Heat-mediated antigen retrieval was performed using 0.01 M citrate buffer (pH 6.0; pre-warmed), and a microwave oven on high power (800 W) for 15 minutes. After cooling, sections were placed in a dark humid chamber and incubated with blocking buffer, which contain 5% w/v BSA, 4% v/v FBS, and 0.1% v/v Triton X-100 in PBS 1x, at room temperature for 1 hour. Then they were incubated with primary antibodies diluted in blocking buffer (for dilutions of primary antibodies see Table 6) at 4°C overnight, and then washed three times with PBS 1x. Immunoreactive elements were visualized with the appropriate secondary antibody labelled with fluorophore (anti-mouse, anti-rabbit; diluted 1:500 in blocking buffer) (Table 7) by treating at room temperature for 2 hours, and then washed three times with PBS 1x. Nuclei were counterstained with Hoechst 33342 (Invitrogen; diluted 1:3000) for 5 minutes, and then washed three times with PBS 1x. The slides were mounted and coverslipped using a temporary mount of 50% of glycerol.

The multiple staining IHC, for detection of two or more targets on one section, was performed as a simultaneous staining. The only difference from the traditional method described above is that the two primary antibodies raised in different host species were

applied simultaneously. Therefore, the primary antibodies mixture can be visualized using a system based on anti-mouse and anti-rabbit secondary antibodies labelled with different fluorochromes (Table 7), allowing the distinction between primary antibodies. This simultaneous staining method is less time-consuming and there is no signal loss with the washes steps than the sequential method, since primary and secondary antibodies can be mixed together in two incubation steps. Though, it requires avoiding all cross-reactivity [144]. The combination used was APP clone 22C11 with APP CT695 (for dilutions see Table 6).

Stained images were obtained with an IX81 Motorized Inverted Microscope (Olympus Corporation, Hamburg, Germany) with an LCPlanFl 20x/0.40 objective lens, and analysed with AnalySIS 3.2 Soft Imaging System GmbH software attached to the IX81.

The pH of prepared solutions was taken into account, for the correct performance of the technique, which had to be adjusted. Negative controls were utilized to assess the specificity of the immunostaining. In the negative control the primary antibody and/or secondary antibody were replaced by PBS 1x.

Table 7: Summary of the secondary antibodies used for detection of the various primary antibodies used in immunohistochemistry.

Antibody	Excitation maximum (nm)	Emission maximum (nm)	Observed colour
Alexa Fluor 594 goat anti-mouse IgG (H+L) (Invitrogen)	590	617	Red
Alexa Fluor 594 goat anti-rabbit IgG (H+L) (Invitrogen)	590	617	Red
Alexa Fluor 488 goat anti-rabbit IgG (H+L) (Invitrogen)	495	519	Green

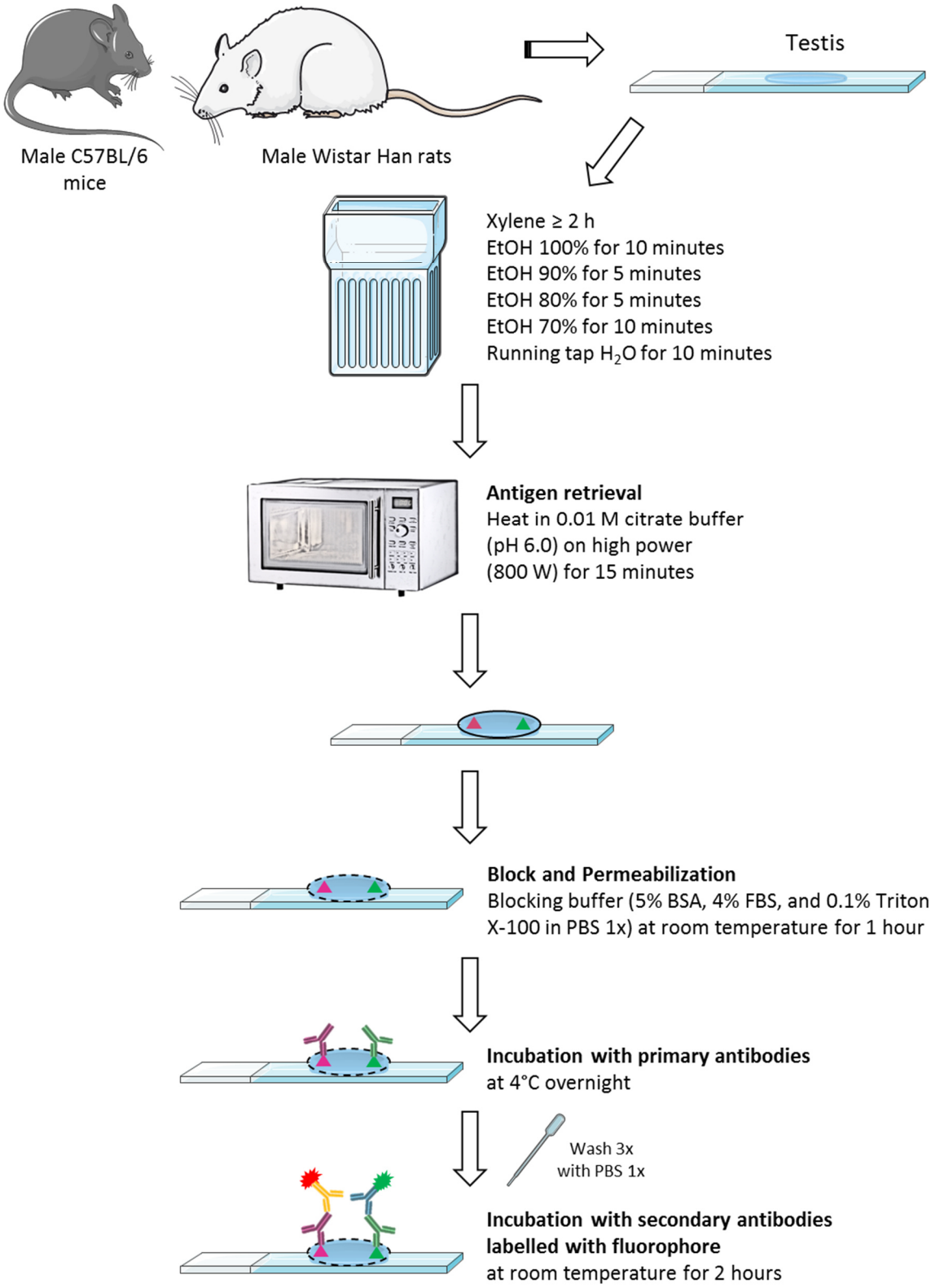

Figure 12: Schematic representation of the fluorescent immunohistochemistry protocol performed in this study, using paraffin-embedded tissue.
Abbreviation: BSA, Bovine Serum Albumin; EtOH, Ethanol; FBS, Foetal Bovine Serum; PBS, Phosphate Buffered Saline.

3.4. Western Blot Analysis

Western blot technique is an analytical method that allows the separation and identification of specific proteins from a complex mixture of proteins extracted from cells or tissues. This technique uses three steps to accomplish this task: i) a mixture of proteins is separated by size (molecular weight), through gel electrophoresis; ii) transfer to a solid support (membrane) producing a band for each protein; and iii) marking target protein, by incubating the membrane, using a proper primary (specific to the protein of interest) and secondary antibody to visualize (immunoblotting). The unbound antibody is washed off leaving only the bound antibody to the protein of interest. The bound antibodies are then detected by developing the film. As the antibodies only bind to the protein of interest, only one band should be visible. The thickness of the band corresponds to the amount of protein present; thus doing a standard can indicate the amount of protein present [145].

After extracting the proteins from the samples, it is important to determine the extract's concentration. This allows to ensure that the samples are being compared on an equivalent basis. Protein concentration is often measured using the bicinchoninic acid (BCA) method, described below. Using the protein concentration allows to measure the mass of the protein (50 μg) that is being loaded into each well. After determining the appropriate volume of the sample, it is diluted into a loading buffer, which contains glycerol that gives density to the samples and so these sink easily into the wells of the gel. A tracking dye (bromophenol blue) is also present in the loading buffer allowing to see how far the separation has progressed. After being diluted into a loading buffer containing Sodium Dodecyl Sulphate (SDS) and a reducing agent (β-mercaptoethanol), the sample is boiled in order to denature the higher order structure, while retaining sulphide bridges. Denaturing the high structure ensures that the negative charge of a.a. is not neutralized, enabling the protein to move in the electric field applied during electrotransfer [145].

Western blot gel electrophoresis uses two different types of agarose gel: stacking and resolving gel. The higher, stacking gel is slightly acidic (pH 6.8) and has a lower acrylamide concentration making a non-restrictive porous gel, which separates protein poorly but allows them to form thin, sharply defined bands. The lower gel, resolving or separating gel, is basic (pH 8.9), and has a higher polyacrylamide content, making the gel's pores narrower. This allow that the smaller proteins to travel more easily and rapidly, than the larger proteins, causing them to separate by their molecular weight. The gel percentage and size depend on the molecular weight of the proteins to be separated. Since proteins when loaded on the gel have a negative charge, as they have been denatured by heating, and will travel toward the positive electrode when a voltage is applied [145].

After separating the protein mixture by molecular weight, it is transferred to a solid support, a membrane. The transfer is done using an electric field oriented perpendicular to the surface of the gel, causing proteins to move out of the gel and onto the membrane. The

membrane is placed between the gel surface and the positive electrode in a sandwich, so that the negatively charged proteins can migrate from the gel to the membrane. The sandwich includes a fibber pad (sponge) at each end, and filter papers to protect the gel and the blotting membrane [145].

3.4.1. Tissue Homogenization

Mouse (n=3) and rat (n=8) testes were removed surgically after the animals were transcardialy perfused with 0.9% saline solution, and stored at -80°C until use. Lysis buffer (50 mM Tris-HCl (pH 8.0), 120 mM NaCl, 4% w/v 3[(3-Cholamidopropyl)dimethylammonio]-propanesulfonic acid (CHAPS)) containing protease inhibitors cocktail were added to tissues, and then homogenized in a variable speed motor drive homogenizer (750-1000 rpm; Yellowline OST 20 Digital; IKA Labortechnik) with a pestle tissue grinder. After, the homogenized tissues were transferred to a sterile tube and centrifuged at 1000 rcf at 4°C for 2 minutes, to separate the proteins from the non-homogenized tissue, like the thick fibrous connective tissue capsule (the tunica albuginea) that covered the testes. The supernatant was transferred to a new sterile tube and then each sample was sonicated twice on ice for 10 seconds (0.5 cycle; 60% amplitude; Sonicator U200S control; IKA Labortechnik). Each sample was made up to 1% SDS and boiled at 90°C for 10 minutes, and stored at -20°C until use.

Lysis buffer containing protease inhibitors was used considering that allows an efficient tissue lysis and protein solubilisation, while prevents protein degradation and interference with the protein´s immunoreactivity and biological activity.

3.4.2. Total Protein Concentration Determination

Total protein concentration of the tissue lysates was determined using the BCA Protein Assay (Thermo Scientific Pierce). This kit is a fast (two-component), high-precision, detergent-compatible assay reagent set to measure total protein concentration compared to protein standards (Table 8). The BCA Protein Assay combines the reduction of Cu^{2+} to Cu^{1+} by protein in an alkaline environment with the highly sensitive and selective colorimetric detection of the cuprous cation (Cu^{1+}) by BCA. The first step of the colour development reaction is the biuret reaction, where peptides containing three or more a.a. residues form a coloured chelate complex (light blue) with cupric ions (Cu^{2+}) in an alkaline medium containing sodium potassium tartrate. In the second reaction occurs the chelation of two molecules of BCA with one reduced cuprous cation, which was formed in step one, resulting in the formation of the intense purple-coloured reaction product. The water-soluble BCA/copper complex displays a strong linear absorbance at 562 nm with increasing protein concentrations over a working range of 20 µg/mL to 2000 µg/mL. The BCA reagent

is approximately 100 times more sensitive than the light blue colour of the first reaction [146].

The reaction that leads to BCA colour development is strongly influenced by four a.a. residues in the a.a. sequence of the protein, which are cysteine, cystine, tyrosine, and tryptophan. Though, the universal peptide backbone also contributes to colour formation, helping to minimize variability caused by protein compositional differences [146].

Table 8: Protein standards used in BCA Protein Assay method.

Protein Standard	BSA 2 mg/mL (µL)	SDS 1% (µL)	Protein Mass (µg)	Protein Concentration (µg/µL)
P0	0	25	0	0.00
P1	1	24	2	0.08
P2	2	23	4	0.16
P3	5	20	10	0.40
P4	10	15	20	0.80
P5	20	5	40	1.60

Abbreviations: BSA, Bovine Serum Albumin; SDS, Sodium Dodecyl Sulphate.

The quantitative analyses of total protein concentration were carried out using four dilutions of the samples (5 µL, 2.5 µL, 1 µL and 0.5 µL, with final volumes of 25 µL that were adjusted with SDS 1%). After preparation of protein standards and samples in a 96 well plate, they were incubated at 37°C for 30 minutes with 200 µL of working reagent (composed of 50 parts of reagent A to 1 part of the reagent B). Immediately after incubation the absorbance was measured at 562 nm using the microplate reader Infinite M200 (Tecan, Männedorf, Switzerland) and analysed with Tecan i-control 1.9 software attached to the Infinite M200. The standard curve was prepared by plotting the absorbance value for each BSA standard against its concentration (Table 8). The total protein concentration of each sample was determined using the standard curve. Duplicates of protein standards and samples were always prepared.

3.4.3. Gradient SDS Polyacrylamide Gel Electrophoresis

The 5-20% gradient SDS polyacrylamide gel were prepared and allowed to polymerize at room temperature for 45 minutes. This resolving gel has a linear progression of acrylamide concentrations (5 to 20%) from top to bottom, resulting in a wider separation range. Next, the stacking gel solution was prepared and loaded on the top of gradient gel.

A comb was inserted and the gel was left to polymerize for 30 minutes at room temperature. Prior to loading the samples on the wells of the stacking gel, ¼ volume of loading buffer 4x (250 mM Tris (pH 6.8), 0.01% w/v bromophenol blue, 2% v/v β-mercaptoethanol, 8% w/v SDS, and 40% v/v glycerol in sterile deionized H_2O) was added to the sonicated samples. After boiling at 90°C for 10 minutes and spinned down, the mass-normalized samples were subjected to electrophoresis on a 7.5 and 5-20% gradient SDS polyacrylamide gel in a Hoefer electrophoresis system at 90 mA for approximately 3 hours.

Precision Plus Protein™ Dual Colour Standards (Bio Rad) was used as molecular weight marker, and were loaded and resolved side-by-side with the samples.

3.4.4. Immunoblotting

After the samples were electrophoresed, proteins were transferred from gel to a nitrocellulose membrane (0.2 µm pore size; Whatman®) at 200 mA for approximately 18 hours. Nitrocellulose membrane was used for its high affinity for protein, its retention abilities, highly versatile (several staining options), and low background.

The membranes were initially hydrated with Tris Buffered Saline (TBS) 1x for 5 minutes at room temperature. Then were incubated with blocking buffer (5% w/v BSA in Tris Buffered Saline-Tween (TBS-T) 1x) at room temperature for 4 hours with gentle agitation and at 4°C overnight. This is a very important step of western blotting, as it prevents antibodies from binding to the membrane non-specifically, reducing the background. After blocking, the proteins of interest were detected incubating the membranes with specific antibodies at room temperature for 4 hours with gentle rocking and at 4°C overnight. The antibodies used were: Anti-APP, clone 22C11 (Chemicon); Anti-APP, PAD CT695 (Invitrogen); Anti-Phospho-APP (Thr668) (Cell Signaling); Anti-Tau, clone Tau-5 (Chemicon); Anti-Phospho-PHF-Tau (pSer202+Thr205), clone AT8 (Thermo Scientific); and Anti-β-Tubulin, clone 2-28-33 (Invitrogen). The antibodies were diluted in 5% w/v BSA in TBS-T 1x, according to the manufacturer's instructions (for dilutions of primary antibodies see Table 6). The membranes were washed with TBS-T 1x, 3 times, 10 minutes each time. Washing is very important as it minimizes background and removes unbound antibody. Bound primary antibodies were detected by an appropriate horseradish peroxidase (HRP) conjugated second antibody (Amersham™ ECL™ Anti-mouse IgG, Horseradish Peroxidase-Linked Species-Specific Whole Antibody (from sheep), and Amersham™ ECL™ Anti-rabbit IgG, Horseradish Peroxidase-Linked Species-Specific Whole Antibody (from donkey); GE Healthcare Life Sciences; diluted 1:5000) after 2 hours at room temperature incubation with gentle agitation. After washing with TBS-T 1x, 3 times, 10 minutes each time, the membranes were incubated with an enhanced chemiluminescence (ECL) Luminata Crescendo Western HRP substrate (Merck Millipore) for 2-5 minutes, or with a homemade ECL detection reagent (100 (0.1 mM 3-aminophthalhydrazide (luminol);

2 mM 4-iodophenol; 50 mM Tris (pH 9.35)) : 1 (hydrogen peroxide)) for 1 minute, both at room temperature. The signal that is produced corresponds to the position of the target protein. This signal was captured on an X-ray film (Amersham Hyperfilm ECL; GE Healthcare Life Sciences), which was developed and fixed in a dark room with the appropriate solutions. The X-ray films were scanned on a GS-800™ Calibrated Densitometer (Bio-Rad Laboratories, Amadora, Portugal) and analysed with the Image Lab™ Software version 5.1 (Bio-Rad Laboratories, Amadora, Portugal).

Chemiluminescence is the most commonly used enzymatic detection system. This method is based on antibodies conjugated to HRP that catalyse the oxidation of luminol in presence of luminol peroxide detection reagent, in a multi-step reaction. The result is the emission of low intensity light at 428 nm [147].

The membranes were incubated with stripping buffer (62.5 mM Tris base, 2% w/v SDS, and 0.7% v/v β-mercaptoethanol in deionized H_2O) at 50°C for 30 minutes with gentle rocking, to stripping for re-probing the membranes. The membranes were washed with TBS-T 1x, 5 times, 15 minutes each time (until the β-mercaptoethanol was totally removed). Then, the membranes were washed 2 times with deionized H_2O, and were allowed to dry until the next re-probing treatment.

The proteins quantifications were normalized against the amount of β-tubulin (clone 2-28-33; 1:1000; Invitrogen) to correct for loading.

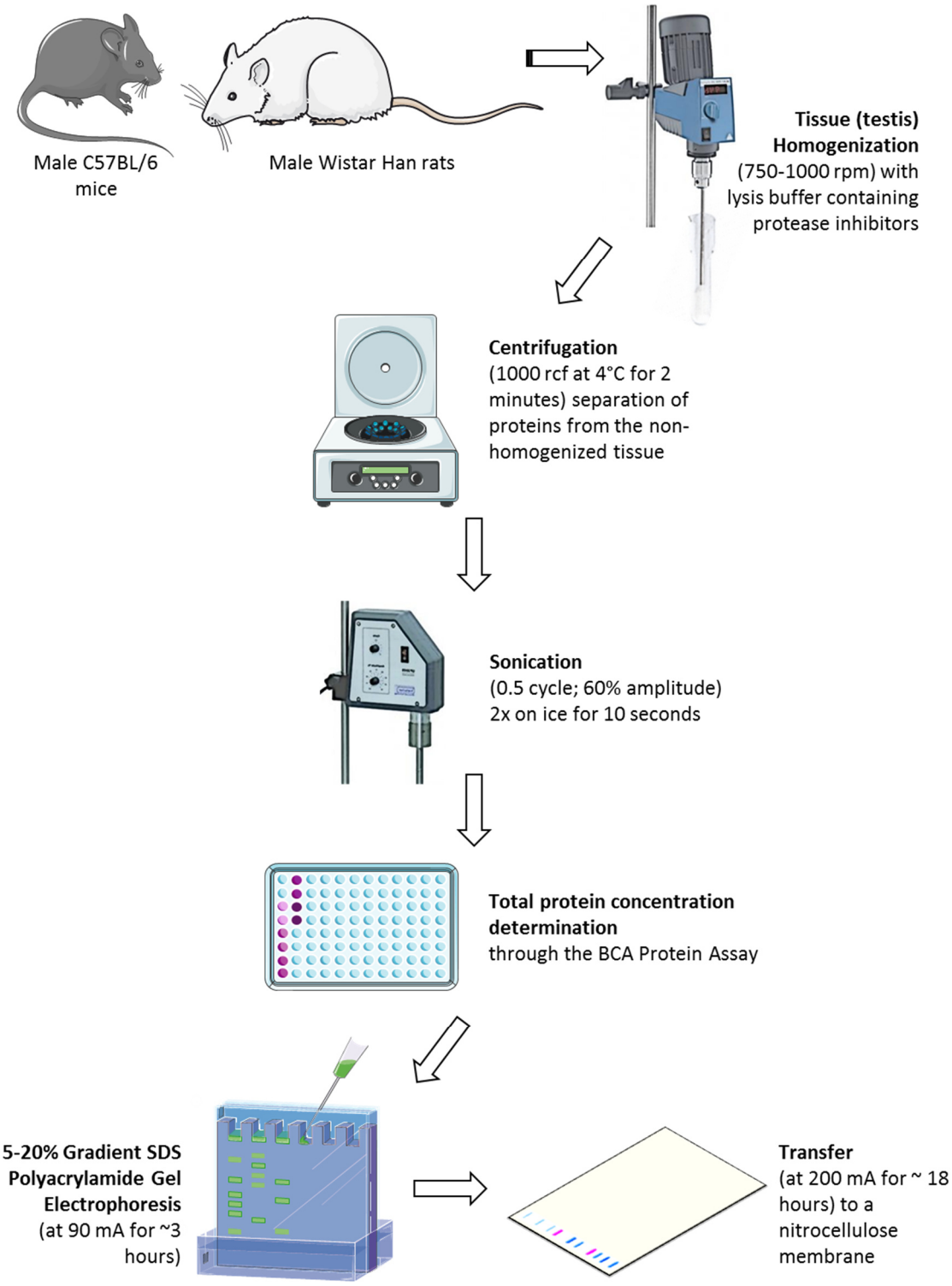

Figure 13: Diagram of the western blot protocol performed in this study, using mouse and rat testes. Abbreviations: BCA, Bicinchoninic Acid; SDS, Sodium Dodecyl Sulphate.

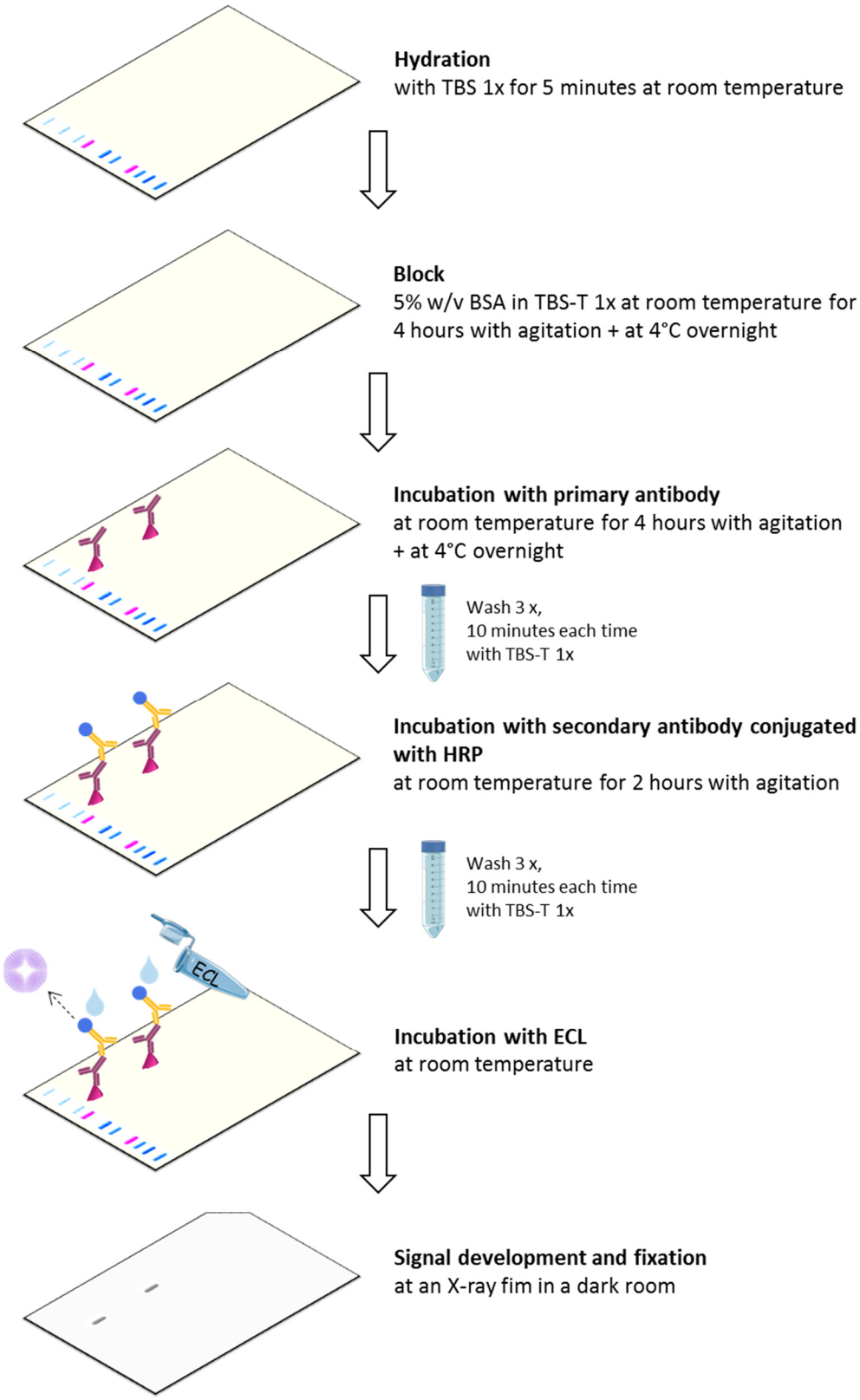

Figure 14: Schematic representation of the immunoblotting protocol performed in this study. Abbreviations: BSA, Bovine Serum Albumin; ECL, Enhanced Chemiluminescence; HRP, horseradish peroxidase; TBS, Tris Buffered Saline; TBS-T, Tris Buffered Saline-Tween.

4. Results – Setting up fluorescent immunohistochemistry

4.1. Abstract

Upon initiating the experiments designed it became apparent that the tissues had autofluorescence, which was interfering with fluorescent IHC performed. Thus, the initial objective was to found in the available literature and test the best possible treatment in order to decrease autofluorescence. The overall aim was to establish the conditions for the subsequent experiments. Antigen retrieval pre-treatment with citrate buffer and an indirect immunofluorescent staining method was the strategy implemented to reduce the autofluorescence problem.

4.2. Results – Detecting Autofluorescence

Autofluorescence was one of the problems in the course of this study. To better evaluate the tissue autofluorescence, fluorescent IHC (on paraffin-embedded tissue) protocol was performed without primary and secondary antibodies incubation. Also, no antigen retrieval pre-treatment was performed, given the fact that this pre-treatment can reduce autofluorescence [142]. The next figures show testis sections from 2-month-old mouse (Figure 15) and 29-month-old rat (Figure 16). Interstitial cells (Figures 15 and 16), as well as myoid cells and Sertoli cells (Figure 16) exhibited elevated levels of autofluorescence. In testis of younger animals, mainly the interstitial cells exhibited fluorescence. In older animals, autofluorescence was observed in myoid cells (peritubular layer of the seminiferous tubules) and in Sertoli cells. Thus, testis autofluorescence appears to be age-related, once it was observed an increase in the autofluorescence levels with ageing, as well as an increase in the cell types affected.

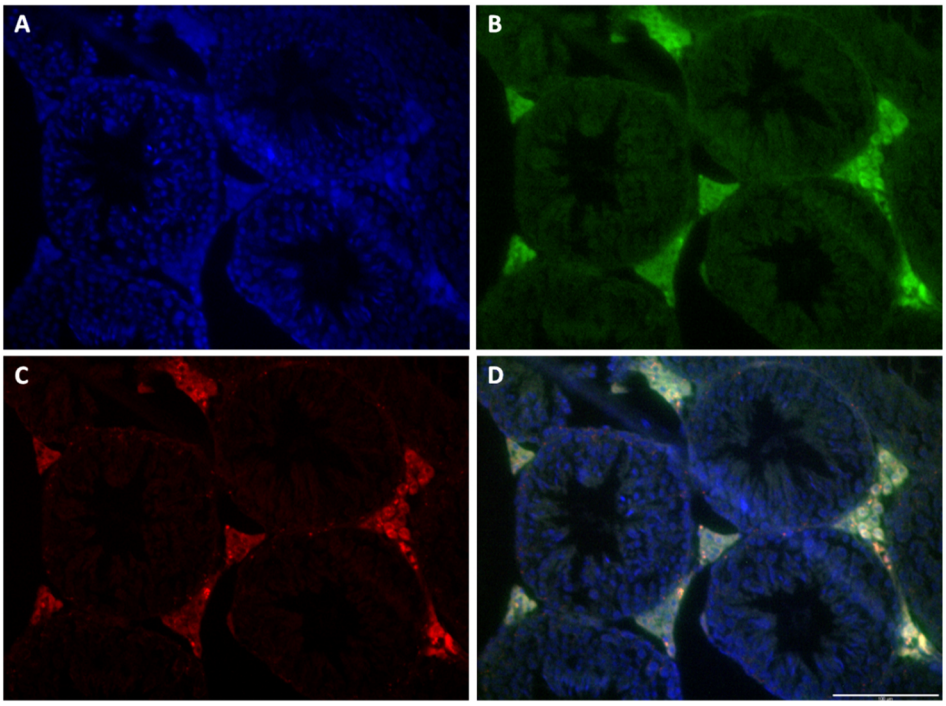

Figure 15: Autofluorescence of testis from 2-month-old mouse.
No antigen retrieval pre-treatment and no primary and secondary antibodies incubations were performed in this section. **A)** Blue signals represent nuclear DNA counterstained with Hoechst 33342 (diluted 1:3000). **B)** and **C)** Green and red signals represent the tissue autofluorescence capture with GFP and TRITC, respectively. **D)** Merged image. Bar = 100 µm. Magnification 200x.

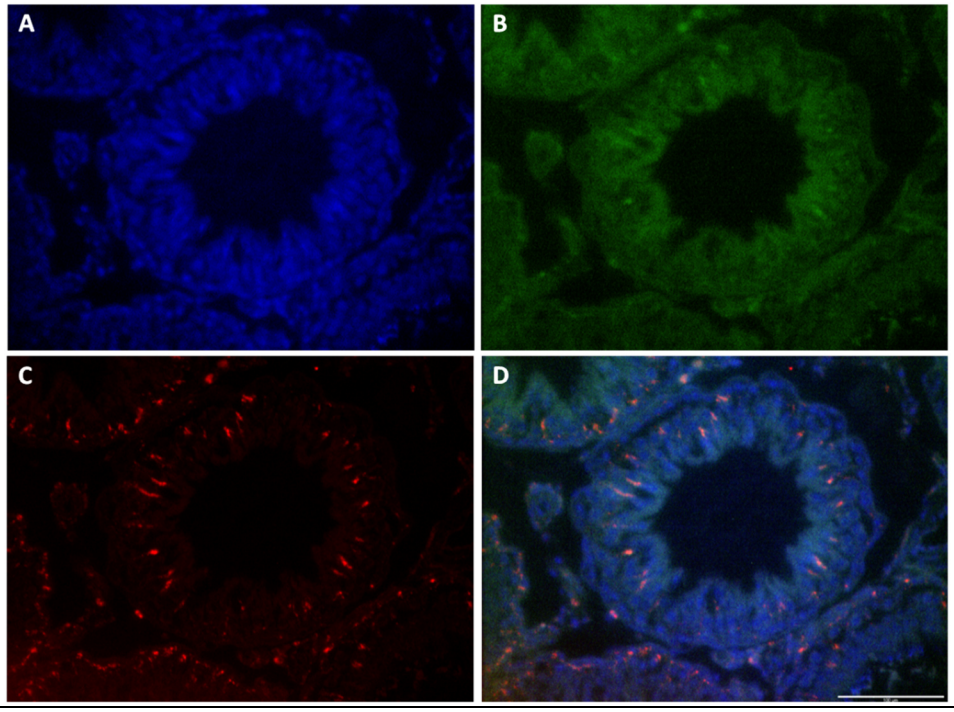

Figure 16: Autofluorescence of testis from 29-month-old rat.
No antigen retrieval pre-treatment and no primary and secondary antibodies incubations were performed in this section. **A)** Blue signals represent nuclear DNA counterstained with Hoechst 33342 (diluted 1:3000). **B)** and **C)** Green and red signals represent the tissue autofluorescence capture with GFP and TRITC, respectively. **D)** Merged image. Bar = 100 µm. Magnification 200x.

These results were consistent with the findings of Miquel and colleagues (1978). They investigated by spectrophotofluorometric and electron microscopic techniques the lipofuscin accumulation in the testis of C57BL/6J mice ranging in age from 4 to 39 month. It was reported that mice testes contained fluorescent substances, which increased linearly until about 24 months. From that age on, no further increase were observed. Through electron microscopy, they showed that spermatogonia were completely free of lipofuscin. In striking contrast, both Sertoli and interstitial cells of Leydig, in old animals, had accumulated very large amounts of pigment. In the Sertoli cells, a process of mitochondrial vacuolation and densification was apparently linked with the genesis of lipofuscin. On the other hand, in the interstitial cells, densification of lipid droplets played a role in the formation of most pigment granules [148].

Ceroid/lipofuscin-type pigments are the responsible for cell and tissue autofluorescence. These pigments are classified and defined as follows:

i. Lipofuscin is an intracellular, age-related, fluorescent, cytoplasmic, non-degradable granular pigment. It is mostly present in secondary lysosomes of post-mitotic cells, such as neurons, cardiac myocytes, and retinal pigment epithelial cells, which forms due to iron-catalysed oxidation/polymerization of protein and lipid residues [149];
ii. Ceroid is a group of biopigments, also with an intralysosomal location, which are quickly produced as a result of several pathologies and experimental conditions, such as x-irradiation, E-vitamin deficiency, starvation, and intoxication. Ceroid is probably similar to lipofuscin and may share the same mechanisms of formation, but it does not accumulate with age. It may be present in a variety of cells, like in the kidney, thymus, pancreas, testis, prostate, seminal vesicles, uterus, and adrenal gland [149,150].

The emission wavelength of the autofluorescent substance ranged from 425 to 700 nm, a range sufficiently broad that could potentially interfere with fluorescence techniques [151].

4.3. Results – Reducing the Autofluorescence

Different strategies have been advanced to combat the inherent diffuse autofluorescence problem, including extraction of the autofluorescent constituents, chemical modification of the fluorochrome, photobleaching methods, and “blocking” the autofluorescent structures. To date, none of these approaches has fully succeeded, in part because effectiveness of the “blocking steps” varies by tissue type and method of processing [142]. Viegas *et al.* (2007) concluded that a combination of short-duration, high-intensity ultraviolet irradiation (2 hours at 30 W) and Sudan Black B was the best protocol to reduce autofluorescence regardless of the extent of vascularity and level of lipofuscin content [152]. A different approach was advocated by Robertson *et al.* (2008) that reported a

combined approach to multiple immunofluorescent labeling of formalin-fixed paraffin-embedded tissue, using antigen retrieval pre-treatment, an indirect immunofluorescent staining method, and confocal laser scanning microscopy to circumvent autofluorescence [153]. Yang and Honaramooz (2012) reported that the intrinsic fluorescence was completely masked after treatment with Sudan Black B for 10-15 minutes of the Piglet testis tissue sections or for 8 minutes of the testis cells [151].

In this study, antigen retrieval pre-treatment and an indirect immunofluorescent staining method was the strategy implemented to combat the autofluorescence problem. This approach wasn't fully effective at completely eliminating the autofluorescence problem. Nonetheless there was a substantial reduction in autofluorescence in the seminiferous tubules, but not in the interstitial space (Figure 17 and 18). Thus, in IHC analysis of the different antibodies tested in this study, was only considered the staining within the seminiferous tubules.

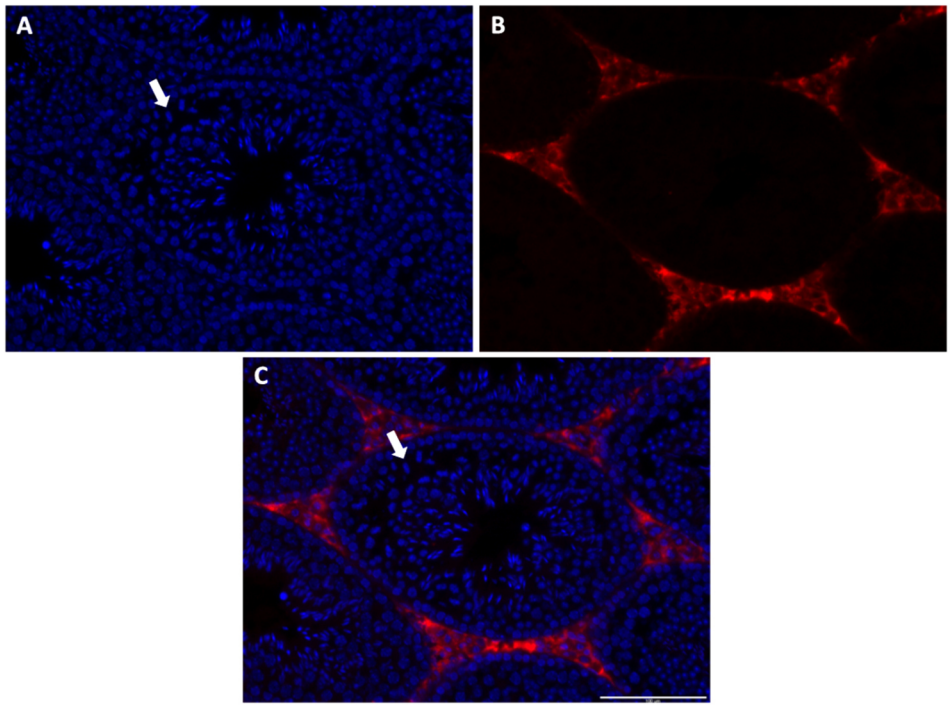

Figure 17: Autofluorescence of testis from 2-month-old mouse, after antigen retrieval pre-treatment. No primary antibody incubation was performed in this section. Spermatocytes during meiotic division (arrows) are present. **A)** Blue signals represent nuclear DNA counterstained with Hoechst 33342 (diluted 1:3000). **B)** Red signals represent the tissue autofluorescence capture with TRITC. **C)** Merged image. Bar = 100 µm. Magnification 200x.

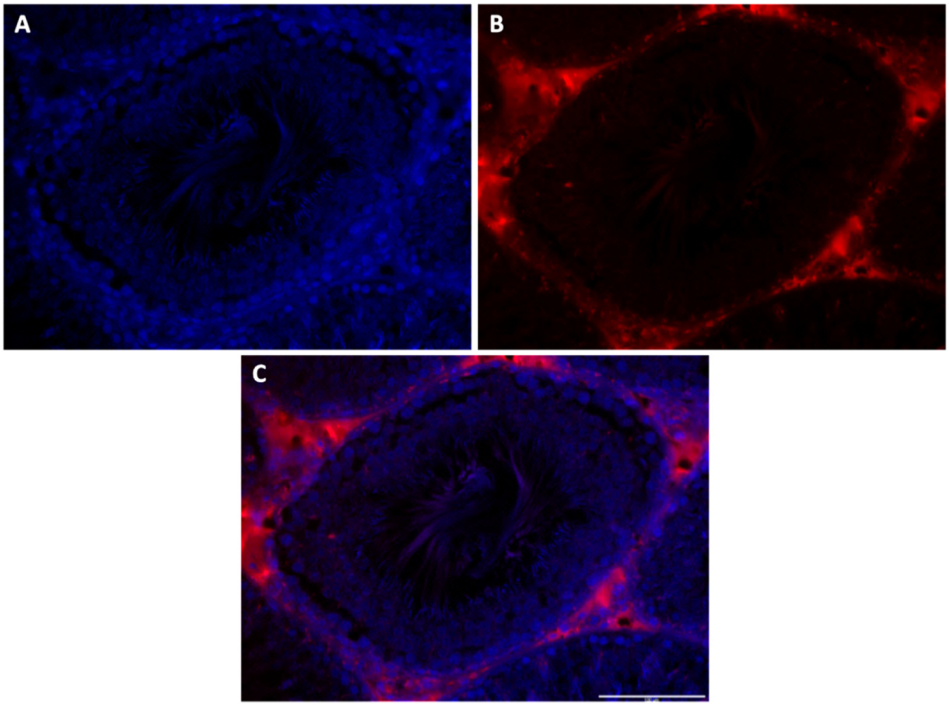

Figure 18: Autofluorescence of testis from 26-month-old rat, after antigen retrieval pre-treatment.
No primary antibodies incubation was performed in this section. **A)** Blue signals represent nuclear DNA counterstained with Hoechst 33342 (diluted 1:3000). **B)** Red signals represent the tissue autofluorescence capture with TRITC. **C)** Merged image. Bar = 100 µm. Magnification 200x.

5. Results – Tau protein, PP1α and PP1γ

5.1. Abstract

Having established ideal conditions to reduce tissue inherent autofluorescence, we work on to test proteins relevant to Tau phosphorylation in testis. Thus, fluorescent IHC was carried out for Tau, phosphorylated Tau, serine/threonine protein phosphatase (PP) 1α, and PP1γ. The seminiferous epithelium of the mammalian testis has a variety of MT networks: an ordered array in Sertoli cells, the manchette, axonemal MTs and in mitotic and meiotic spindles. These abundant MT networks are reflected by a diversity of MAPs. Thus, the testis are an abundant source for studies of MTs and MAPs [73].

The overall aim was to analyse the Tau protein expression and its dynamics of phosphorylation patterns during spermatogenesis.

Results showed that all cells of spermatogenic lineage express Tau protein. Phosphorylated Tau (Ser202 and Thr205) is localized all over spermatogonia, spermatocytes and early (round) spermatids. PP1α and PP1γ are expressed throughout spermatogenesis.

5.2. Results – Tau

IHC using the monoclonal anti-Tau, clone Tau-5 antibody detected the localization of total-Tau protein during spermatogenesis. Tau was detected throughout spermatogenesis, all over the cells in a diffuse way (Figures 19).

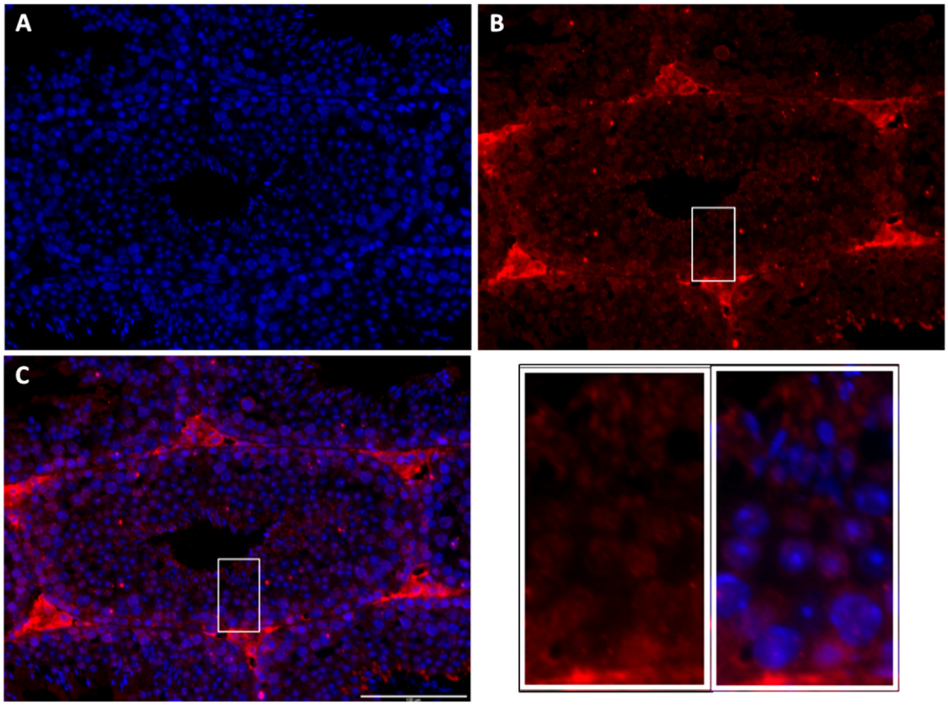

Figure 19: Tau protein expression in testis from 6-month-old mouse.
A) Blue signals represent nuclear DNA counterstained with Hoechst 33342 (diluted 1:3000). **B)** Red signals represent immunostaining with anti-Tau-5 (diluted 1:200). **C)** Merged image. Bar = 100 µm. Magnification 200x.

5.3. Results – Tau Phosphorylation

IHC using the monoclonal anti-phospho-PHF-Tau (Ser202+Thr205), clone AT8 antibody detected Tau protein only when phosphorylated (simultaneously) at Ser202 and Thr205 during spermatogenesis. AT8 was localized all over spermatogonia, spermatocytes and early (round) spermatids (Figures 20 and 21) in a diffuse way. We observed a decrease in the AT8 expression pattern between the ages of 3-month-old (Figure 20) and 15-month-old (Figure 21). It was necessary to increase the exposure time from 100 milliseconds to 500 milliseconds, respectively.

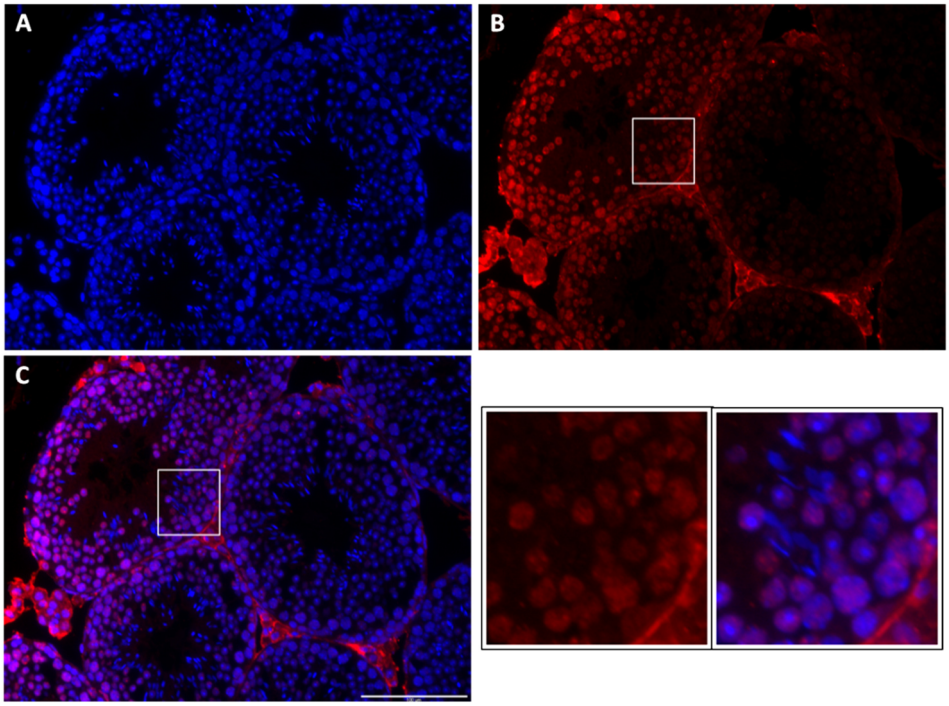

Figure 20: Phosphorylated Tau (Ser202 and Thr205) expression in testis from 3-month-old mouse.
This section and the section in Figure 27 are serial sections each other. **A)** Blue signals represent nuclear DNA counterstained with Hoechst 33342 (diluted 1:3000). **B)** Red signals represent immunostaining with anti-AT8 (diluted 1:100). **C)** Merged image. Bar = 100 µm. Magnification 200x.

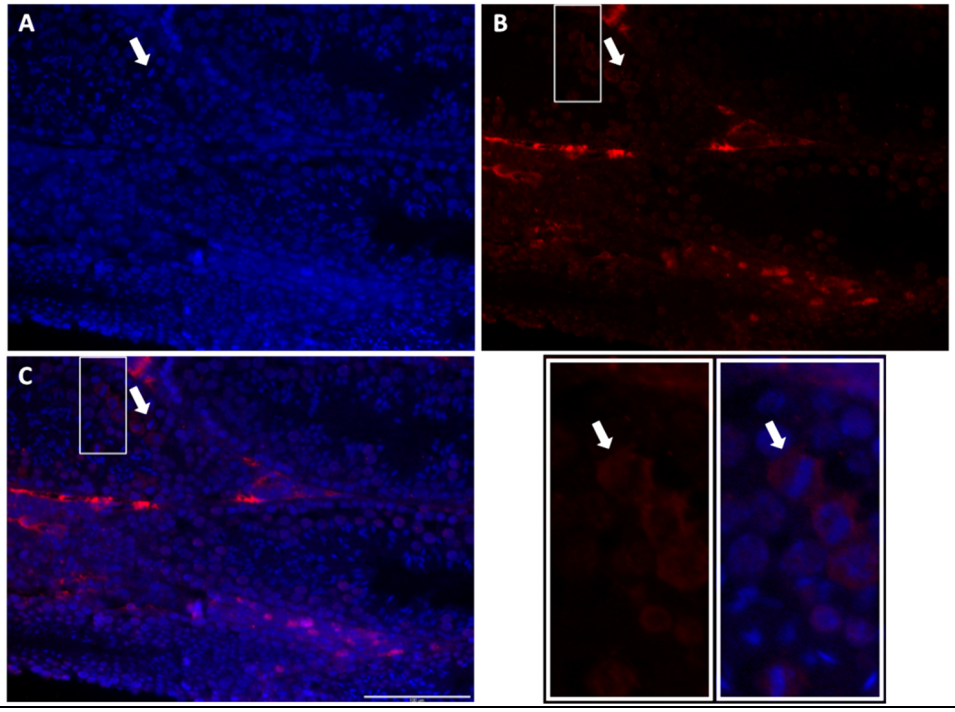

Figure 21: Phosphorylated Tau (Ser202 and Thr205) expression in testis from 15-month-old mouse.
This section and the section in Figure 28 are serial sections each other. Spermatocytes during meiotic division (arrows) are present. **A)** Blue signals represent nuclear DNA counterstained with Hoechst 33342 (diluted 1:3000). **B)** Red signals represent immunostaining with anti-AT8 (diluted 1:100). **C)** Merged image. Bar = 100 µm. Magnification 200x.

5.4. Results – PP1α

IHC using the polyclonal anti-PP1α antibody detected total Serine/Threonine Protein Phosphatase PP1α during spermatogenesis. All cells of spermatogenic lineage exhibited a diffuse cytoplasmic stain with this antibody (Figure 22). PP1α was localized all over cells including around the nucleus, and presented higher intensity in spermatogonia (Figure 22B).

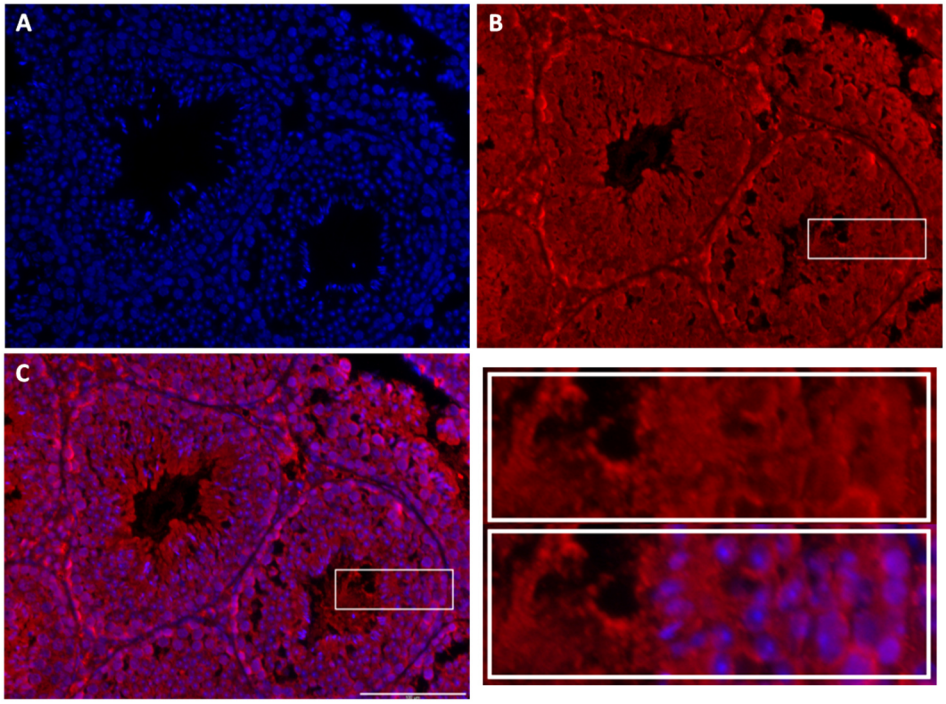

Figure 22: PP1α expression in testis from 2-month-old mouse.
This section and the section in Figure 23, 24 and 25 are serial sections each other. **A)** Blue signals represent nuclear DNA counterstained with Hoechst 33342 (diluted 1:3000). **B)** Red signals represent immunostaining with anti-PP1α (diluted 1:250). **C)** Merged image. Bar = 100 µm. Magnification 200x.

5.5. Results – PP1γ

IHC using the polyclonal anti-PP1γ antibody detected both Serine/Threonine Protein Phosphatase PP1γ isoforms (PP1γ1 and PP1γ2) during spermatogenesis. All cells of spermatogenic lineage presented a diffuse cytoplasmic stain with this antibody (Figure 23). PP1γ was localized all over cells including around the nucleus, and stained more intensely the spermatogonia and the late (elongated) spermatids heads and midpieces (Figure 23B).

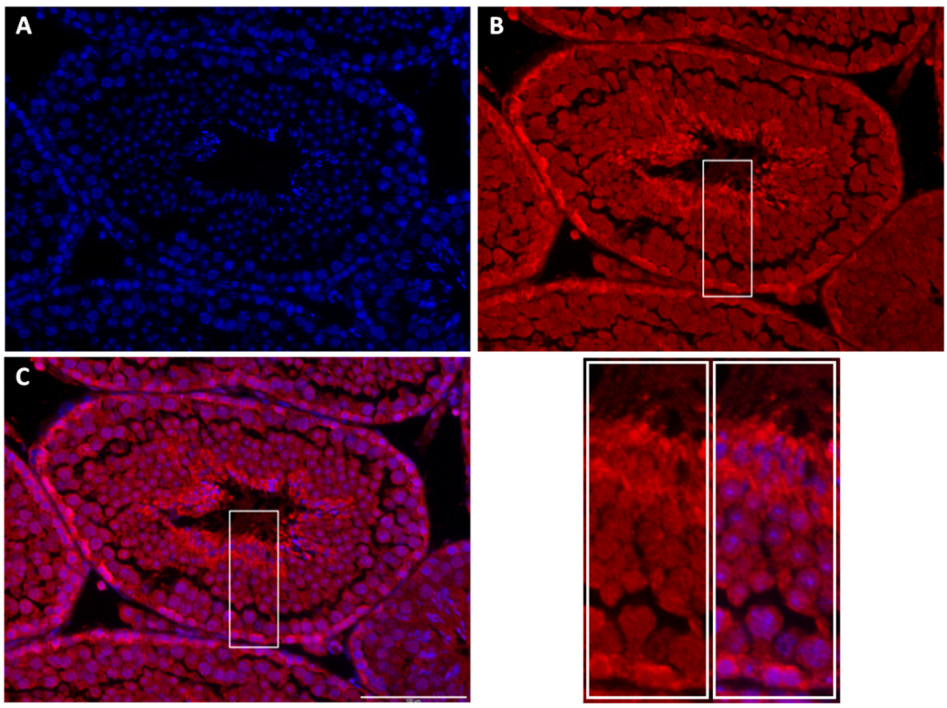

Figure 23: PP1γ expression in testis from 2-month-old mouse.
This section and the section in Figure 22, 24 and 25 are serial sections each other. **A)** Blue signals represent nuclear DNA counterstained with Hoechst 33342 (diluted 1:3000). **B)** Red signals represent immunostaining with anti-PP1γ (diluted 1:500). **C)** Merged image. Bar = 100 µm. Magnification 200x.

5.6. Discussion

Tau promotes assembly of tubulin *in vitro* [86] and stabilizes MTs against depolymerization *in vivo* [154,155]. Grundke-Iqbal *et al.* (1986) described that an increase in Tau protein phosphorylation reduces its affinity for MTs, which results in neuronal cytoskeleton destabilization [87]. In opposition, the function of Tau protein and its phosphorylation in the testis has only recently begun to be characterized [73].

In this immunohistochemichal analysis we studied Tau's expression and its phosphorylation patterns in the testis. Total-Tau expression, detected by anti-Tau-5, was constantly observed from spermatogonia to late (elongated) spermatids (Figure 19). Although, anti-AT8, which detect phosphorylated Tau at Ser202 and Thr205, was localized from spermatogonia to early (round) spermatids (Figure 20 and 21). These findings are in agreement with H. Inoue *et al.* (2014) findings [73]. They used a battery of antibodies to study Tau phosphorylation patterns in the C57BL/6 mice testis at 12 weeks of age. Phosphorylated Tau (P-Tau^{S199,S202}, AT8, AT100 and AT270) was especially localized in spermatocytes during meiosis in their study, as well as in ours (arrows in Figure 21). They also reported that the expression of acetylated tubulin was inversely weakened during the same stage. This, according to the authors, suggests that Tau phosphorylation is specific during meiosis. In addition, Tau protein might be phosphorylated at AD-specific sites in meiosis. Thus, Tau phosphorylation and MT deacetylation may contribute to spermatogenesis, particularly in meiosis [73].

In this study, we observed a decrease in AT8 expression pattern between the ages of 3-month-old (Figure 20) and 15-month-old (Figure 21), in a way that was necessary to increase the exposure time from 100 milliseconds to 500 milliseconds, respectively. In order to test this hypothesis, we used western blot analysis to confirm the decrease of Tau and phosphorylated Tau expression with age. Unfortunately, despite our best efforts, we did not detect any signal with this approach using anti-Tau-5 and anti-AT8. After carefully examination of all possible explanations, we concluded that either the concentration of the primary antibody was not appropriate, or the antigen was present in low concentration [145,147]. Thus, as future work, we should attempt another western blot analysis, starting to increase primary antibody and/or the antigen concentration. If this new attempt does not succeed, we should try other techniques, such as immunoprecipitation.

In the adult rat brain, alternative splicing of the primary transcript of Tau generates six isoforms with an apparent molecular weight between 48 and 67 kDa. Still, Gu *et al.* (1996) suggested a testis-specific isoform when they reported that Tau protein was detected in two major bands in rat testis at 34 and 37 kDa after alkaline phosphatase treatment [66]. More recently, it was reported that this protein was detected in some bands with apparent molecular weight between 37 and 40 kDa in the mouse testis. Additionally,

it was confirmed that Tau isoform-D (identified as P10637-5 in uniprot), of 38.961 kDa, is the isoform expressed in mouse testis [73].

PP1 isoforms belong to the family of serine/threonine protein phosphatases, which is involved in Tau dephosphorylation [88], as previously mentioned. The role of PP1 has been implicated in various eukaryotic processes including metabolism, cell cycle regulation, apoptosis, etc. In mammals, three genes, Ppp1ca, Ppp1cb, and Ppp1cc, encode four PP1 isoforms: PP1α, PP1β, PP1γ1 and PP1γ2. Ppp1cc gene alternative splicing generates the isoforms PP1γ1 and PP1γ2. All four PP1 isoforms are virtually identical (approximately 90% identity) except at their extreme C-terminal. Even though PP1γ1, PP1α and PP1β are ubiquitous, PP1γ2 is mainly restricted to adult testis [156,157]. Ppp1cc gene null mutation, which eliminates both splice variants, results in male infertility due to disruptions in spermatogenesis [158,159]. Females appear normal suggesting that the PP1α and PP1β can substitute for the PP1γ isoforms in all tissues except testis [157–159]. Curiously, loss of PP1α appears to have no apparent phenotype [157].

Both PP1α (Figure 22) and PP1γ (Figure 23) were detected throughout spermatogenesis. Although our PP1γ findings are in agreement with that Chakrabarti *et al.* (2007) described, the PP1α are not [159]. In adult mice testis, PP1γ2 was described to be localized in the cytoplasm of secondary spermatocytes, round spermatids, and elongated spermatids, as well as in testicular and epididymal spermatozoa. However, its expression was weak in spermatogonia, pachytene spermatocytes, and interstitial cells. Additionally, PP1γ1 expression was observed in interstitial cells, whereas much weaker expression was observed in all stages of spermatogenesis, in both the cytoplasm and nuclei of all cells. PP1α expression was reported in the cytoplasm of interstitial cells, peritubular cells, spermatogonia, and pachytene spermatocytes in adult mice testis [159].

6. Results – APP and its phosphorylation

6.1. Abstract

Work from our group has previously identified that APP is expressed in sperm. Therefore we work on to address if APP is also expressed in testis. Further, given the specific relevance of protein phosphorylation in signalling cascades, we also included the study of APP phosphorylated on Thr668. Thus, fluorescent IHC was carried out for APP, phosphorylated APP (Thr668), and γ-Tubulin.

The overall aim was to analyse APP expression and its dynamics of phosphorylation patterns during spermatogenesis.

Results showed that APP is expressed throughout spermatogenesis. Surprisingly, results were dramatic in its phosphorylation pattern.

6.2. Results – APP

IHC using anti-APP 22C11 and anti-APP CT695 antibodies detected total-APP during spermatogenesis. The monoclonal antibody anti-APP 22C11 recognizes the N-terminal epitope of APP and APLP2, and the polyclonal antibody anti-CT is specific for APP and reacts with the intracellular domain of all transmembrane APP isoforms. All cells of spermatogenic lineage and Sertoli cells displayed a diffuse cytoplasmic stain with APP 22C11 (Figure 24) and APP CT695 (Figure 25). APP 22C11 was localized all over cells except around the nucleus, and stained more intensely the spermatocytes (Figure 24B). In contrast, APP CT695 was localized all over cells including around the nucleus, and stained more intensely the spermatogonia (Figure 25B).

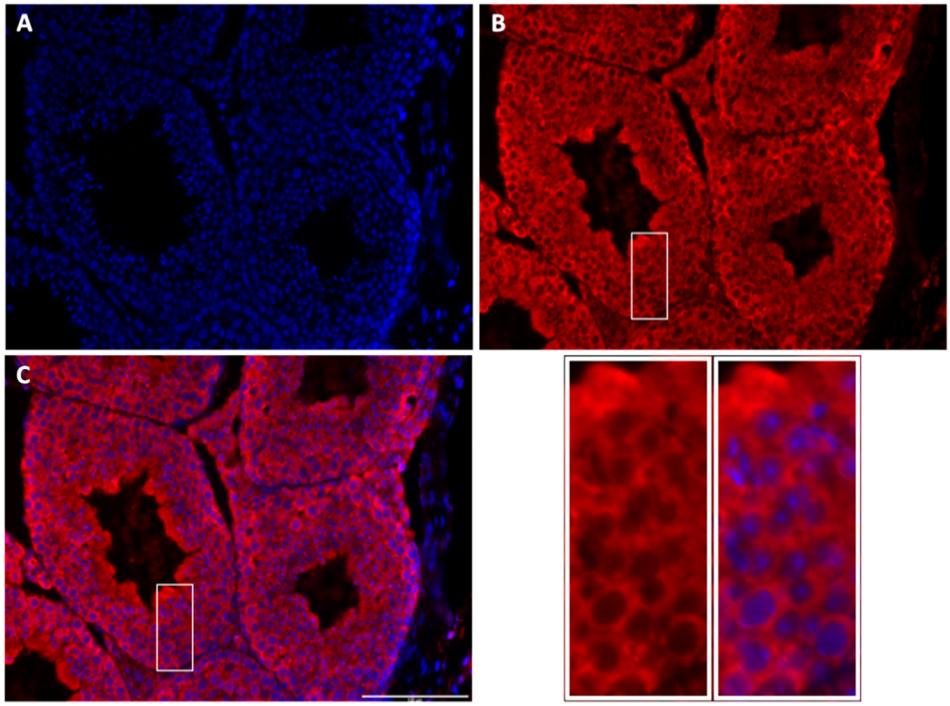

Figure 24: APP expression in testis from 2-month-old mouse.
This section and the section in Figure 22, 23 and 25 are serial sections each other. **A)** Blue signals represent nuclear DNA counterstained with Hoechst 33342 (diluted 1:3000). **B)** Red signals represent total-APP and APLP2 immunostained with APP 22C11 (diluted 1:20). **C)** Merged image. Bar = 100 µm. Magnification 200x.

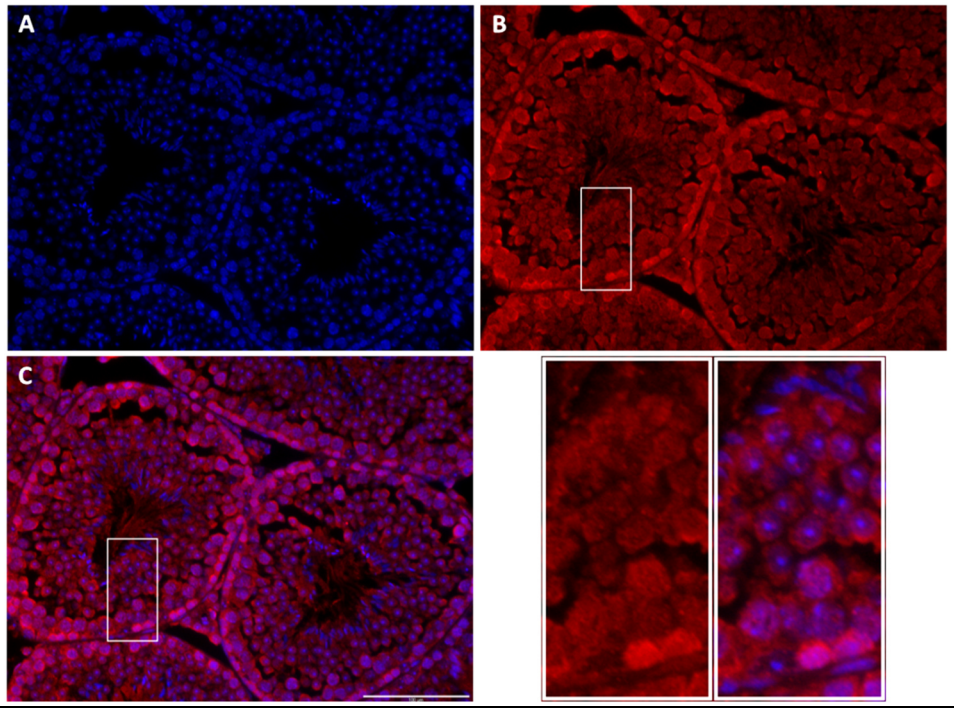

Figure 25: APP expression in testis from 2-month-old mouse.
This section and the section in Figure 22, 23 and 24 are serial sections each other. **A)** Blue signals represent nuclear DNA counterstained with Hoechst 33342 (diluted 1:3000). **B)** Red signals represent total-APP and C-Terminal Fragment immunostained with APP CT695 (diluted 1:100). **C)** Merged image. Bar = 100 µm. Magnification 200x.

Given that both anti-APP 22C11 and anti-APP CT695 antibodies detect not only APP, but also other proteins (APLP2) and fragments (sAPPα and β, and CTFs), a double staining IHC using these two antibodies was performed. This was performed to localize the full-length form of APP during spermatogenesis. All cells of spermatogenic lineage and Sertoli cells shown a diffuse cytoplasmic stain for both APP CT695 (Figure 26B) and APP 22C11 (Figure 26C).

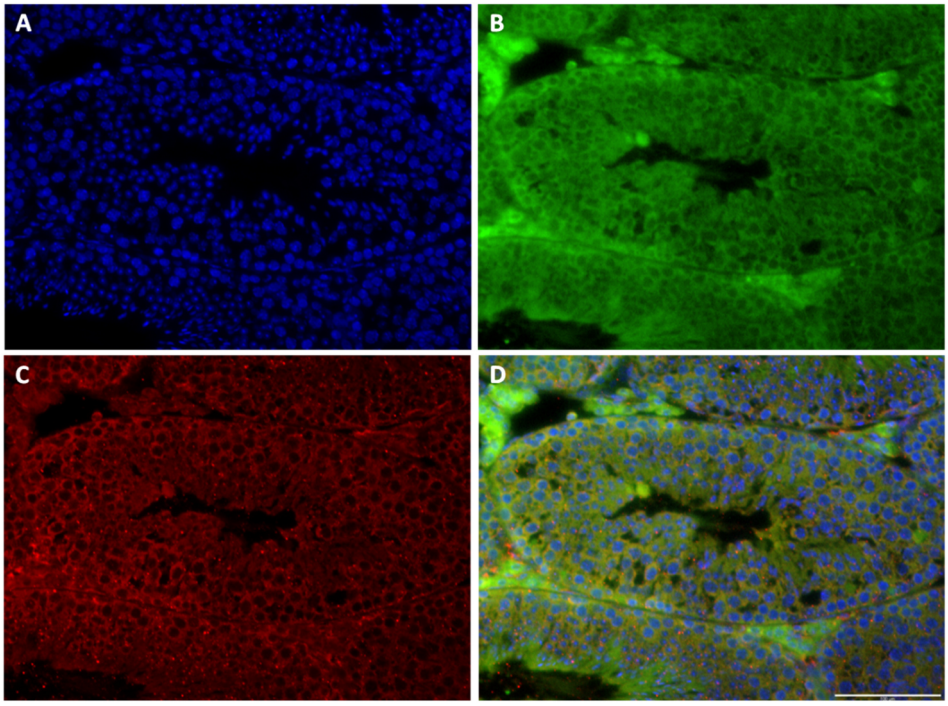

Figure 26: APP expression in testis from 6-month-old mouse.
A) Blue signals represent nuclear DNA counterstained with Hoechst 33342 (diluted 1:3000). **B)** Green signals represent total-APP and C-Terminal Fragment immunostained with APP CT695 (diluted 1:100). **C)** Red signals represent total-APP and APLP2 immunostained with APP 22C11 (diluted 1:20). **D)** Merged image. Bar = 100 µm. Magnification 200x.

6.3. Results – APP Phosphorylation

IHC using the polyclonal anti-phospho-APP (Thr668) antibody detected different isoforms of endogenous APP only when phosphorylated at Thr668 (in the APP695 isoform) during spermatogenesis. All cells of spermatogenic lineage and Sertoli cells showed a weak diffuse cytoplasmic stain with this antibody. An intense focal stain was observed in what appears to be the spermatocyte nuclei, under the form of a condensate spot (Figures 27 and 28). Curiously, spermatocytes during meiosis intensely stained with this antibody all over the cell (arrows in Figure 27 and 28). There seem to be no major differences in the expression pattern between the ages of 3-month-old (Figure 27) and 15-month-old (Figure 28).

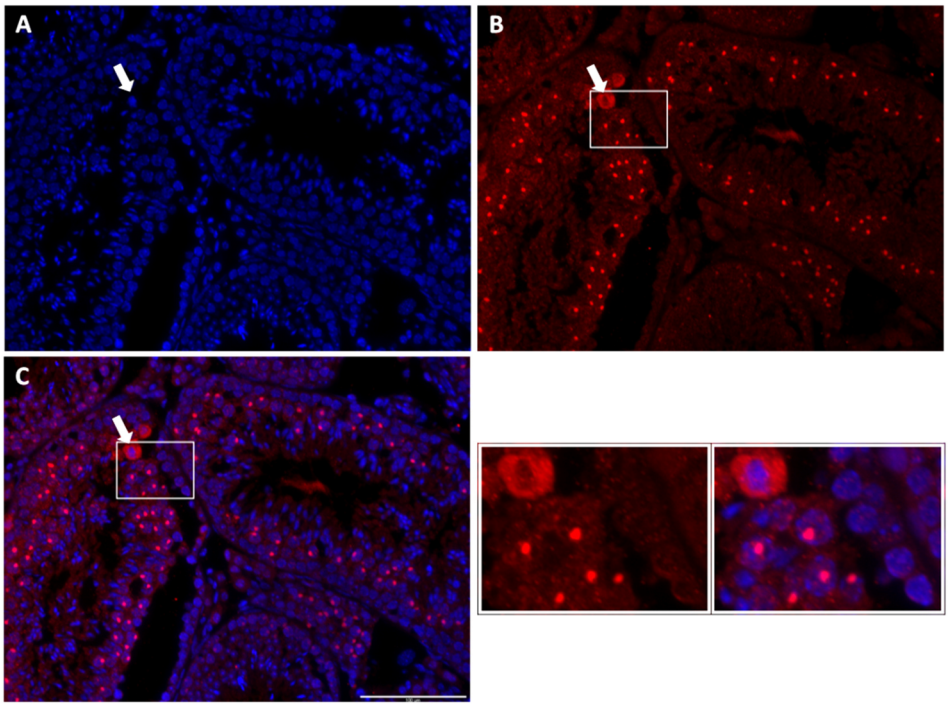

Figure 27: Phosphorylated APP (Thr668) expression in testis from 3-month-old mouse.
This section and the section in Figure 20 are serial sections each other. Spermatocytes during meiotic division (arrows) are present. **A)** Blue signals represent nuclear DNA counterstained with Hoechst 33342 (diluted 1:3000). **B)** Red signals represent immunostaining with anti-phospho-APP (Thr668) (diluted 1:400). **C)** Merged image. Bar = 100 µm. Magnification 200x.

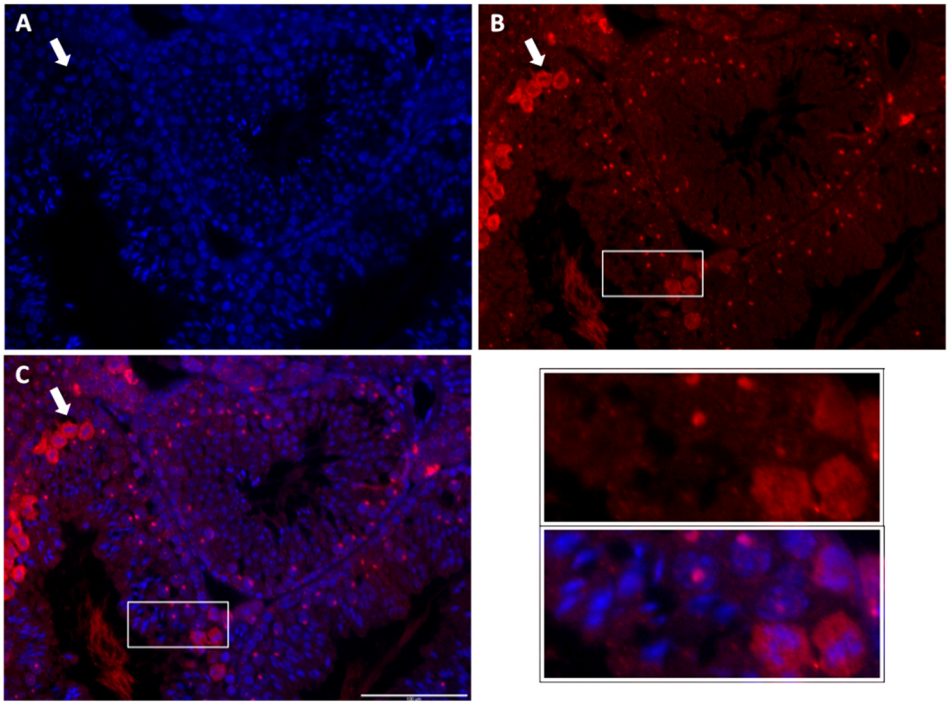

Figure 28: Phosphorylated APP (Thr668) expression in testis from 15-month-old mouse.
This section and the section in Figure 21 are serial sections each other. Spermatocytes during meiotic division (arrows) are present. **A)** Blue signals represent nuclear DNA counterstained with Hoechst 33342 (diluted 1:3000). **B)** Red signals represent immunostaining with anti-phospho-APP (Thr668) (diluted 1:400). **C)** Merged image. Bar = 100 µm. Magnification 200x.

6.4. Results – γ-Tubulin

IHC using the polyclonal anti-γ-Tubulin antibody detected total γ-Tubulin protein during spermatogenesis. At first glance, this antibody seems to be staining throughout the cytoplasm of all spermatogenic cells. However, after a closer observation, all cells of spermatogenic lineage seem to display a focal cytoplasmic stain, the centrosome (a pair of centrioles) (Figure 29).

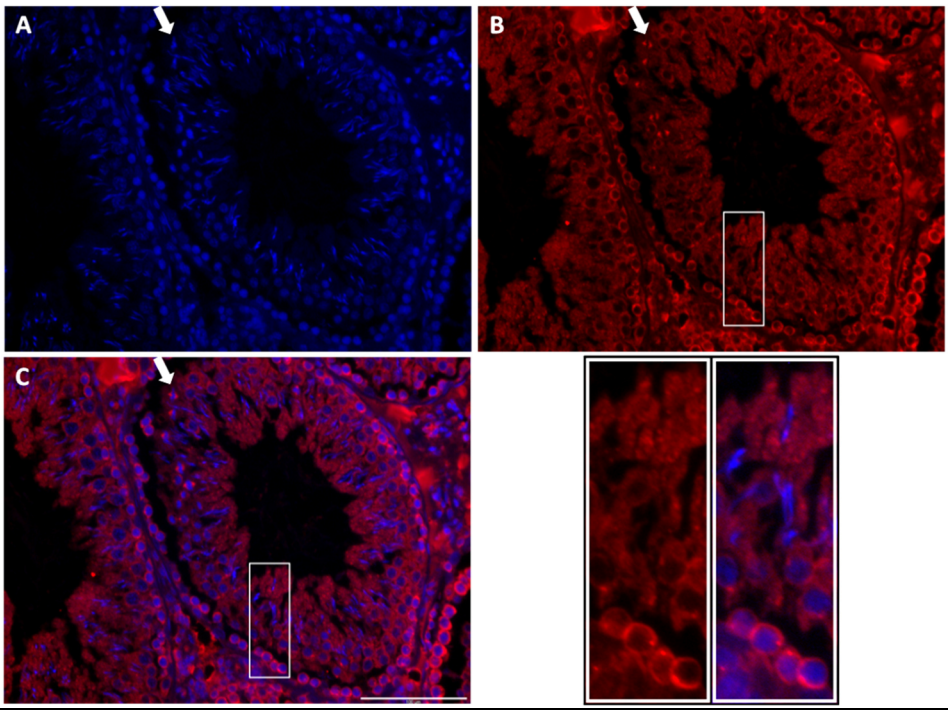

Figure 29: γ-Tubulin expression in testis from 26-month-old rat.
Spermatocytes during meiotic division (arrows) are present. **A)** Blue signals represent nuclear DNA counterstained with Hoechst 33342 (diluted 1:3000). **B)** Red signals represent immunostaining with anti-γ-Tubulin (diluted 1:500). **C)** Merged image. Bar = 100 µm. Magnification 200x.

6.5. Results – APP Western Blot Analysis

In mice testis at 2 and 6 months of age, the anti-APP clone 22C11 antibody, which recognizes the N-terminal epitope of APP and APLP2, detected two major bands with apparent molecular mass of 107 kDa and 104 kDa, and two minor bands of 54 kDa and 42 kDa (Figure 30 – Mouse). In rats testis at 5, 26 and 29 months of age, the same antibody detected one major band with apparent molecular mass of 110 kDa, and three minor bands of 74 kDa, 54 kDa and 43 kDa (Figure 30 – Rat).

Equal amounts (50 µg) of protein were loaded, and β-tubulin (50 kDa) was used as loading control.

Figure 31 is the graphic representation of the relative protein expression of APP (APP/β-Tubulin) in testes from mice and rats, based on the quantification of immunoblot in Figure 30. There is a tendency to decrease in APP expression between the ages of 2-month-old and 6-month-old (Figure 30 and 31 – Mouse).

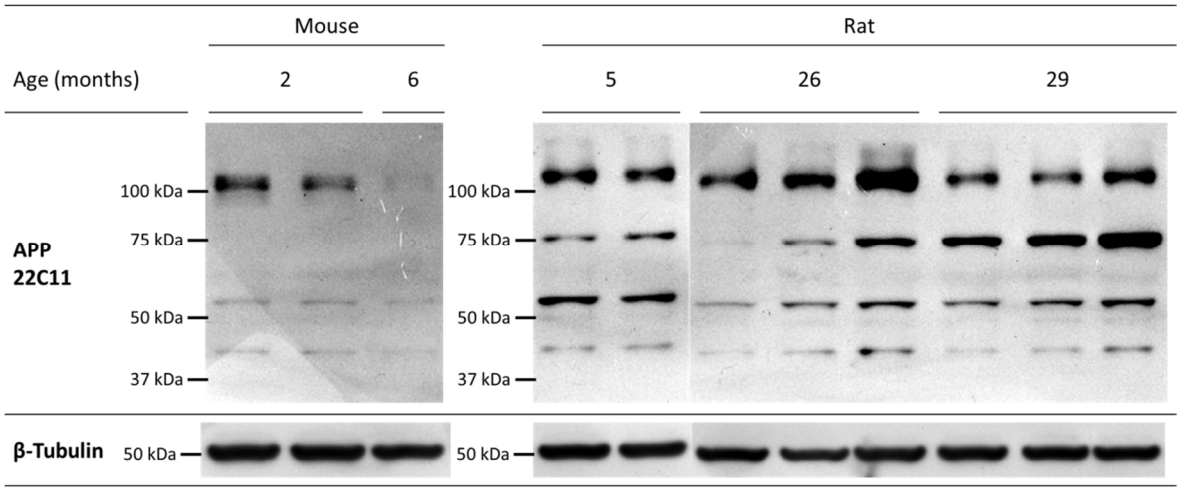

Figure 30: APP expression through western blot analysis of testes from 2-month-old (n = 2) and 6-month-old (n = 1) mice, and of testes from 5-month-old (n = 2), 26-month-old (n = 3) and 29-month-old (n = 3) rats. APP was detected by anti-APP clone 22C11 (diluted 1:250). In mice this antibody detected two major bands with molecular mass of 107 kDa and 104 kDa, and two minor bands with molecular mass of 54 kDa and 42 kDa. In rats this antibody detected one major band with molecular mass of 110 kDa, and three minor bands with molecular mass of 74 kDa, 54 kDa and 43 kDa. β-Tubulin (diluted 1:1000) was used as a loading control.

Using the anti-APP CT695 and anti-phospho-APP (Thr668), results show non-specific binding.

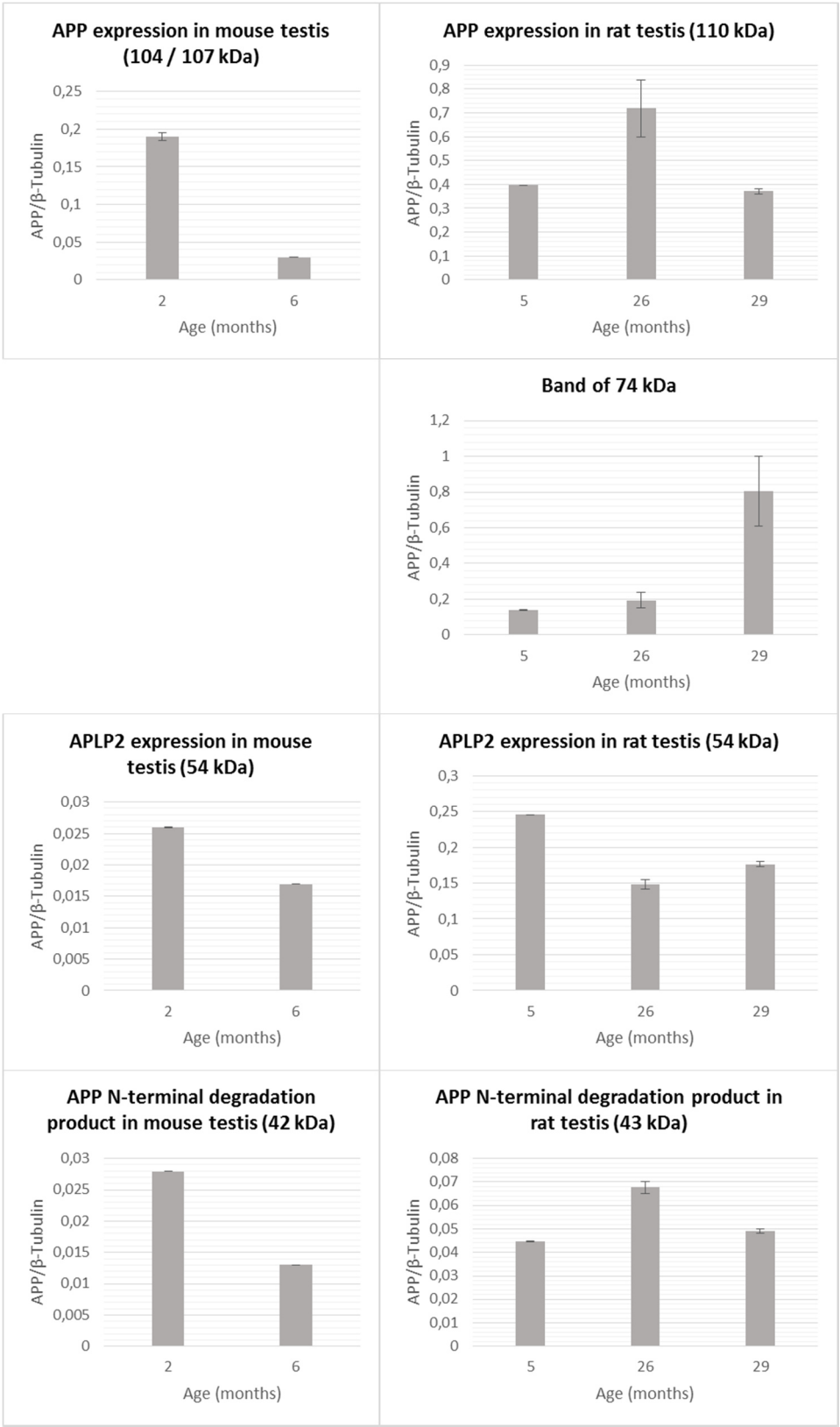

Figure 31: Relative protein expression of APP in testes from 2-month-old (n = 2) and 6-month-old (n = 1) mice (on the left), and in testes from 5-month-old (n = 2), 26-month-old (n = 3) and 29-month-old (n = 3) rats (on the right), based on the quantification of immunoblot in Figure 30. Data presented as mean ± standard error of the mean. β-Tubulin was used as a loading control.

6.6. Discussion

In human testis, APP is described to be a 184 Fragments Per Kilobase of transcript per Million fragments mapped (FPKM) in RNA sequencing expression analysis, and as a protein is localized in cells in seminiferous ducts at low levels [160]. Mice and rats were used as models in this study, once the homology of APP sequence between these two animals and human is approximately 97% for the three major APP isoforms [161].

IHC was performed to investigate the localization of total-APP and its phosphorylation patterns in testis. This technique indicated not only APP expression but also its phosphorylation patterns in mouse testis. APP expression, detected by anti-APP 22C11 and anti-APP CT695 antibodies, was constantly observed from spermatogonia to late (elongated) spermatids (Figures 24-26), and in the non-proliferating and supporting Sertoli cells. This finding is in agreement with studies demonstrating that the APP gene is expressed in the two cell types that compose the epithelium in the seminiferous tubules. Shoji *et al.* (1990) have described the presence of APP by immunocytochemistry only during sperm formation in the acrosome and the growing tail of spermatids [122]. Beer *et al.* (1995) reported that APP is highly expressed in soma and processes of Sertoli cells, and at low levels in germ cells in the testes of young adult Wistar rats [123].

APP 22C11 was localized all over cells except around the nucleus (Figure 24B), while APP CT695 was localized all over cells including around the nucleus (Figure 25B). This suggests that CTFs, probably AICD, are in nucleus, and is in agreement with findings that described that this fragment is involved in nuclear signalling, as a transcription factor [162]. Evidence indicates that only the amyloidogenic pathway generates AICD capable of nuclear signalling, due to the subcellular compartmentalization of APP processing [162].

Thr668 is a major phosphorylation site within APP that can be phosphorylated by a number of kinases [163]. CDK5 [40] and glycogen synthase kinase (GSK) 3β [41] phosphorylate APP at Thr668 in post-mitotic neurons, whereas CDK1 phosphorylate APP in dividing cells [33]. The c-Jun N-terminal kinase (JNK) 1 and JNK2 also phosphorylate APP at Thr668, after a cellular stress signal [42], while JNK3 phosphorylates APP during neuronal differentiation [39]. The phosphorylation of APP at Thr668 results in a significant conformational change that may affect interactions with binding partners and consequently impact its subcellular localization and metabolism [164]. Phosphorylation at this residue is a normal process associated with neurite extension, anterograde transport of vesicular cargo into neurites, and in signalling to the nucleus [39,165–168]. A recent study has shown that non-phosphorylated forms (at Thr668) of C-terminal APP fragments are associated with lipid raft-like microdomains where the γ-secretase complex (amyloidogenic) resides, whereas Thr668-phosphorylated C-terminal fragments reside predominantly in cytoplasmic fractions [169]. Hence phosphorylation regulates the localization of APP and thus affects its processing by γ-secretase [169].

In contrast with total-APP localization, anti-phospho-APP (Thr668) antibody was especially localized in what appears to be the spermatocyte nuclei (Figures 27 and 28), in the present study. We suspect that this staining in the nuclei represent phosphorylated AICD (at Thr668). Supporting this idea are the findings reported to Chang *et al.* (2006), which showed that the phosphorylation of AICD at Thr668 is required for its binding to Fe65 and its translocation into the nucleus. Additionally, phosphorylation of AICD at Thr668 induce GSK-3β expression, which leads to increased Tau phosphorylation at the Ser202 and Thr205 and neurotoxicity [168]. However, it is still controversial how AICD becomes localized in the nucleus. Nakaya and Suzuki (2006) reported that AICD translocation into the nucleus is not dependent on AICD phosphorylation. Additionally, FE65-dependent gene transactivation mediated by AICD in the nucleus are regulated by APP phosphorylation [170].

The anti-phospho-APP (Thr668) was also especially localized in spermatocytes during meiosis (arrows in Figures 27 and 28), suggesting that APP phosphorylation is specific during meiosis. In contrast, total-APP expression was not specific during meiosis, once during the meiotic division no major alterations in the expression pattern were observed. Additionally, it may be suggested that APP might be phosphorylated at AD-specific sites in meiosis. Thus, as future work, we should confirm if phosphorylated AICD is really in nuclei, and if so, attempt to identify the sub-nuclear structure where it is and its function there.

In a similar way, phosphorylation of APP at Thr668 is also mitosis-specific [33,45,171]. Suzuki and colleagues (1994) reported that APP is phosphorylated at Thr668 by CDK1/CDC2 kinase *in vitro*, and in a cell cycle-dependent manner *in vivo* [33]. At the G_2/M phase of the cell cycle, when CDC2 kinase is most active, APP phosphorylation is maximal. Additionally, the levels of mature APP and immature APP do not change significantly. However, immature APP is altered qualitatively. Furthermore, the level of the secreted extracellular N-terminal domain (sAPP) is decreased, and that of the truncated intracellular C-terminal fragment (APP_{COOH}) is increased. Thus, and considering that APP isoforms are ubiquitously expressed in cells, cell cycle-regulated phosphorylation of these proteins may be important in modulating their normal physiological functions and/or their metabolism [33]. Besides that, Judge *et al.* (2011) described that cell cycle activation not only induced the phosphorylation and proteolytic processing of APP (Aβ generation), but also affected the localization of phosphorylated APP in cells. Mitotic cells showed centrosome specific localization of phosphorylated APP [171]. Additionally, another study proposed that the phosphorylation of structural or transient components of centrosomes may affect cell cycle dependent processes such as centrosome duplication and MT nucleation [172] (reviewed in Judge *et al.*, 2011 [171]). Thus, in addition to enhanced proteolytic cleavage, APP phosphorylation may influence cell proliferation through its association with the cell cycle machinery. The co-localization of phosphorylated APP with MPM2, a metaphase protein marker, further reiterates APP's role as a growth-promoting molecule. Therefore, it is possible that high levels of phosphorylated APP may promote proliferation in dividing cells and centrosome

duplication or chromosome mis-segregation and cell death in post-mitotic neurons [171]. APP's function as a mitogenic molecule is evident from the fact that its upregulation is associated with cancers of different organs [173,174] (reviewed in Judge *et al.*, 2011 [171]), like testicular germ cell tumours [175]. It has also been reported that APP and PS1 associate with other proteins at the centrosome and localize to centrosomes [176,177] (reviewed in Judge *et al.*, 2011 [171]).

Sandbrink *et al.* (1994) described relative amounts of differential expression of APP messenger ribonucleic acids (mRNAs) in peripheral tissue. In Wistar rats (7 or 8 months old), the main isoform expressed is APP770 (47%), followed by APP751 and L-APP752 (20% each), L-APP733 (7%), APP695 and L-APP696 (4% both), L-APP677 (2%), and APP714 (<1%). Thus, KPI domain encoding APP mRNA isoforms are the principal isoforms expressed in testis (94%) [178]. These findings and the expected molecular weight of each isoform are summarized in Table 9.

Table 9: Relative amounts of APP species in rat testis and their expected size.

APP species	Relative Quantity (mRNA) [178]	Expected size [179]
APP770	47%	146 kDa (mature) 129 kDa (sAPP) 116 kDa (immature)
APP751	20%	139 kDa (mature) 123 kDa (sAPP) 112 kDa (immature)
L-APP752	20%	
L-APP733	7%	
APP714	<1%	
APP695 and L-APP696	4%	125 kDa (mature) 109 kDa (sAPP) 106 kDa (immature)
L-APP677	2%	

Abbreviations: APP, Amyloid Precursor Protein; mRNA, messenger Ribonucleic Acid; sAPP, soluble Amyloid Precursor Protein.

Through western blot analysis we detected two major bands with apparent molecular mass of 107 kDa and 104 kDa in mice testis, and one band at 110 kDa in rats testis (Figure

30). The major bands at 107 kDa (mouse) and 110 kDa (rat) probably represent full-length APP770, once that is the main isoform expressed in testis [178]. The band at 104 kDa (mouse) may represents APLP2 [124]. The minor band at 74 kDa (rat) was also found in mouse brain [180] and in previous work from our group with 22C11 and C-terminal antibodies, but has not yet been identified. Whereas the band at 54 kDa (mouse and rat) it may be an APLP2 variant, and was described to be present in human sperm [124]. The minor band at 42 kDa in mouse and at 43 kDa in rat probably represent an APP N-terminal cleavage product, and was recently described to be present in human embryonic stem cells [181]. Although these APP cleavage products were reported to be in different types of cells, the functional significance of these products is still unknown [181].

Similarly to Tau study, we attempted to evaluate the ageing influence in APP expression and its phosphorylation, through the western blot analysis. Spermatogenesis begins at around day 8 in mouse [182], and at approximately 5 days of age in rat [183]. The sexual maturity is reached at 7 to 10 weeks in mouse [182], and at about 6 weeks in rat [183]. When 24-month-old, rats are mostly in a state of testicular regression [184]. There is a tendency to decrease in APP expression between the ages of 2-month-old and 6-month-old (Figure 30 and 31 – Mouse), using anti-APP 22C11. In rats, results of western blot analysis were inconsistent (Figure 30 and 31 – Rat), and was not possible to establish a logical conclusion. Statistical analysis could not be done, due to sample size ($n < 3$ in the majority of analysed ages). Thus, future work should increase the sample size and the age range in both mouse and rat to reach a most valid conclusion.

Despite our best efforts, we obtained non-specific bindings in the western blot analysis using anti-APP CT695 and anti-phospho-APP (Thr668). After analysing all possible explanations, we concluded that polyclonal antibodies aren't the best choice to use on tissue homogenization. Therefore, as future work, we should attempt other techniques to accomplish this aim, like immunoprecipitation.

7. Conclusion

In summary, this study comprised a detailed analysis of APP and Tau expression, as well as their phosphorylation patterns, during spermatogenesis (Table 10). Our results over Tau protein and its phosphorylation pattern are consistent with those previously published by H. Inoue *et al.* (2014) [73]. PP1γ results are also in agreement with that Chakrabarti *et al.* (2007) described [159]. However, PP1α results were not in conformity with what has been published.

In this study, APP results are the major novel. There is a marked contrast in the distribution of total-APP and phosphorylated APP at Thr668. We demonstrate that site-specific APP phosphorylation is specifically localized during spermatogenesis. Furthermore, APP phosphorylation may play a critical role in the meiosis process, probably related with its normal physiological functions and/or its metabolism.

Table 10: Summary of relative expression of addressed proteins throughout spermatogenesis.

	Spermatogonia	**Spermatocytes**	**Spermatocytes in meiosis**	**Round spermatids**	**Elongated spermatids**
APP	++	++	++	++	++
Phospho-APP (Thr668)	+	++	+++	+	+
Tau protein	++	+	n.d.	+	++
Phospho-Tau (Ser202 + Thr205)	++	++	+++ ($P\text{-}Tau^{S199,\ S202}$)[73]	++	-
PP1α	+++	++	n.d.	++	++
PP1γ	+++	++	n.d.	++	+++
γ-Tubulin	+++	++	++	++	++

Abbreviations: -, negative immunostaining; +, weak immunostaining; ++, moderate immunostaining; +++, strong immunostaining; n.d., not detected; APP, Amyloid Precursor Protein; PP, Serine/Threonine Protein Phosphatase; Ser, Serine; Thr, Threonine.

Future perspectives:

- Study how ageing influences APP and Tau protein expression and their phosphorylation in testis through another technique than western blot analysis, like immunoprecipitation, as well as increasing the sample size and the age range;
- Study other APP and Tau phosphorylatable residues in spermatogenesis, in order to unravel their importance in meiosis;
- Confirm whether phosphorylated AICD is present in spermatocyte nuclei, and identify the sub-nuclear structure where it is and its function there.

8. References

1. Bilkei-Gorzo, A. Genetic mouse models of brain ageing and Alzheimer's disease. *Pharmacology & Therapeutics* **142**(2): 244–257 (2014).

2. Stelzmann, R. A., Schnitzlein, H. N. and Murtagh, F. R. An English translation of Alzheimer's 1907 paper, "Über eine eigenartige Erkankung der Hirnrinde." *Clinical Anatomy* **8**: 429–431 (1995).

3. Thies, W. and Bleiler, L. 2013 Alzheimer's disease facts and figures. *Alzheimer's & Dementia: The Journal of the Alzheimer's Association* **9**(2): 208–245 (2013).

4. Dementia statistics. *Alzheimer's Disease International (ADI)* (2013). at <http://www.alz.co.uk/research/statistics> (Accessed March 03, 2014).

5. Dementia: a public health priority. *World Health Organization (WHO)* (2012). at <http://www.med.upenn.edu/aging/documents/WHO-ADIdementia_report_final.pdf> (Accessed March 01, 2014).

6. Hebert, L. E., Weuve, J., Scherr, P. A. and Evans, D. A. Alzheimer disease in the United States (2010-2050) estimated using the 2010 census. *Neurology* **80**(19): 1778–1783 (2013).

7. Dementia cases set to triple by 2050 but still largely ignored. *World Health Organization (WHO)* (2012). at <http://www.who.int/mediacentre/news/releases/2012/> (Accessed March 03, 2014).

8. Selkoe, D. J. Cell biology of protein misfolding: the examples of Alzheimer's and Parkinson's diseases. *Nature Cell Biology* **6**(11): 1054–1061 (2004).

9. Mineur, Y. S., McLoughlin, D., Crusio, W. E. and Sluyter, F. Genetic mouse models of Alzheimer's disease. *Neural Plasticity* **12**: 299–310 (2005).

10. Francis, P. T. Analysis of post-mortem brain from people with Alzheimer's disease: a vital element in understanding the disease and developing new treatments. *The Journal of Quality Research in Dementia* (4): 13–16 (2007).

11. Gouras, G. K., Xu, H., Jovanovic, J. N., Buxbaum, J. D., Wang, R., Greengard, P., Relkin, N. R. and Gandy, S. Generation and regulation of beta-amyloid peptide variants by neurons. *Journal of Neurochemistry* **71**(5): 1920–1925 (1998).

12. Kumar, V., Abbas, A. K., Aster, J. C. and Fausto, N. *Robbins and Cotran Pathologic Basis of Disease*. 1464 (Saunders Elsevier, 2009).

13. Wakabayashi, T. and De Strooper, B. Presenilins: members of the gamma-secretase quartets, but part-time soloists too. *Physiology (Bethesda, Md.)* **23**: 194–204 (2008).

14. Götz, J., Streffer, J. R., David, D., Schild, A., Hoerndli, F., Pennanen, L., Kurosinski, P. and Chen, F. Transgenic animal models of Alzheimer's disease and related disorders: histopathology, behavior and therapy. *Molecular Psychiatry* **9**(7): 664–683 (2004).

15. PSEN1. (2013). at <http://ghr.nlm.nih.gov/gene/PSEN1> (Accessed March 10, 2014).

16. PSEN2. (2008). at <http://ghr.nlm.nih.gov/gene/PSEN2> (Accessed March 10, 2014).

17. Canevelli, M., Piscopo, P., Talarico, G., Vanacore, N., Blasimme, A., Crestini, A., Tosto, G., Troili, F., Lenzi, G. L., Confaloni, A. and Bruno, G. Familial Alzheimer's disease sustained by presenilin 2

mutations: systematic review of literature and genotype-phenotype correlation. *Neuroscience and biobehavioral reviews* **42**: 170–9 (2014).

18. Dumanchin, C., Camuzat, A., Campion, D., Verpillat, P., Hannequin, D., Dubois, B., Saugier-Veber, P., Martin, C., Penet, C., Charbonnier, F., Agid, Y., Frebourg, T. and Brice, A. Segregation of a missense mutation in the microtubule-associated protein tau gene with familial frontotemporal dementia and parkinsonism. *Human Molecular Genetics* **7**(11): 1825–1829 (1998).

19. Imtiaz, B., Tolppanen, A.-M., Kivipelto, M. and Soininen, H. Future directions in Alzheimer's disease from risk factors to prevention. *Biochemical Pharmacology* **88**(4): 661–670 (2014).

20. Jacobsen, K. T. and Iverfeldt, K. Amyloid precursor protein and its homologues: a family of proteolysis-dependent receptors. *Cellular and Molecular Life Sciences* **66**(14): 2299–2318 (2009).

21. Kang, J., Lemaire, H. G., Unterbeck, A., Salbaum, J. M., Masters, C. L., Grzeschik, K. H., Multhaup, G., Beyreuther, K. and Müller-Hill, B. The precursor of Alzheimer's disease amyloid A4 protein resembles a cell-surface receptor. *Nature* **325**(6106): 733–736 (1987).

22. Dyrks, T., Weidemann, A., Multhaup, G., Salbaum, J. M., Lemaire, H. G., Kang, J., Müller-Hill, B., Masters, C. L. and Beyreuther, K. Identification, transmembrane orientation and biogenesis of the amyloid A4 precursor of Alzheimer's disease. *The EMBO Journal* **7**(4): 949–957 (1988).

23. Ling, Y., Morgan, K. and Kalsheker, N. Amyloid precursor protein (APP) and the biology of proteolytic processing: relevance to Alzheimer's disease. *The International Journal of Biochemistry & Cell Biology* **35**(11): 1505–1535 (2003).

24. Suzuki, T. and Nakaya, T. Regulation of amyloid beta-protein precursor by phosphorylation and protein interactions. *The Journal of Biological Chemistry* **283**(44): 29633–29637 (2008).

25. Yamada, T., Sasaki, H., Dohura, K., Goto, I. and Sakaki, Y. Structure and expression of the alternatively-spliced forms of mRNA for the mouse homolog of Alzheimer's disease amyloid beta protein precursor. *Biochemical and Biophysical Research Communications* **158**(3): 906–912 (1989).

26. Yamada, T., Sasaki, H., Furuya, H., Miyata, T., Goto, I. and Sakaki, Y. Complementary DNA for the mouse homolog of the human amyloid beta protein precursor. *Biochemical and Biophysical Research Communications* **149**(2): 665–671 (1987).

27. De Strooper, B., Vassar, R. and Golde, T. The secretases: enzymes with therapeutic potential in Alzheimer disease. *Nature reviews. Neurology* **6**(2): 99–107 (2010).

28. Lichtenthaler, S., Wang, R., Grimm, H., Uljon, S. N., Masters, C. L. and Beyreuther, K. Mechanism of the cleavage specificity of Alzheimer's disease γ-secretase identified by phenylalanine-scanning mutagenesis of the transmembrane domain of the amyloid precursor. *Proceedings of the National Academy of Sciences of the United States of America* **96**(6): 3053–3058 (1999).

29. Struhl, G. and Adachi, A. Requirements for presenilin-dependent cleavage of notch and other transmembrane proteins. *Molecular Cell* **6**(3): 625–636 (2000).

30. Parent, A. T. and Thinakaran, G. Modeling presenilin-dependent familial Alzheimer's disease: emphasis on presenilin substrate-mediated signaling and synaptic function. *International Journal of Alzheimer's Disease* **2010**: 11 pages (2010).

31. Eggert, S., Paliga, K., Soba, P., Evin, G., Masters, C. L., Weidemann, A. and Beyreuther, K. The proteolytic processing of the amyloid precursor protein gene family members APLP-1 and APLP-2 involves alpha-, beta-, gamma-, and epsilon-like cleavages: modulation of APLP-1 processing by n-glycosylation. *The Journal of Biological Chemistry* **279**(18): 18146–18156 (2004).

32. Nakagawa, K., Kitazume, S., Oka, R., Maruyama, K., Saido, T. C., Sato, Y., Endo, T. and Hashimoto, Y. Sialylation enhances the secretion of neurotoxic amyloid-beta peptides. *Journal of Neurochemistry* **96**(4): 924–933 (2006).

33. Suzuki, T., Oishi, M., Marshak, D. R., Czernik, A. J., Nairn, A. C. and Greengard, P. Cell cycle-dependent regulation of the phosphorylation and metabolism of the Alzheimer amyloid precursor protein. *The EMBO Journal* **13**(5): 1114–1122 (1994).

34. Oishi, M., Nairn, A. C., Czernik, A. J., Lim, G. S., Isohara, T., Gandy, S. E., Greengard, P. and Suzuki, T. The cytoplasmic domain of Alzheimer's amyloid precursor protein is phosphorylated at Thr654, Ser655, and Thr668 in adult rat brain and cultured cells. *Molecular Medicine (Cambridge, Mass.)* **3**(2): 111–123 (1997).

35. Lee, M.-S., Kao, S.-C., Lemere, C. A., Xia, W., Tseng, H.-C., Zhou, Y., Neve, R., Ahlijanian, M. K. and Tsai, L.-H. APP processing is regulated by cytoplasmic phosphorylation. *The Journal of Cell Biology* **163**(1): 83–95 (2003).

36. Feyt, C., Pierrot, N., Tasiaux, B., Van Hees, J., Kienlen-Campard, P., Courtoy, P. J. and Octave, J.-N. Phosphorylation of APP695 at Thr668 decreases gamma-cleavage and extracellular Abeta. *Biochemical and Biophysical Research Communications* **357**(4): 1004–1010 (2007).

37. Takahashi, K., Niidome, T., Akaike, A., Kihara, T. and Sugimoto, H. Phosphorylation of amyloid precursor protein (APP) at Tyr687 regulates APP processing by alpha- and gamma-secretase. *Biochemical and Biophysical Research Communications* **377**(2): 544–549 (2008).

38. Gandy, S., Czernik, A. J. and Greengard, P. Phosphorylation of Alzheimer disease amyloid precursor peptide by protein kinase C and Ca2+/calmodulin-dependent protein kinase II. *Proceedings of the National Academy of Sciences of the United States of America* **85**(16): 6218–6221 (1988).

39. Kimberly, W. T., Zheng, J. B., Town, T., Flavell, R. A. and Selkoe, D. J. Physiological regulation of the beta-amyloid precursor protein signaling domain by c-Jun N-terminal kinase JNK3 during neuronal differentiation. *The Journal of Neuroscience: The Official Journal of the Society for Neuroscience* **25**(23): 5533–5543 (2005).

40. Iijima, K., Ando, K., Takeda, S., Satoh, Y., Seki, T., Itohara, S., Greengard, P., Kirino, Y., Nairn, A. C. and Suzuki, T. Neuron-specific phosphorylation of Alzheimer's beta-amyloid precursor protein by cyclin-dependent kinase 5. *Journal of Neurochemistry* **75**(3): 1085–1091 (2000).

41. Aplin, A. E., Gibb, G. M., Jacobsen, J. S., Gallo, J. M. and Anderton, B. H. In vitro phosphorylation of the cytoplasmic domain of the amyloid precursor protein by glycogen synthase kinase-3beta. *Journal of neurochemistry* **67**(2): 699–707 (1996).

42. Taru, H. and Suzuki, T. Facilitation of stress-induced phosphorylation of beta-amyloid precursor protein family members by X11-like/Mint2 protein. *The Journal of Biological Chemistry* **279**(20): 21628–21636 (2004).

43. Suzuki, T., Ando, K., Isohara, T., Oishi, M., Lim, G. S., Satoh, Y., Wasco, W., Tanzi, R. E., Nairn, A. C., Greengard, P., Gandy, S. E. and Kirino, Y. Phosphorylation of Alzheimer beta-amyloid precursor-like proteins. *Biochemistry* **36**(15): 4643–4649 (1997).

44. Ando, K., Iijima, K. I., Elliott, J. I., Kirino, Y. and Suzuki, T. Phosphorylation-dependent regulation of the interaction of amyloid precursor protein with Fe65 affects the production of beta-amyloid. *The Journal of Biological Chemistry* **276**(43): 40353–40361 (2001).

45. Pastorino, L., Sun, A., Lu, P.-J., Zhou, X. Z., Balastik, M., Finn, G., Wulf, G., Lim, J., Li, S.-H., Li, X., Xia, W., Nicholson, L. K. and Lu, K. P. The prolyl isomerase Pin1 regulates amyloid precursor protein processing and amyloid-beta production. *Nature* **440**(7083): 528–534 (2006).

46. Liou, Y.-C., Sun, A., Ryo, A., Zhou, X. Z., Yu, Z.-X., Huang, H.-K., Uchida, T., Bronson, R., Bing, G., Li, X., Hunter, T. and Lu, K. P. Role of the prolyl isomerase Pin1 in protecting against age-dependent neurodegeneration. *Nature* **424**(6948): 556–561 (2003).

47. Drechsel, D. N., Hyman, A. A., Cobb, M. H. and Kirschner, M. W. Modulation of the dynamic instability of tubulin assembly by the microtubule-associated protein tau. *Molecular Biology of the Cell* **3**(10): 1141–1154 (1992).

48. LoPresti, P., Szuchet, S., Papasozomenos, S. C., Zinkowski, R. P. and Binder, L. I. Functional implications for the microtubule-associated protein tau: localization in oligodendrocytes. *Proceedings of the National Academy of Sciences* **92**(22): 10369–10373 (1995).

49. Ebneth, A. Overexpression of Tau Protein Inhibits Kinesin-dependent Trafficking of Vesicles, Mitochondria, and Endoplasmic Reticulum: Implications for Alzheimer's Disease. *The Journal of Cell Biology* **143**(3): 777–794 (1998).

50. McDermott, J. B., Aamodt, S. and Aamodt, E. ptl-1, a Caenorhabditis elegans gene whose products are homologous to the tau microtubule-associated proteins. *Biochemistry* **35**(29): 9415–9423 (1996).

51. Goedert, M., Baur, C. P., Ahringer, J., Jakes, R., Hasegawa, M., Spillantini, M. G., Smith, M. J. and Hill, F. PTL-1, a microtubule-associated protein with tau-like repeats from the nematode Caenorhabditis elegans. *Journal of Cell Science* **109**(Pt 11): 2661–2672 (1996).

52. Irminger-Finger, I., Laymon, R. A. and Goldstein, L. S. Analysis of the primary sequence and microtubule-binding region of the Drosophila 205K MAP. *The Journal of Cell Biology* **111**(6 Pt 1): 2563–2572 (1990).

53. Cambiazo, V., González, M. and Maccioni, R. B. DMAP-85: a tau-like protein from Drosophila melanogaster larvae. *Journal of Neurochemistry* **64**(3): 1288–1297 (1995).

54. Liu, Y., Xia, J., Ma, D., Faber, D. S. and Fischer, I. Tau-like proteins in the nervous system of goldfish. *Neurochemical Research* **22**(12): 1511–1516 (1997).

55. Yin, H. S., Chou, H. C. and Chiu, M. M. Changes in the microtubule proteins in the developing and transected spinal cords of the bullfrog tadpole: induction of microtubule-associated protein 2c and enhanced levels of Tau and tubulin in regenerating central axons. *Neuroscience* **67**(3): 763–775 (1995).

56. Lee, G., Cowan, N. and Kirschner, M. The primary structure and heterogeneity of tau protein from mouse brain. *Science (New York, N.Y.)* **239**(4837): 285–288 (1988).

57. Kosik, K. S. and Finch, E. A. MAP2 and tau segregate into dendritic and axonal domains after the elaboration of morphologically distinct neurites: an immunocytochemical study of cultured rat cerebrum. *The Journal of Neuroscience: The Official Journal of the Society for Neuroscience* **7**(10): 3142–3153 (1987).

58. Himmler, A., Drechsel, D., Kirschner, M. W. and Martin, D. W. Tau consists of a set of proteins with repeated C-terminal microtubule-binding domains and variable N-terminal domains. *Molecular and Cellular Biology* **9**(4): 1381–1388 (1989).

59. Himmler, A. Structure of the bovine tau gene: alternatively spliced transcripts generate a protein family. *Molecular and Cellular Biology* **9**(4): 1389–1396 (1989).

60. Nelson, P. T., Stefansson, K., Gulcher, J. and Saper, C. B. Molecular evolution of tau protein: implications for Alzheimer's disease. *Journal of Neurochemistry* **67**(4): 1622–1632 (1996).

61. Goedert, M., Spillantini, M. G., Potier, M. C., Ulrich, J. and Crowther, R. A. Cloning and sequencing of the cDNA encoding an isoform of microtubule-associated protein tau containing four tandem repeats: differential expression of tau protein mRNAs in human brain. *The EMBO Journal* **8**(2): 393–399 (1989).

62. Goedert, M., Spillantini, M. G., Jakes, R., Rutherford, D. and Crowther, R. A. Multiple isoforms of human microtubule-associated protein tau: sequences and localization in neurofibrillary tangles of Alzheimer's disease. *Neuron* **3**(4): 519–526 (1989).

63. Tucker, R. P. The roles of microtubule-associated proteins in brain morphogenesis: a review. *Brain Research. Brain Research Reviews* **15**(2): 101–120

64. Chin, S. S. and Goldman, J. E. Glial inclusions in CNS degenerative diseases. *Journal of Neuropathology and Experimental Neurology* **55**(5): 499–508 (1996).

65. Ingelson, M., Vanmechelen, E. and Lannfelt, L. Microtubule-associated protein tau in human fibroblasts with the Swedish Alzheimer mutation. *Neuroscience Letters* **220**(1): 9–12 (1996).

66. Gu, Y., Oyama, F. and Ihara, Y. Tau is widely expressed in rat tissues. *Journal of Neurochemistry* **67**(3): 1235–1244 (1996).

67. Vanier, M. T., Neuville, P., Michalik, L. and Launay, J. F. Expression of specific tau exons in normal and tumoral pancreatic acinar cells. *Journal of Cell Science* **111**(1): 1419–1432 (1998).

68. MAPT microtubule-associated protein tau [Homo sapiens (human)]. (2014). at <http://www.ncbi.nlm.nih.gov/gene/4137> (Accessed May 26, 2014).

69. Pittman, A. M., Fung, H.-C. and de Silva, R. Untangling the tau gene association with neurodegenerative disorders. *Human Molecular Genetics* **15**(2): R188–195 (2006).

70. P10636 (TAU_HUMAN). (2014). at <http://www.uniprot.org/uniprot/P10636> (Accessed May 21, 2014).

71. Neve, R. L., Harris, P., Kosik, K. S., Kurnit, D. M. and Donlon, T. A. Identification of cDNA clones for the human microtubule-associated protein tau and chromosomal localization of the genes for tau and microtubule-associated protein 2. *Molecular Brain Research* **1**(3): 271–280 (1986).

72. Buée, L., Bussière, T., Buée-Scherrer, V., Delacourte, A. and Hof, P. R. Tau protein isoforms, phosphorylation and role in neurodegenerative disorders. *Brain Research. Brain Research Reviews* **33**(1): 95–130 (2000).

73. Inoue, H., Hiradate, Y., Shirakata, Y., Kanai, K., Kosaka, K., Gotoh, A., Fukuda, Y., Nakai, Y., Uchida, T., Sato, E. and Tanemura, K. Site-specific phosphorylation of Tau protein is associated with deacetylation of microtubules in mouse spermatogenic cells during meiosis. *FEBS Letters* **588**(11): 2003–2008 (2014).

74. Kosik, K. S., Kowall, N. W. and McKee, A. Along the way to a neurofibrillary tangle: a look at the structure of tau. *Annals of Medicine* **21**(2): 109–112 (1989).

75. Kosik, K. S., Orecchio, L. D., Bakalis, S. and Neve, R. L. Developmentally regulated expression of specific tau sequences. *Neuron* **2**(4): 1389–1397 (1989).

76. Goedert, M. and Jakes, R. Expression of separate isoforms of human tau protein: correlation with the tau pattern in brain and effects on tubulin polymerization. *The EMBO Journal* **9**(13): 4225–4230 (1990).

77. Lee, G., Neve, R. L. and Kosik, K. S. The microtubule binding domain of tau protein. *Neuron* **2**(6): 1615–1624 (1989).

78. Binder, L. I. The distribution of tau in the mammalian central nervous system. *The Journal of Cell Biology* **101**(4): 1371–1378 (1985).

79. Kosik, K. S. Tau protein and Alzheimer's disease. *Current Opinion in Cell Biology* **2**(1): 101–104 (1990).

80. Sergeant, N., Bretteville, A., Hamdane, M., Caillet-Boudin, M.-L., Grognet, P., Bombois, S., Blum, D., Delacourte, A., Pasquier, F., Vanmechelen, E., Schraen-Maschke, S. and Buée, L. Biochemistry of Tau in Alzheimer's disease and related neurological disorders. *Expert Review of Proteomics* **5**(2): 207–224 (2008).

81. Hanger, D. P., Betts, J. C., Loviny, T. L., Blackstock, W. P. and Anderton, B. H. New phosphorylation sites identified in hyperphosphorylated tau (paired helical filament-tau) from Alzheimer's disease brain using nanoelectrospray mass spectrometry. *Journal of Neurochemistry* **71**(6): 2465–2476 (1998).

82. Morishima-Kawashima, M., Hasegawa, M., Takio, K., Suzuki, M., Yoshida, H., Titani, K. and Ihara, Y. Proline-directed and non-proline-directed phosphorylation of PHF-tau. *The Journal of Biological Chemistry* **270**(2): 823–829 (1995).

83. Buée, L., Troquier, L., Burnouf, S., Belarbi, K., Van der Jeugd, A., Ahmed, T., Fernandez-Gomez, F., Caillierez, R., Grosjean, M.-E., Begard, S., Barbot, B., Demeyer, D., Obriot, H., Brion, I., Buée-Scherrer, V., Maurage, C.-A., Balschun, D., D'hooge, R., Hamdane, M., Blum, D. and Sergeant, N. From tau phosphorylation to tau aggregation: what about neuronal death? *Biochemical Society transactions* **38**(4): 967–972 (2010).

84. Lindwall, G. and Cole, R. D. Phosphorylation affects the ability of tau protein to promote microtubule assembly. *The Journal of Biological Chemistry* **259**(8): 5301–5305 (1984).

85. Biernat, J., Gustke, N., Drewes, G., Mandelkow, E. M. and Mandelkow, E. Phosphorylation of Ser262 strongly reduces binding of tau to microtubules: distinction between PHF-like immunoreactivity and microtubule binding. *Neuron* **11**(1): 153–163 (1993).

86. Weingarten, M. D., Lockwood, A. H., Hwo, S. Y. and Kirschner, M. W. A protein factor essential for microtubule assembly. *Proceedings of the National Academy of Sciences* **72**(5): 1858–1862 (1975).

87. Grundke-Iqbal, I., Iqbal, K., Tung, Y. C., Quinlan, M., Wisniewski, H. M. and Binder, L. I. Abnormal phosphorylation of the microtubule-associated protein tau (tau) in Alzheimer cytoskeletal pathology. *Proceedings of the National Academy of Sciences* **83**(13): 4913–4917 (1986).

88. Wang, J.-Z., Xia, Y.-Y., Grundke-Iqbal, I. and Iqbal, K. Abnormal hyperphosphorylation of tau: sites, regulation, and molecular mechanism of neurofibrillary degeneration. *Journal of Alzheimer's Disease* **33 Suppl 1**: S123–S139 (2013).

89. Lee, G. and Leugers, C. J. Tau and tauopathies. *Progress in Molecular Biology and Translational Science* **107**: 263–293 (2012).

90. Lee, V. M., Goedert, M. and Trojanowski, J. Q. Neurodegenerative tauopathies. *Annual Review of Neuroscience* **24**: 1121–1159 (2001).

91. Hernández, F. and Avila, J. Tauopathies. *Cellular and Molecular Life Sciences* **64**(17): 2219–2233 (2007).

92. Ludolph, A. C., Kassubek, J., Landwehrmeyer, B. G., Mandelkow, E., Mandelkow, E.-M., Burn, D. J., Caparros-Lefebvre, D., Frey, K. A., de Yebenes, J. G., Gasser, T., Heutink, P., Höglinger, G., Jamrozik, Z., Jellinger, K. A., Kazantsev, A., Kretzschmar, H., Lang, A. E., Litvan, I., Lucas, J. J., McGeer, P. L., Melquist, S., Oertel, W., Otto, M., Paviour, D., Reum, T., Saint-Raymond, A., Steele, J. C., Tolnay, M., Tumani, H., van Swieten, J. C., Vanier, M. T., Vonsattel, J.-P., Wagner, S. and Wszolek, Z. K. Tauopathies with parkinsonism: clinical spectrum, neuropathologic basis, biological markers, and treatment options. *European Journal of Neurology: The Official Journal of the European Federation of Neurological Societies* **16**(3): 297–309 (2009).

93. Hanger, D. P., Anderton, B. H. and Noble, W. Tau phosphorylation: the therapeutic challenge for neurodegenerative disease. *Trends in Molecular Medicine* **15**(3): 112–119 (2009).

94. Alonso, A. C., Zaidi, T., Grundke-Iqbal, I. and Iqbal, K. Role of abnormally phosphorylated tau in the breakdown of microtubules in Alzheimer disease. *Proceedings of the National Academy of Sciences* **91**(12): 5562–5566 (1994).

95. Alonso, A. C., Grundke-Iqbal, I. and Iqbal, K. Alzheimer's disease hyperphosphorylated tau sequesters normal tau into tangles of filaments and disassembles microtubules. *Nature Medicine* **2**(7): 783–787 (1996).

96. Gustke, N., Steiner, B., Mandelkow, E.-M., Biernat, J., Meyer, H. E., Goedert, M. and Mandelkow, E. The Alzheimer-like phosphorylation of tau protein reduces microtubule binding and involves Ser-Pro and Thr-Pro motifs. *FEBS Letters* **307**(2): 199–205 (1992).

97. Ivy, G. O., Kitani, K. and Ihara, Y. Anomalous accumulation of τ and ubiquitin immunoreactivities in rat brain caused by protease inhibition and by normal aging: a clue to PHF pathogenesis? *Brain Research* **498**(2): 360–365 (1989).

98. Grundke-Iqbal, I., Iqbal, K., Quinlan, M., Tung, Y., Zaidi, M. and Wisniewski, H. Microtubule-associated protein tau. A component of Alzheimer paired helical filaments. *The Journal of Biological Chemistry* **261**(13): 6084–6089 (1986).

99. Berger, Z., Roder, H., Hanna, A., Carlson, A., Rangachari, V., Yue, M., Wszolek, Z., Ashe, K., Knight, J., Dickson, D., Andorfer, C., Rosenberry, T. L., Lewis, J., Hutton, M. and Janus, C. Accumulation of pathological tau species and memory loss in a conditional model of tauopathy. *The Journal of Neuroscience: The Official Journal of the Society for Neuroscience* **27**(14): 3650–3662 (2007).

100. Iqbal, K., Liu, F., Gong, C.-X., Alonso, A. D. C. and Grundke-Iqbal, I. Mechanisms of tau-induced neurodegeneration. *Acta Neuropathologica* **118**(1): 53–69 (2009).

101. Rapoport, M., Dawson, H. N., Binder, L. I., Vitek, M. P. and Ferreira, A. Tau is essential to β-amyloid-induced neurotoxicity. *Proceedings of the National Academy of Sciences of the United States of America* **99**(9): 6364–6369 (2002).

102. Roberson, E. D., Scearce-Levie, K., Palop, J. J., Yan, F., Cheng, I. H., Wu, T., Gerstein, H., Yu, G.-Q. and Mucke, L. Reducing endogenous tau ameliorates amyloid beta-induced deficits in an Alzheimer's disease mouse model. *Science (New York, N.Y.)* **316**(5825): 750–754 (2007).

103. Ke, Y. D., Suchowerska, A. K., van der Hoven, J., De Silva, D. M., Wu, C. W., van Eersel, J., Ittner, A. and Ittner, L. M. Lessons from tau-deficient mice. *International Journal of Alzheimer's Disease* **2012**: 8 pages (2012).

104. Singh, K. and Jaiswal, D. Human male infertility: a complex multifactorial phenotype. *Reproductive Sciences* **18**(5): 418–425 (2011).

105. Hunter, D., Anand-Ivell, R., Danner, S. and Ivell, R. Models of in vitro spermatogenesis. *Spermatogenesis* **2**(1): 32–43 (2012).

106. Okabe, M., Ikawa, M. and Ashkenas, J. Male infertility and the genetics of spermatogenesis. *American Journal of Human Genetics* **62**(6): 1274–1281 (1998).

107. Ross, M. H. and Pawlina, W. in *Histology: a text and atlas: with correlated cell and molecular biology* 784–829 (Wolters Kluwer, Lippincott Williams & Wilkins, 2011).

108. Jamsai, D. and O'Bryan, M. K. Mouse models in male fertility research. *Asian Journal of Andrology* **13**(1): 139–151 (2011).

109. Junqueira, L. C. and Carneiro, J. *Basic Histology: Text and Atlas*. (McGraw-Hill Medical, 2005).

110. Mescher, A. *Junqueira's Basic Histology: Text and Atlas*. (McGraw-Hill Medical, 2010).

111. Hess, R. A. and Renato de Franca, L. Spermatogenesis and cycle of the seminiferous epithelium. *Advances in Experimental Medicine and Biology* **636**: 1–15 (2008).

112. França, L. R., Ogawa, T., Avarbock, M. R., Brinster, R. L. and Russell, L. D. Germ cell genotype controls cell cycle during spermatogenesis in the rat. *Biology of Reproduction* **59**(6): 1371–1377 (1998).

113. Johnson, L., Petty, C. S. and Neaves, W. B. A comparative study of daily sperm production and testicular composition in humans and rats. *Biology of Reproduction* **22**(5): 1233–1243 (1980).

114. Hwang, K., Yatsenko, A. N., Jorgez, C. J., Mukherjee, S., Nalam, R. L., Matzuk, M. M. and Lamb, D. J. Mendelian genetics of male infertility. *Annals of the New York Academy of Sciences* **1214**(The Year in Human and Medical Genetics): E1–E17 (2010).

115. Sharma, R., Biedenharn, K. R., Fedor, J. M. and Agarwal, A. Lifestyle factors and reproductive health: taking control of your fertility. *Reproductive Biology and Endocrinology* **11**: 66 (2013).

116. Krausz, C. in *The Genetics of Male Infertility* (ed. Carrell, D. T.) 275–289 (Humana Press, 2007). doi:10.1007/978-1-59745-176-5

117. Savvas, M. and Hamoda, H. in *Frontiers in Gynecological Endocrinology* (eds. Genazzani, A. R. & Brincat, M.) 119–125 (Springer International Publishing, 2014). doi:10.1007/978-3-319-03494-2_11

118. Zheng, H., Jiang, M., Trumbauer, M. E., Sirinathsinghji, D. J., Hopkins, R., Smith, D. W., Heavens, R. P., Dawson, G. F. R., Boyce, S., Conner, M. W., Stevens, K. A., Slunt, H. H., Sisoda, S. S., Chen, H. Y. and Van der Ploeg, L. H. β-Amyloid Precursor Protein-Deficient Show Reactive Gliosis and Decreased Locomotor Activity. *Cell* **81**(4): 525–531 (1995).

119. Zheng, H. and Jiang, M. Mice deficient for the amyloid precursor protein gene. *Annals of the New York Academy of Sciences* (908): 421–426 (1996).

120. Koch, C. Von, Zheng, H. and Chen, H. Generation of APLP2 KO mice and early postnatal lethality in APLP2/APP double KO mice. *Neurobiology of Aging* **18**(6): 661–669 (1997).

121. Fisher, S. Expression of the amyloid precursor protein gene in mouse oocytes and embryos. *Proceedings of the National Academy of Sciences of the United States of America* **88**(5): 1779–1782 (1991).

122. Shoji, M. and Kawarabayashi, T. Alzheimer amyloid beta-protein precursor in sperm development. *American Journal of Pathology* **137**(5): 1027–1032 (1990).

123. Beer, J., Masters, C. L. and Beyreuther, K. Cells from peripheral tissues that exhibit high APP expression are characterized by their high membrane fusion activity. *Neurodegeneration* **4**(1): 51–59 (1995).

124. Fardilha, M., Vieira, S. I., Barros, A., Sousa, M., Da Cruz e Silva, O. a B. and Da Cruz e Silva, E. F. Differential distribution of Alzheimer's amyloid precursor protein family variants in human sperm. *Annals of the New York Academy of Sciences* **1096**: 196–206 (2007).

125. Harada, A., Oguchi, K., Okabe, S., Kuno, J., Terada, S., Ohshima, T., Sato-Yoshitake, R., Takei, Y., Noda, T. and Hirokawa, N. Altered microtubule organization in small-calibre axons of mice lacking tau protein. *Nature* **369**(6480): 488–491 (1994).

126. Dawson, H. N., Ferreira, A., Eyster, M. V, Ghoshal, N., Binder, L. I. and Vitek, M. P. Inhibition of neuronal maturation in primary hippocampal neurons from tau deficient mice. *Journal of Cell Science* **114**(Pt 6): 1179–1187 (2001).

127. Tucker, K. L., Meyer, M. and Barde, Y. A. Neurotrophins are required for nerve growth during development. *Nature Neuroscience* **4**(1): 29–37 (2001).

128. Lei, P., Ayton, S., Finkelstein, D. I., Spoerri, L., Ciccotosto, G. D., Wright, D. K., Wong, B. X. W., Adlard, P. A., Cherny, R. A., Lam, L. Q., Roberts, B. R., Volitakis, I., Egan, G. F., McLean, C. A., Cappai, R., Duce, J. A. and Bush, A. I. Tau deficiency induces parkinsonism with dementia by impairing APP-mediated iron export. *Nature Medicine* **18**(2): 291–295 (2012).

129. Ikegami, S., Harada, A. and Hirokawa, N. Muscle weakness, hyperactivity, and impairment in fear conditioning in tau-deficient mice. *Neuroscience Letters* **279**(3): 129–132 (2000).

130. Ashman, J. B., Hall, E. S., Eveleth, J. and Boekelheide, K. Tau, the neuronal heat-stable microtubule-associated protein, is also present in the cross-linked microtubule network of the testicular spermatid manchette. *Biology of Reproduction* **46**(1): 120–129 (1992).

131. Klein, T. and Bischoff, R. Active metalloproteases of the A Disintegrin and Metalloprotease (ADAM) family: biological function and structure. *Journal of Proteome Research* **10**(1): 17–33 (2011).

132. Luo, Y., Bolon, B., Kahn, S., Bennett, B. D., Babu-Khan, S., Denis, P., Fan, W., Kha, H., Zhang, J., Gong, Y., Martin, L., Louis, J. C., Yan, Q., Richards, W. G., Citron, M. and Vassar, R. Mice deficient in BACE1, the Alzheimer's beta-secretase, have normal phenotype and abolished beta-amyloid generation. *Nature Neuroscience* **4**(3): 231–232 (2001).

133. Dominguez, D., Tournoy, J., Hartmann, D., Huth, T., Cryns, K., Deforce, S., Serneels, L., Camacho, I. E., Marjaux, E., Craessaerts, K., Roebroek, A. J. M., Schwake, M., D'Hooge, R., Bach, P., Kalinke, U., Moechars, D., Alzheimer, C., Reiss, K., Saftig, P. and De Strooper, B. Phenotypic and biochemical analyses of BACE1- and BACE2-deficient mice. *The Journal of Biological Chemistry* **280**(35): 30797–30806 (2005).

134. Arduengo, P. M., Appleberry, O. K., Chuang, P. and L'Hernault, S. W. The presenilin protein family member SPE-4 localizes to an ER/Golgi derived organelle and is required for proper cytoplasmic partitioning during Caenorhabditis elegans spermatogenesis. *Journal of Cell Science* **111**(24): 3645–3654 (1998).

135. Dirami, G., Ravindranath, N., Achi, M. V and Dym, M. Expression of Notch pathway components in spermatogonia and Sertoli cells of neonatal mice. *Journal of andrology* **22**(6): 944–52

136. Shen, J., Bronson, R. T., Chen, D. F., Xia, W., Selkoe, D. J. and Tonegawa, S. Skeletal and CNS defects in Presenilin-1-deficient mice. *Cell* **89**(4): 629–639 (1997).

137. Herreman, A., Hartmann, D., Annaert, W., Saftig, P., Craessaerts, K., Serneels, L., Umans, L., Schrijvers, V., Checler, F., Vanderstichele, H., Baekelandt, V., Dressel, R., Cupers, P., Huylebroeck, D., Zwijsen, A., Van Leuven, F. and De Strooper, B. Presenilin 2 deficiency causes a mild pulmonary phenotype and no changes in amyloid precursor protein processing but enhances the embryonic lethal phenotype of presenilin 1 deficiency. *Proceedings of the National Academy of Sciences of the United States of America* **96**(21): 11872–11877 (1999).

138. *Bancroft's Theory and Practice of Histological Techniques*. 576 (Churchill Livingstone, 2013).

139. Boenisch, T. in *Immunohistochemical Staining Methods Education Guide* (eds. Kumar, G. L. & Rudbeck, L.) 1–10 (Dako, 2009).

140. Boenisch, T. in *Immunohistochemical Staining Methods Education Guide* (eds. Kumar, G. L. & Rudbeck, L.) 1–10 (Dako, 2009).

141. Da Cruz e Silva, E. F., Fox, C. A., Ouimet, C. C., Gustafson, E., Watson, S. J. and Greengard, P. Differential expression of protein phosphatase 1 isoforms in mammalian brain. *The Journal of neuroscience : the official journal of the Society for Neuroscience* **15**(5 Pt 1): 3375–89 (1995).

142. Shi, S.-R., Shi, Y. and Taylor, C. R. Antigen retrieval immunohistochemistry: review and future prospects in research and diagnosis over two decades. *The Journal of Histochemistry and Cytochemistry: Official Journal of the Histochemistry Society* **59**(1): 13–32 (2011).

143. Snider, J. Blocking Strategies for IHC. at <http://www.piercenet.com/method/blocking-strategies-ihc#optimizing> (Accessed September 3, 2014).

144. Christensen, N. K. and Winther, L. in *Immunohistochemical Staining Methods Education Guide* (eds. Kumar, G. L. & Rudbeck, L.) 103–108 (Dako, 2009).

145. Mahmood, T. and Yang, P.-C. Western blot: technique, theory, and trouble shooting. *North American Journal of Medical Sciences* **4**(9): 429–434 (2012).

146. Thermo Scientific Pierce. Pierce™ BCA Protein Assay Kit. at <https://www.piercenet.com/instructions/2161296.pdf> (Accessed August 18, 2014).

147. *Western Blotting: Principles and Methods*. 192 pages (GE Healthcare Life Sciences).

148. Miquel, J., Lundgren, P. R. and Johnson, J. E. Spectrophotofluorometric and Electron Microscopic Study of Lipofuscin Accumulation in the Testis of Aging Mice. *Journal of Gerontology* **33**(1): 5–19 (1978).

149. Terman, A. and Brunk, U. T. Lipofuscin. *The International Journal of Biochemistry & Cell Biology* **36**(8): 1400–1404 (2004).

150. Yin, D. and Brunk, U. Autofluorescent Ceroid/Lipofuscin . *Free Radical and Antioxidant Protocols* **108** : 217–227 (1998).

151. Yang, Y. and Honaramooz, A. Characterization and quenching of autofluorescence in piglet testis tissue and cells. *Anatomy Research International* **2012**: 10 pages (2012).

152. Viegas, M. S., Martins, T. C., Seco, F. and do Carmo, A. An improved and cost-effective methodology for the reduction of autofluorescence in direct immunofluorescence studies on formalin-fixed paraffin-embedded tissues. *European Journal of Histochemistry* **51**(1): 59–66

153. Robertson, D., Savage, K., Reis-Filho, J. S. and Isacke, C. M. Multiple immunofluorescence labelling of formalin-fixed paraffin-embedded (FFPE) tissue. *BMC Cell Biology* **9**: 13 (2008).

154. Drubin, D. G. and Kirschner, M. W. Tau protein function in living cells. *The Journal of Cell Biology* **103**(6 Pt 2): 2739–2746 (1986).

155. Kanai, Y., Takemura, R., Oshima, T., Mori, H., Ihara, Y., Yanagisawa, M., Masaki, T. and Hirokawa, N. Expression of multiple tau isoforms and microtubule bundle formation in fibroblasts transfected with a single tau cDNA. *The Journal of Cell Biology* **109**(3): 1173–1184 (1989).

156. Fardilha, M., Esteves, S. L. C., Korrodi-Gregório, L., Pelech, S., da Cruz E Silva, O. A. B. and da Cruz E Silva, E. Protein phosphatase 1 complexes modulate sperm motility and present novel targets for male infertility. *Molecular Human Reproduction* **17**(8): 466–477 (2011).

157. Li, J., Sinha, N., Vijayaraghavan, S. and Chen, Y. Expression of Protein Phosphatase PP1 Isoforms in Developing Mouse Embryos. *Biology of Reproduction* **85**(Meeting Abstract): 255 (2011).

158. Varmuza, S., Jurisicova, A., Okano, K., Hudson, J., Boekelheide, K. and Shipp, E. B. Spermiogenesis is impaired in mice bearing a targeted mutation in the protein phosphatase 1cgamma gene. *Developmental Biology* **205**(1): 98–110 (1999).

159. Chakrabarti, R., Kline, D., Lu, J., Orth, J., Pilder, S. and Vijayaraghavan, S. Analysis of Ppp1cc-null mice suggests a role for PP1gamma2 in sperm morphogenesis. *Biology of Reproduction* **76**(6): 992–1001 (2007).

160. The Human Protein Atlas. APP. at <http://www.proteinatlas.org/ENSG00000142192/tissue> (Accessed October 22, 2014).

161. Podlisny, M. B., Tolan, D. R. and Selkoe, D. J. Homology of the amyloid beta protein precursor in monkey and human supports a primate model for beta amyloidosis in Alzheimer's disease. *The American journal of pathology* **138**(6): 1423–35 (1991).

162. Konietzko, U. AICD nuclear signaling and its possible contribution to Alzheimer's disease. *Current Alzheimer Research* **9**(2): 200–216 (2012).

163. Acevedo, K. M., Opazo, C. M., Norrish, D., Challis, L. M., Li, Q.-X., White, A. R., Bush, A. I. and Camakaris, J. Phosphorylation of amyloid precursor protein at threonine 668 is essential for its copper-responsive trafficking in SH-SY5Y neuroblastoma cells. *The Journal of Biological Chemistry* **289**(16): 11007–11019 (2014).

164. Ramelot, T. A. and Nicholson, L. K. Phosphorylation-induced structural changes in the amyloid precursor protein cytoplasmic tail detected by NMR. *Journal of Molecular Biology* **307**(3): 871–884 (2001).

165. Muresan, Z. and Muresan, V. Coordinated transport of phosphorylated amyloid-beta precursor protein and c-Jun NH2-terminal kinase-interacting protein-1. *The Journal of Cell Biology* **171**(4): 615–625 (2005).

166. Ando, K., Oishi, M., Takeda, S., Iijima, K., Isohara, T., Nairn, A. C., Kirino, Y., Greengard, P. and Suzuki, T. Role of phosphorylation of Alzheimer's amyloid precursor protein during neuronal differentiation. *The Journal of Neuroscience: The Official Journal of the Society for Neuroscience* **19**(11): 4421–4427 (1999).

167. Muresan, Z. and Muresan, V. A phosphorylated, carboxy-terminal fragment of beta-amyloid precursor protein localizes to the splicing factor compartment. *Human Molecular Genetics* **13**(5): 475–488 (2004).

168. Chang, K.-A., Kim, H.-S., Ha, T.-Y., Ha, J.-W., Shin, K. Y., Jeong, Y. H., Lee, J.-P., Park, C.-H., Kim, S., Baik, T.-K. and Suh, Y.-H. Phosphorylation of amyloid precursor protein (APP) at Thr668 regulates the nuclear translocation of the APP intracellular domain and induces neurodegeneration. *Molecular and Cellular Biology* **26**(11): 4327–4338 (2006).

169. Matsushima, T., Saito, Y., Elliott, J. I., Iijima-Ando, K., Nishimura, M., Kimura, N., Hata, S., Yamamoto, T., Nakaya, T. and Suzuki, T. Membrane-microdomain localization of amyloid β-precursor protein (APP) C-terminal fragments is regulated by phosphorylation of the cytoplasmic Thr668 residue. *The Journal of Biological Chemistry* **287**(23): 19715–19724 (2012).

170. Nakaya, T. and Suzuki, T. Role of APP phosphorylation in FE65-dependent gene transactivation mediated by AICD. *Genes to Cells: devoted to molecular & cellular mechanisms* **11**(6): 633–645 (2006).

171. Judge, M., Hornbeck, L., Potter, H. and Padmanabhan, J. Mitosis-specific phosphorylation of amyloid precursor protein at threonine 668 leads to its altered processing and association with centrosomes. *Molecular Neurodegeneration* **6**: 80 (2011).

172. Vandré, D. D., Centonze, V. E., Peloquin, J., Tombes, R. M. and Borisy, G. G. Proteins of the mammalian mitotic spindle: phosphorylation/dephosphorylation of MAP-4 during mitosis. *Journal of Cell Science* **98 (Pt 4)**: 577–588 (1991).

173. Hansel, D. E., Rahman, A., Wehner, S., Herzog, V., Yeo, C. J. and Maitra, A. Increased expression and processing of the Alzheimer amyloid precursor protein in pancreatic cancer may influence cellular proliferation. *Cancer Research* **63**(21): 7032–7037 (2003).

174. Casas, C., Sergeant, N., Itier, J.-M., Blanchard, V., Wirths, O., van der Kolk, N., Vingtdeux, V., van de Steeg, E., Ret, G., Canton, T., Drobecq, H., Clark, A., Bonici, B., Delacourte, A., Benavides, J., Schmitz, C., Tremp, G., Bayer, T. A., Benoit, P. and Pradier, L. Massive CA1/2 neuronal loss with intraneuronal and N-terminal truncated Abeta42 accumulation in a novel Alzheimer transgenic model. *The American Journal of Pathology* **165**(4): 1289–1300 (2004).

175. Yamada, Y., Fujimura, T., Takahashi, S., Takayama, K., Urano, T., Murata, T., Obinata, D., Ouchi, Y., Homma, Y. and Inoue, S. Clinical significance of amyloid precursor protein in patients with testicular germ cell tumor. *Advances in Urology* **2013**(Article ID 348438): 6 pages (2013).

176. Nizzari, M., Venezia, V., Bianchini, P., Caorsi, V., Diaspro, A., Repetto, E., Thellung, S., Corsaro, A., Carlo, P., Schettini, G., Florio, T. and Russo, C. Amyloid precursor protein and Presenilin 1 interaction studied by FRET in human H4 cells. *Annals of the New York Academy of Sciences* **1096**: 249–257 (2007).

177. Nizzari, M., Venezia, V., Repetto, E., Caorsi, V., Magrassi, R., Gagliani, M. C., Carlo, P., Florio, T., Schettini, G., Tacchetti, C., Russo, T., Diaspro, A. and Russo, C. Amyloid precursor protein and Presenilin1 interact with the adaptor GRB2 and modulate ERK 1,2 signaling. *The Journal of Biological Chemistry* **282**(18): 13833–13844 (2007).

178. Sandbrink, R., Masters, C. L. and Beyreuther, K. Beta A4-amyloid protein precursor mRNA isoforms without exon 15 are ubiquitously expressed in rat tissues including brain, but not in neurons. *The Journal of Biological Chemistry* **269**(2): 1510–1517 (1994).

179. Caporaso, G. L., Gandy, S. E., Buxbaum, J. D., Ramabhadran, T. V and Greengard, P. Protein phosphorylation regulates secretion of Alzheimer beta/A4 amyloid precursor protein. *Proceedings of the National Academy of Sciences of the United States of America* **89**(7): 3055–9 (1992).

180. Vella, L. J. and Cappai, R. Identification of a novel amyloid precursor protein processing pathway that generates secreted N-terminal fragments. *FASEB Journal: Official Publication of the Federation of American Societies for Experimental Biology* **26**(7): 2930–2940 (2012).

181. Porayette, P., Gallego, M. J., Kaltcheva, M. M., Bowen, R. L., Vadakkadath Meethal, S. and Atwood, C. S. Differential processing of amyloid-beta precursor protein directs human embryonic stem cell proliferation and differentiation into neuronal precursor cells. *The Journal of Biological Chemistry* **284**(35): 23806–23817 (2009).

182. Lewis, S. A., Lee, M. G. and Cowan, N. J. Five mouse tubulin isotypes and their regulated expression during development. *The Journal of Cell Biology* **101**(3): 852–861 (1985).

183. Sengupta, P. A Scientific Review of Age Determination for a Laboratory Rat: How Old is it in Comparison with Human Age? *Biomedicine International* **2**: 81–89 (2011).

184. Paul, C. and Robaire, B. Impaired function of the blood-testis barrier during aging is preceded by a decline in cell adhesion proteins and GTPases. *PloS One* **8**(12): e84354 (2013).

9. Appendix

Immunohistochemistry Solutions

Blocking Buffer (20 mL)

0.1% v/v Triton X-100 ..... 20 µL
4% v/v Foetal Bovine Serum (FBS)..... 800 µL
5% w/v Bovine Serum Albumin (BSA)..... 1 g
Phosphate Buffered Saline (PBS) 1x ..... make up to 20 mL
Store at 4°C

Citric Acid Solution, Sodium Citrate Solution, and Sodium Citrate Buffer

a) 0.1 M Citric Acid Solution (1 L)

Citric Acid Monohydrate ($C_6H_8O_7.H_2O$) ..... 21.01 g
Deionized H_2O..... make up to 1 L
Store at 4°C

b) 0.1 M Sodium Citrate Solution (1 L)

Trisodium Citrate Dihydrate ($Na_3C_6H_5O_7.2H_2O$) ..... 29.41 g
Deionized H_2O..... make up to 1 L
Store at 4°C

c) 0.01 M Sodium Citrate Buffer, pH 6.0 (500 mL)

Citric Acid Solution (0.1 M stock solution) ..... 9 mL
Sodium Citrate Solution (0.1 M stock solution) ..... 41 mL
Deionized H_2O..... make up to 500 mL
Adjust pH to 6.0 ± 0.2 and store at 4°C

Ethanol 90%, 80% and 70%

	EtOH 90%	EtOH 80%	EtOH 70%
Ethanol absolute	450 mL	400 mL	350 mL
Deionized H_2O	50 mL	100 mL	150 mL

Phosphate Buffered Saline (PBS) 1x, pH 7.4 (500 mL)

For a final volume of 500 mL, dissolve one pack of BupH™ Modified Dulbecco's Phosphate Buffered Saline Pack (Thermo Scientific Pierce) in deionized H_2O. Final composition: 0.002 M Potassium Phosphate; 0.008 M Sodium Phosphate; 0.01 M Potassium Chloride; 0.14 M Sodium Chloride. Store at 4°C.

Western Blot Analysis Solutions

Ammonium Persulphate (APS) 10% (10 mL)

10% w/v APS.....1 g
Deionized H_2O .....make up to 10 mL
Store at 4°C by a maximum of one week

Loading Buffer (LB) 4x (10 mL)

Tris (1 M, pH 6.8 stock solution) .....2.5 mL
0.01% w/v Bromophenol Blue.....1 mg
2% v/v β-mercaptoethanol .....2 mL
8% w/v SDS.....0.8 g
40% v/v glycerol .....4 mL
Deionized H_2O .....make up to 10 mL

Lower Gel Buffer (LGB) 4x, pH 8.9 (500 mL)

Tris base.....90.825 g
Sodium Dodecyl Sulphate (SDS).....2 g
Deionized H_2O .....make up to 500 mL
Adjust pH to 8.9 ± 0.2 and store at 4°C

Lysis Buffer (20 mL)

Tris-HCl, pH 8.0 (50 mM, pH 8.0 stock solution).....1 mL
NaCl (120 mM stock solution).....2.4 mL
4% w/v 3[(3-Cholamidopropyl)dimethylammonio]-propanesulfonic acid (CHAPS)
.....0.8 g
Protease Inhibitors:

Leupeptin (5 mg/mL stock solution) ..... 4 µL
Pepstatin A (1 mg/mL stock solution in DMSO)..... 132.2 µL
Aprotinin (2.1 mg/mL stock solution) ..... 240 µL
Phenylmethylsulfonyl Fluoride (PMSF) (100 mM stock solution) 977.8 µL
Benzamidine (200 mM stock solution) ..... 1000 µL
Sterile Deionized H_2O ..... make up to 20 mL

Resolving Gel (lower gel), 1 system – 5-20% gradient SDS polyacrylamide gel

	5%	**20%**
Sterile Deionized H_2O	17.4 mL	2.2 mL
LGB	7.5 mL	7.5 mL
Acrylamide 30%	5 mL	20 mL
APS	150 µL	150 µL
N,N,N',N'-Tetramethylethylenediamine (TEMED)	15 µL	15 µL

Running Buffer 10x, pH 8.3 (1 L)

Tris base ..... 30.3 g (250 mM)
Glycine ..... 150.14 g (2 M)
1% w/v Sodium Dodecyl Sulphate (SDS) ..... 10 g
Deionized H_2O..... make up to 1 L
Adjust pH to 8.3 ± 0.2

Sodium Dodecyl Sulphate (SDS) 10% (10 mL)

10% w/v SDS ..... 1 g
Deionized H_2O..... make up to 10 mL

Stacking gel (upper gel), 1 system – 3.5% SDS polyacrylamide gel

Sterile Deionized H_2O ..... 13.2 mL
Upper Gel Buffer (UGB) ..... 4 mL
Acrylamide 30% ..... 2.4 mL
SDS 10% ..... 200 µL
APS ..... 200 µL
N,N,N',N'-Tetramethylethylenediamine (TEMED) ..... 20 µL

Transfer Buffer 10x (2 L)

Tris base.....60.57 g
Glycine.....280.0 g
Deionized H_2O.....make up to 2 L

Transfer Buffer 1x, pH 8.3 (1 L)

Transfer 10x.....100 mL
Methanol.....200 mL
Deionized H_2O.....make up to 1 L
Adjust pH to 8.3 ± 0.2

1 M Tris, pH 6.8 (150 mL)

Tris base.....30.3 g
Deionized H_2O.....make up to 150 mL
Adjust pH to 6.8 ± 0.2

Upper Gel Buffer (UGB) 5x, pH 6.8 (500 mL)

Tris base.....37.845 g
Deionized H_2O.....make up to 500 mL
Adjust pH to 6.8 ± 0.2 and store at 4°C

Immunoblotting Solutions

ECL detection reagent

Solution A:

3-aminophthalhydrazide (luminol) (20 mM stock solution in DMSO)
.....1.25 mL (0.1 mM)
4-iodophenol (100 mM stock solution in DMSO).....5 mL (2 mM)
Tris (0.1 M, pH 9.35 stock solution).....125 mL (50 mM)
Deionized H_2O.....make up to 250 mL
Protect from light store at 4°C

Solution B: hydrogen peroxide

Store at 4°C and just before use add 100 Solution A : 1 Solution B.

Stripping Buffer, pH 6.7 (500 mL)

Tris base ..... 3.78 g (62.5 mM)
2% w/v SDS ..... 10 g
Deionized H_2O ..... make up to 500 mL
Adjust pH to 6.7 ± 0.2
Just before use add 0.7% v/v β-mercaptoethanol ..... 3.5 mL

Tris Buffered Saline (TBS) 10x, pH 8.0 (1L)

Tris base ..... 12.11 g (100 mM)
NaCl ..... 87.66 g (1.5 M)
Deionized H_2O ..... make up to 1 L
Adjust pH to 8.0 ± 0.2 and store at 4°C

Tris Buffered Saline (TBS) 1x, pH 8.0 (1L)

TBS 10x, pH 8.0 ..... 100 mL
Deionized H_2O ..... make up to 1 L
Final composition: 10 mM Tris base; 150 mM Sodium Chloride.

Tris Buffered Saline-Tween (TBS-T) 10x, pH 8.0 (1L)

Tris base ..... 12.11 g (100 mM)
NaCl ..... 87.66 g (1.5 M)
Deionized H_2O ..... make up to 1 L
Adjust pH to 8.0 ± 0.2 and store at 4°C
1% v/v Tween-20 ..... 10 mL

Tris Buffered Saline-Tween (TBS-T) 1x, pH 8.0 (1L)

TBS-T 10x, pH 8.0 ..... 100 mL
Deionized H_2O ..... make up to 1 L
Final composition: 10 mM Tris base; 150 mM Sodium Chloride; 0.1% v/v Tween-20.